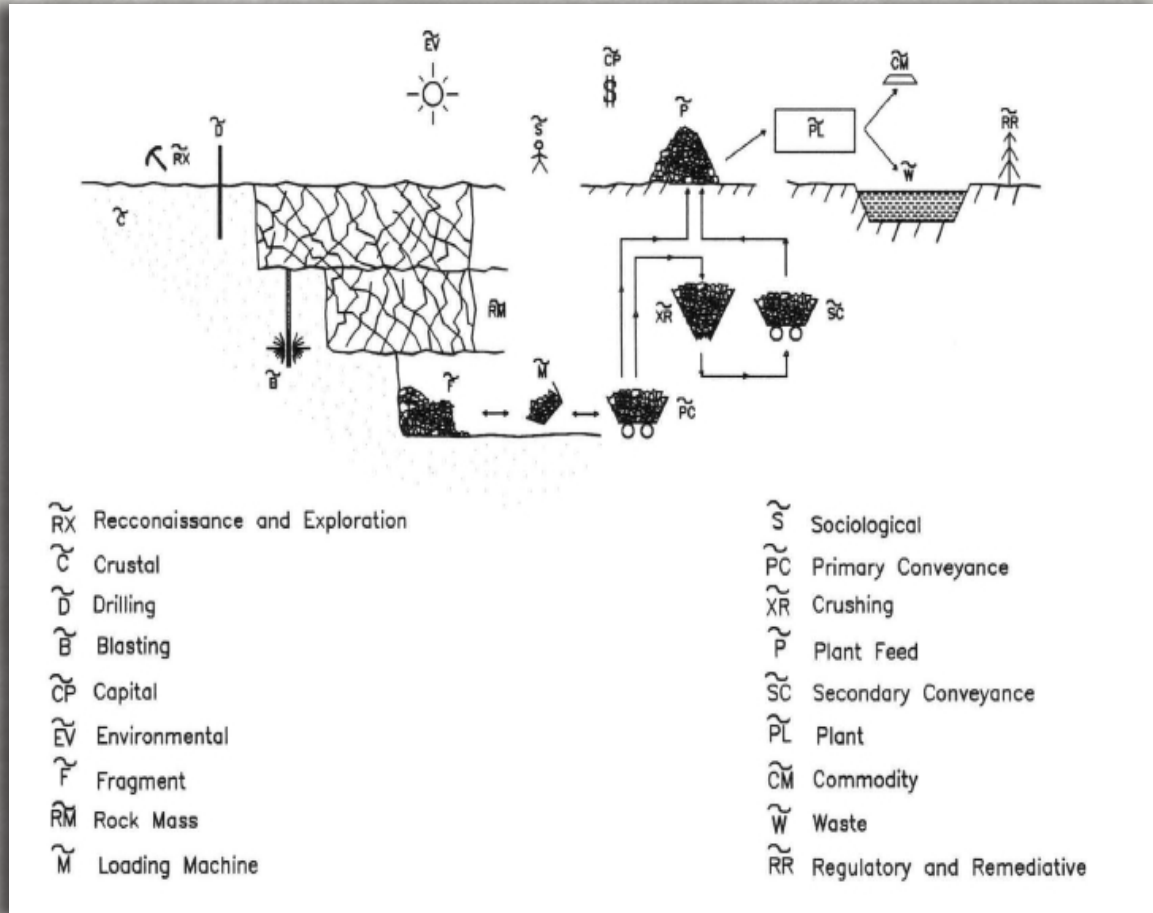


A MODEL FOR MINIMIZING THE COST OF ROCK MASS EXCAVATION

Robert Mansel Ford
University of Arizona



CONTRIBUTED REPORT CR-12-C

May 2012

Arizona Geological Survey

www.azgs.az.gov | repository.azgs.az.gov

Arizona Geological Survey Contributed Report CR-12-C

A Model for Minimizing Rock Mass Excavation

May 2012

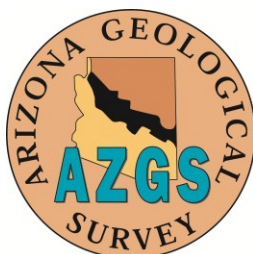
Robert Mansel Ford
University of Arizona

Arizona Geological Survey Contributed Report Series

The Contributed Report Series provides non-AZGS authors with a forum for publishing documents concerning Arizona geology. While review comments may have been incorporated, this document does not necessarily conform to AZGS technical, editorial, or policy standards.

The Arizona Geological Survey issues no warranty, expressed or implied, regarding the suitability of this product for a particular use. Moreover, the Arizona Geological Survey shall not be liable under any circumstances for any direct, indirect, special, incidental, or consequential damages with respect to claims by users of this product.

The author(s) is solely responsible for the data and ideas expressed herein.



A MODEL FOR MINIMIZING THE COST OF ROCK MASS EXCAVATION

by

Robert Mansel Ford

Copyright © Robert Mansel Ford 1997

A Thesis Submitted to the Faculty of the

DEPARTMENT OF MINING AND GEOLOGICAL ENGINEERING

In Partial Fulfillment of the Requirements
For the Degree of

MASTER OF SCIENCE
WITH A MAJOR IN MINING ENGINEERING

In the Graduate College

THE UNIVERSITY OF ARIZONA

1997

STATEMENT BY AUTHOR

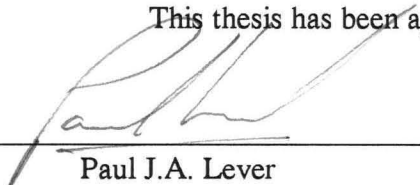
This thesis has been submitted in partial fulfillment of requirements for an advanced degree at the University of Arizona and is deposited in the University Library to be made available to borrowers under rules of the Library.

Brief quotations from this thesis are allowable without special permission, provided that accurate acknowledgment of source is made. Requests for permission for extended quotation from or reproduction of this manuscript in whole or in part may be granted by the copyright holder.

Signed: Robert M. and For

APPROVAL BY THESIS DIRECTOR

This thesis has been approved on the date shown below:



Paul J.A. Lever
Associate Professor of Mining Engineering

8/1/97

Date

ACKNOWLEDGMENTS

“ In operation, the tractors were strung out in a long staggered formation, the lead tractor being directed for much of the time by the company commander circling overhead in a small helicopter. The large number of bomb craters made the job of maneuvering the large tracked vehicles most difficult. The heat was oppressive (hovering around 130 degrees F. in the tractor cabs) and the work was truly arduous. But the morale of the men seemed very high, despite their 15 hour work days, seven days a week, wet season and dry. The company was proud of its abilities and accomplishments and, we are told, was among the rare units in Vietnam without a drug problem. ”

Pfeiffer and Westing (1971) --- *Land War*

Acknowledgment must first be extended to Noel Rytter, Brad Holsapple, and Dennis Greene of the Caterpillar Corporation; they had courage, initiative, and foresight to facilitate the funding of a solicited proposal that was originally directed towards an attempt to quantify the fragmentation parameters that affect the performance of large loading machines. I am also much indebted to the authors of the original proposal to Caterpillar Inc., Drs. John Kemeny and Paul Lever of the University of Arizona Department of Mining and Geological Engineering, for many discussions relating fragmentation to blasting and loading machine performance. I also appreciate the efforts of Dr. Fei-yu Wang, of the U. of A. Dept. of Systems and Industrial Engineering, who took time from a busy schedule to serve upon my thesis committee.

Thanks must also be extended to the following fellow graduate students studying within the Department: to Kirsten Girdner for the exceptional image processing work she contributed; to Mehmet Sari and Umut Alev for the work they performed to quantify the cycle time characteristics of large loading machines; and to Zhou Zhen for the many mathematical arguments. And many thanks to Mike Porter, an Administrative Secretary within the Department, for his efforts in helping me decipher the University's official thesis formatting manual.

DEDICATION

To Basil, Jesse, Doran, and Paco.

“A sterile landscape covers the ore, there is as good as the best for
all the forbidding appearance,
There is the mine, there are the miners,
The forge-furnace is there, the melt is accomplish'd, the hammers-
men are at hand with their tongs and hammers,
What always served and always serves is at hand.”

Walt Whitman (1881) --- *Leaves of Grass*

TABLE OF CONTENTS

LIST OF FIGURES	8
LIST OF TABLES	12
ABSTRACT	13
1. INTRODUCTION.....	14
1.1 The Stages of Rock Mass Size Reduction	16
1.2 The Objectives of Rock Mass Size Reduction	17
1.3 The Scope of the Research.....	19
1.4 The Direction of the Current Research.....	20
1.5 The Fragmentation and Rock Mass Descriptors - In Brief	23
1.6 Analytical Tools Utilized in the Research	23
1.6.1 Digital Image Analysis	24
1.6.2 Regression Analysis	25
1.7 The Research Objective	25
1.8 A Summary of the Work.....	26
2. A MATHEMATICAL FORMULATION FOR TOTAL EXCAVATION COST.....	27
2.1 The Dollar Cost per Ton of Blasting	28
2.2 The Dollar Cost per Ton of Loading Machines.....	31
2.3 The Equation for the Total Cost of Excavation	33
3. COLLECTION, PROCESSING, ANALYSIS, AND MODELING OF THE EXPERIMENTAL DATA.....	36
3.1 The Scope of the Loading Machine Database.....	36
3.2 Collection of the Experimental Data.....	36
3.3 Description of the Experimental Data	38
3.4 Experimental Data Processing.....	38
3.4.1 Sampling Theory	39
3.4.2 Cycle Timing Analysis	40
3.4.3 Machine Production.....	42
3.4.3.1 Idealizations Regarding Site Average Machine Production	43
3.4.4 Determination of Rock Fragment Size Distribution	43
3.4.4.1 The Fragment Shape Descriptors.....	45
3.4.4.2 The Expression for Apparent Screen Size	46
3.4.4.3 Idealizations Regarding Characterization of the Site Fragment Size Distribution	47
3.4.5 Determination of Rock Mass Size Distribution.....	48

TABLE OF CONTENTS - *continued*

3.4.5.1	Idealizations Regarding Characterization of the Site Rock Mass Size Distribution	49
3.5	Linear Regression Analysis	50
3.5.1	The Method of Least Variation	51
3.5.2	Assessing the Quality of a Linear Regression	53
3.6	Statistics and the Linear Model	57
3.7	Theoretical Frequency Distributions	58
3.7.1	The Normal Distribution	60
3.7.2	The Weibull Distribution	62
3.7.2.1	Step-wise Frequency Shifts in the Observed Frequency Data	65
3.7.2.2	The Rosin-Rammler Particle Size Distribution	68
3.7.3	The F Distribution (Fisher-Snedecor Form)	71
3.7.3.1	The Analysis of Rock Strength Variance	72
3.7.4	Student's t Distribution	78
3.8	Representation of Regression Analysis Results	80
3.9	Uncertainty Analysis	81
4.	ROCK MASS FRAGMENTATION MODELS	83
4.1	Open-Pit Blasting Terminology	84
4.2	The Blastonium Construct	87
4.3	The Kuznetsov Mean Fragment Size Theory	91
4.4	The Kuz-Ram Fragmentation Model	94
4.4.1	The Kuznetsov Equation in Powder Factor Form	95
4.4.2	The Rock Mass Blastability Factor	95
4.4.3	Estimators for the Parameters of the Weibull Distribution	96
4.5	Weibull Distribution Parameter Comparisons: SPLIT Vs. Kuz-Ram	98
4.6	A New Model for the Explosive Induced Fragmentation of Rock Mass	101
4.6.1	A Proposed Time Domain Form of Weibull's Strength-Volume Relationship	104
4.6.2	A Proposed Relationship between Explosive Energy and Size Reduction	105
4.6.3	Validation of the Weibull Blasting Index Fragmentation Model	106
4.6.4	The Uniformity of Fragment Size Distributions	111
4.7	The Equivalence of the Kuznetsov Hardness Parameter	113
4.8	A Summary of Results for the Determination of the Rock Mass Specific Energy Term	118
4.9	Estimators for Fragment Screen Size Distribution Scale Parameters	120
4.10	The Estimated Cost of the Explosive Mode of Size Reduction	121
5.	PRODUCTION AND COST ESTIMATORS FOR LOADING MACHINES	123

TABLE OF CONTENTS - *continued*

5.1	Machine Production and Total Cycle Time.....	123
5.2	Total Cycle Time and Fragment Screen Size Considerations.....	125
5.3	Machine Production Estimators	128
5.4	Shear Cycle Time and Machine Production	132
5.5	The Machine Cost Estimator	135
6.	DRILL PRODUCTIVITY AND THE STRENGTH OF ROCK MASS.....	137
6.1	The Observed Drill and Strength Data.....	138
6.2	The Bauer and Calder Rotary Drilling Penetration Rate Formula.....	139
6.3	An Estimator for Rock Mass Strength.....	141
6.4	Drilling Machine Costs.....	143
7.	THE TOTAL EXCAVATION COST MODEL	145
7.1	The Total Excavation Cost Estimator.....	146
7.2	Minimization of the Total Cost of Excavation	148
7.3	Minimization of the Total Cost of Excavation Subject to a Powder Column Constraint.....	152
7.4	Minimization of the Total Cost of Excavation Subject to Powder Column and Rock Mass Volume Constraints	156
7.5	The Range of Ground Conditions used for the Excavation Cost Modeling....	160
7.6	Loading Machines used for the Excavation Cost Modeling.....	161
7.7	Machine Cost Equilibration for the Excavation Cost Modeling	162
8.	RESULTS AND CONCLUSIONS	163
8.1	Total Estimated Excavation Costs for the Different Machines over the Range of Observed Rock Mass Chunk Screen Size Distribution Scale Parameters.....	165
8.2	Total Estimated Excavation Costs for the Different Machines over the Range of Rock Mass Strengths	168
8.3	Total Estimated Excavation Costs for the Different Machines over the Range of Rock Mass Densities	171
8.4	An Inconsistency of the Current Form of the Excavation Cost Model.....	173
9.	FUTURE WORK	175
9.1	Redefining Loading Machine Productivity.....	176
9.2	Crushing Implications	182
9.3	Drilling Work	187
	APPENDIX: DATA TABLES	189
	REFERENCES.....	198

LIST OF FIGURES

Figure 1.1	Symbolic Representation of the Descriptor Sets Defining the Extraction and Concentration of a Mineral or Metallic Crustal Commodity.....	18
Figure 3.1	Methodology for Determination of Fragment Size Distribution	44
Figure 3.2	Methodology for Determination of Rock Mass Chunk Size Distribution.....	49
Figure 3.3	Best Fitting Large Front End Loaders Production Trend Line for Fragment Scale Parameter Observations	53
Figure 3.4	Graphical Depiction of Residual, Regression, and Total Deviation Between an Observed and Predicted Value	54
Figure 3.5	A Residual Scatterplot for the Large Front End Loaders	56
Figure 3.6	Observed and Normal Models of Frequency Distributions for the Load Cycle Time of a Large Front End Loader Operating at Site Au6SA	62
Figure 3.7	Observed and Weibull Model Frequency Distributions for Fragment Size at Site Cu2SD.....	65
Figure 3.8	Observed and Modeled Frequency and Cumulative Frequency Distributions for Fragment Size at Site Cu2SD.....	67
Figure 3.9	Graphical Determination of Weibull Scale and Shape Parameters for Site Cu2SD.....	70
Figure 3.10	F distributions with 1 and 37 degrees of freedom for the Graphical Determination of Risk Level for Analysis of Variance on Site Rock Strengths	76
Figure 3.11	t Distributions with 38 Degrees of Freedom for Graphical Determination of Confidence Intervals for Rock Strength Population Mean.....	79
Figure 4.1	Open Pit Blasting Terminology	85

LIST OF FIGURES - *Continued*

Figure 4.2	The 1 meter Cube of Blastonium before the Stage 1 Detonation.....	89
Figure 4.3	Comparison of Fragment Size Distribution Scale Parameters: SPLIT Vs. Kuz-Ram.....	100
Figure 4.4	Comparison of Fragment Size Distribution Shape Parameters: SPLIT Vs. Kuz-Ram.....	100
Figure 4.5	Average Weibull Frequency Distributions of Size for the Rock Mass Cells and Fragments Composing the Experimental Data Set	102
Figure 4.6	Average Rosin-Rammler Size Distributions for the Rock Mass Cells and Fragments Composing the Experimental Data Set.....	103
Figure 4.7	Comparison of Fragment Size Distribution Scale Parameters: SPLIT Vs. Weibull Model.....	110
Figure 4.8	Comparison of Fragment Size Distribution Shape Parameters: SPLIT Vs. Uniformity Model.....	112
Figure 4.9	Comparison of Mean Fragment Sizes : SPLIT Vs. Kuznetsov Model.....	114
Figure 4.10	Comparison of Mean Fragment Sizes : SPLIT Vs. Kuznetsov Model.....	116
Figure 5.1	The Observed and Modeled Average Total Cycle Times for Large Front End Loaders Over the Range of the Observed Data	127
Figure 5.2	The Observed and Modeled Average Total Cycle Times for Large Front End Loaders Extended Out Toward the Bucket Width	128
Figure 5.3	Estimated Average Perfect Cycle Times for the Different Machine Ranks	131
Figure 5.4	Estimated Average Perfect Productions for the Different Machine Ranks	132
Figure 5.5	Estimated Average Total Cycle Times for the Different Machine Ranks	133

LIST OF FIGURES - *Continued*

Figure 5.6	Estimated Average Total Cycle Times for the Different Machine Ranks over 90 inches of 100 th Percentile Screen Size Range	134
Figure 5.7	Estimated Average Total Productions for the Different Machine Ranks over 225 inches of 100 th Percentile Screen Size Range	135
Figure 6.1	Rotary Drill Penetration Rate Vs. Observed Rock Strength for Three Sites at Mine Cu2	139
Figure 6.2	Estimated Rock Mass Strength (Bauer & Calder Model) Vs. Observed Drill Penetration Rate for Three Sites at Mine Cu2	142
Figure 8.1	Estimated Excavation Costs over the Rock Mass Chunk Screen Size Scale Parameter Range.....	166
Figure 8.2	Mean Fragment Sizes Estimated by the Model over the Rock Mass Chunk Screen Size Scale Parameter Range	166
Figure 8.3	Machine Costs Vs. Rock Mass Chunk Screen Size Scale Parameter	168
Figure 8.4	Estimated Excavation Costs over the Range of Rock Mass Strength	169
Figure 8.5	Mean Fragment Sizes Estimated by the Model over the Range of Rock Mass Strength	169
Figure 8.6	Machine Costs Vs. Rock Mass Strength.....	170
Figure 8.7	Estimated Excavation Costs over the Rock Mass Density Range	171
Figure 8.8	Mean Fragment Sizes Estimated by the Model over the Range of Rock Mass Density.....	172
Figure 9.1	Modeled Average Total Cycle Times for Large Front End Loaders Corresponding to 2 Different Bucket Widths.....	177
Figure 9.2	Estimated Excavation Costs over the Rock Mass Chunk Screen Size Scale Parameter Range: Large Front End Loader with Redefined Production Function	178

LIST OF FIGURES - *Continued*

Figure 9.3	Mean Fragment Sizes Estimated by the Model over the Rock Mass Chunk Screen Size Scale Parameter Range: Large Front End Loader with Redefined Production Function	179
Figure 9.4	Machine Costs Estimated by the Model over the Rock Mass Chunk Screen Size Scale Parameter Range: Large Front End Loader with Redefined Production Function	179
Figure 9.5	Rock Volumes and Powder Columns Estimated by the Model over the Rock Mass Chunk Screen Size Scale Parameter Range: Large Front End Loader with Redefined Production Function	180

LIST OF TABLES

Table 2.1	Physical Variables within the Excavation Cost Equation.....	34
Table 2.2	Machine Constants within the Excavation Cost Equation	34
Table 2.3	Cost Constants within the Excavation Cost Equation	35
Table 2.4	Physical Constants within the Excavation Cost Equation.....	35
Table 2.5	Functions within the Excavation Cost Equation.....	35
Table 3.1	Comparison of Results for Observed and Modeled Fragment Size Frequency Distribution for Site Cu2SD	67
Table 4.1	The Size Reduction of Cubic Blastonium	90
Table 4.2	The Kuznetsov Hardness Parameter and Associated Rock Physical Characteristics	92
Table 5.1	Perfect Machine Production for Different Types and Classes of Loading Machines	130
Table 6.1	Rotary Penetration Rate, Bit Diameter, and Rock Strength Data for Three Sites at Mine Cu2	138
Table 7.1	The Ground Condition Variables used in the Cost Model.....	160
Table 7.2	Summary of Loading Machine Data Used in the Cost Modeling.....	161

ABSTRACT

A mathematical model can minimize the total cost of rock mass excavation. The total excavation cost model consists of functions defining the owning and operating costs for a drill, explosive and auxiliary explosive loading equipment, and an excavating machine. These functions contain variables that describe certain remotely sensed physical features of both the pre-blasted rock mass volume and the fragments that result from blasting. Remote sensing was performed within operating open pit Gold and Copper mines located within the Western United States. For a remotely sensed rock mass, the model automatically determines the rock mass volume and the explosive mass that result in minimum total excavation cost. The model estimated minimum total excavation cost for different loading machines over a range of rock mass conditions that are characteristic of those observed within the mines. The results suggest that a model including the cost of a comminutive process for minimizing the cost of reducing the size of rock mass is feasible.

1. INTRODUCTION

“ The gold which the Griffins dig up consists of rock encrusted with golden drops like fiery sparks; they quarry the gold with the power of their hard beaks. These creatures are found in India and are sacred to the sun, having the size and strength of lions whom they excel by reason of their wings; and they can vanquish elephants and great serpents. The tiger, however, they cannot vanquish, for he excels them by his fleetness...”

Philostratus (2nd/3rd Century) --- *Life of Appolonius of Tyana*

Minimizing the cost of reducing the size of rock mass is a basic function of the mining process. Three principal modes of rock mass size reduction are drilling, blasting, and comminution (crushing and grinding). Each of these modes utilizes a distinctly different process to fracture rock and thereby reduce it's size. The fracture processes of these different modes are all related to the fact that rock is “weak” when subjected to tensile stresses. Currently there is no unified theory relating the principal modes of rock mass size reduction, merely much empirical evidence that a “weak” mass of rock will drill, blast, crush, and grind easier than a “strong” mass of rock. A considerable amount of such evidence exists (in the form of capital costs and energy consumptions for the various modes of size reduction) throughout the mining literature, but it is difficult to utilize this data to form any sort of conclusion relating to what may be the most cost effective arrangement of the different modes of size reduction.

The mass specific energy (MJ/ton) consumed by a size reducing process can be stated as:

$$E_r = k_m f(R) \quad (1.1)$$

where k_m is a physical constant relating the per unit mass resistance of the material to the reductive mode, and f is a function acting on some definition of mass size reduction R .

As an example, the energy consumption of a comminutive process appears to be well characterized by Bond's formula [Wills, 1992]:

$$W = 10 W_i \left(\frac{1}{\sqrt{P}} - \frac{1}{\sqrt{F}} \right) \quad (1.2)$$

where W is the energy consumption (kW-hr/ton) of the comminutive machine, W_i is the rock's work index (kW-hr/ton) , and P and F are the screen size values (microns) for which 80% of the product and feed particles pass.

There currently exists no relationship of a form similar to formula 1.1 above for the explosive mode of size reduction. However, before a rock mass volume can be blasted into fragments:

1. At least some portion of its volume must be reduced by drilling;
2. at least some portion of the rock mass surface area is exposed enabling the observation of pre-existing cracks and fracture boundaries that decompose the volume into discrete "chunks" of rock mass.

If the drill penetration rate can be related to the resistance of the rock mass to the explosive mode of size reduction, and if image analysis can be utilized to obtain both the pre and post blast mass size distributions, then it will be possible to formulate an expression of form analogous to Equation 1.1 above for the explosive mode of size reduction. Then for example the cost of blasting a rock mass composed of chunks of different sizes into a fragment size distribution could be precisely determined. If

properties of these fragments could then be related to the costs of subsequent loading, crushing, and grinding operations, then a formulation for the total cost of size reduction can be attained. The challenging aspect of such a formulation is that both the strength and structural features of the rock mass can change rapidly on the spatial scale, similar to the grade of the commodity contained within the rock. So a total cost formulation that accounts for such variation in rock mass conditions will be of considerable value towards achieving the lowest total cost of size reduction.

1.1 The Stages of Rock Mass Size Reduction

Mining operations generally utilize three distinct stages of rock mass size reduction. The first stage consists of size reduction via the mode of explosive blasting, which is almost always performed for the purpose of practical material handling. The reduction ratio (here defined as [mean mass start size/mean mass finish size]) of this primary stage appears to be about 1 order of magnitude (10^1). Sometimes the fragments produced by blasting are transported directly to waste dumps, or as in the case of leaching operations, blasted ore fragments are leached in-situ or else moved onto horizontal pads for subsequent solution recovery of the ore commodity; in either event blasting is the only mode of size reduction procedure utilized. The second stage of size reduction is a comminutive mode characterized by mechanical crushing. Crushing is performed for a variety of reasons, including: 1) attaining a specific fragment size range for subsequent leaching operations; 2) reducing the size of blasted fragments for efficient conveyor belt handling operations; 3) pre-sizing material for subsequent grinding

operations. The reduction ratio observed in typical crushing operations also appears to be about one order of magnitude. The third stage, grinding (or milling) is also a comminutive reductive mode. Grinding is performed to produce particles finer than those attainable by crushing, usually to physically separate waste rock (called “tailings”) from elements or compounds of valuable commodity to permit their subsequent concentration. The reduction ratios observed in grinding can vary from one to four orders of magnitude. Then for a mass of rock undergoing all three stages of size reduction, the overall reduction ratio can range from about 3 to 6 orders of magnitude, and the total energy expenditure per unit mass can be considerable. So long as the cost of this expenditure is somewhat less than the value of contained commodity, the rock mass may be profitably reduced in size.

1.2 The Objectives of Rock Mass Size Reduction

The objective of rock mass size reduction is commodity production. Figure 1 presents, in symbolic schematic form, the major descriptor sets thought to influence the production of commodity from a massive deposit being mined by the open pit method. Descriptor sets representing the equipment and processes of other mining methods and mass stream layouts could be defined in similar fashion. On Figure 1 the grinding mode of size reduction is represented by processes that occur within a “plant”, where the plant represents any overall process (i.e. flotation, gravity concentration, leaching, etc.) used for concentrating the commodity. Beginning with the left hand side of Figure 1:

- A crustal descriptor provides generalized geological and hydrological information as provided principally by geophysical reconnaissance and exploration;

- exploratory and production drilling information is provided by the drilling descriptor;
- the blast descriptor describes the explosive mode of size reduction acting on the rock mass;
- information concerning the fragmented rock mass is provided by the fragment descriptor;
- loading machine and primary conveyance descriptors describe the transport of the mass stream into either a crusher or the plant feed stockpile;
- a secondary conveyance (belt or truck) descriptor gives data on an alternate form of mass stream transport when the crushing mode of size reduction is utilized;
- the plant descriptor supplies information relating to the subdivision of the principal mass stream into its commodity and waste constituents;
- environmental (climatic), sociological, Capital, and regulatory and remediative descriptors are included as they all influence the rate and cost of processing rock mass.

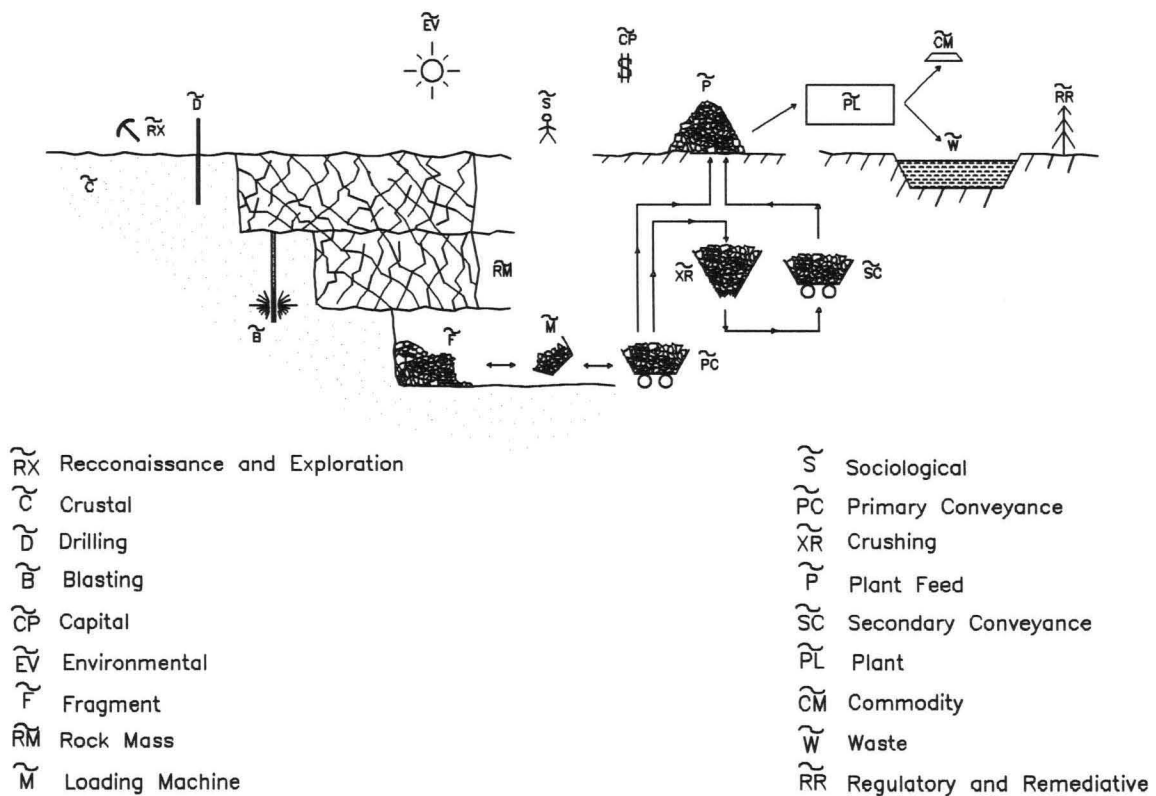


Figure 1.1 - Symbolic Representation of the Descriptor Sets Defining the Extraction and Concentration of a Mineral or Metallic Crustal Commodity

There are different objective functions for a system producing commodity from rock mass. The typical objective function appears to be one of cost minimization:

$$\text{Given } \frac{dM_{\text{cm}}}{dt}, \text{ Minimize } \frac{dC_{\text{tot}}}{dM_{\text{cm}}} \quad (1.3)$$

where M_{cm} is commodity mass, t is time, and C_{tot} is the total cost incurred by the procurement, size reduction, handling, concentrating, and remediative processes performed upon the rock mass. Another important objective function appears to be totally unrelated to cost minimization:

$$\text{Given } CP_{t_0}, \text{ Maximize } \frac{dM_{\text{cm}}}{dt} \quad (1.4)$$

Where CP_{t_0} represents a capital quantity that is suddenly available at time t_0 .

1.3 The Scope of the Research

The overall scope of the current research is perhaps best explained with the following lists of hypothetical observations and constraints, and the single hypothetical concluding argument:

Given hypothetical observations:

1. A mass of rock exists which exhibits spatial variance with respect to commodity grade, strength, density, and structural features;
2. the rock mass is to be successively reduced in size by blasting, crushing, and grinding;
3. before the rock mass can be blasted, at least some portion of it's volume must be reduced by drilling;
4. drilling and grinding are inferred to be the most expensive modes of reducing the size of the rock mass;

5. blasting is inferred to be the least expensive mode of size reduction;
6. the expense of the crushing mode of size reduction is inferred to be somewhere between the expense incurred by the processes of 4) and 5) above;
7. after the rock is blasted, it must be loaded and transported to some location distal to the drilling and blasting site for subsequent crushing;
8. after the material is crushed, it must be transported to some location distal to the crushing site for subsequent grinding; the mode of transport may be different than that used in 7) above.

Given hypothetical constraints:

1. Because of practical operational constraints pertaining to fly-rock, slope stability, and/or seismic considerations, there exists an upper limitation on the explosive mass that may be introduced into the rock mass to permit size reduction by blasting;
2. because of practical considerations pertaining to material handling (loading and conveyance) there exists a lower limitation on the explosive mass that may be introduced into the rock mass.

Concluding hypothetical argument:

1. There exists some allocation of the different modes of size reduction by drilling, blasting, crushing, and grinding, such that while subject to the explosive mass constraints, the total cost incurred by the overall size reduction and handling processes performed upon the mass of rock will be minimized.

1.4 The Direction of the Current Research

The observational data set utilized for this thesis is described within Chapter 3. The data was originally gathered for the purpose of attempting to characterize the relationship between rock fragmentation and the production performance of large loading machines. The data was obtained from a wide variety of different mining sites and includes a large assortment of different machines. The data is composed of information concerning: 1) The uniaxial compressive strength of rock mass; 2) the structural features (video imagery and

hand drawn maps) of the exposed faces of rock mass; 3) the energy content and spatial distribution of the explosives used to blast the rock mass; 4) video imagery of the fragments produced by the blasts; and 5) video images of the machines loading fragments into off-road haul trucks.

The data contains no information concerning the comminutive modes of size reduction, and only limited information concerning the primary mode of conveyance (trucks) occurring subsequent to fragment loading. Of most importance is the fact that the data set does not include any machine cost data (owning nor operating) nor commodity grade information. Thus the scope of the research, as outlined in Section 1.3 above, is forced to shrink considerably. The research will now concentrate on the cost relationships between: 1) Drilling; 2) the explosive mode of size reduction, and 3) the performance of loading machines. Then the lists of hypothetical observations, constraints, and arguments previously presented can be altered to the following:

Given hypothetical observations:

1. A mass of rock exists which is to be reduced in size by blasting;
2. the dimensions of the rock mass are known;
3. the density of the rock mass can be approximated;
4. before the rock mass can be blasted, at least some portion of it's volume must be reduced by drilling, and at least some portion of its outer surface area can be monitored and analyzed to provide data concerning pre-existing flaws, fractures, and joints; and the mass, energy content, and location of the explosive introduced into the drill hole is known;
5. the rate (ft/hr) at which the drill of known diameter penetrates the rock mass can be monitored;

6. the owning and operating costs (\$/hr) of the drill can be approximated;
7. the explosive cost (\$ /lb.) and the owning and operating cost (\$/hr) of the explosive loading equipment can be approximated;
8. after the rock mass is blasted, the fragment muckpile can be monitored to provide a fragment descriptor set;
9. the rock mass fragments must be subsequently machine excavated;
10. the rate of machine excavation can be monitored;
11. the machine owning and operating costs (\$/hr) can be approximated;
12. the drilling cost (\$/ton) is inferred to be a function of the information within 2), 3), 5) and 6) above;
13. the cost (\$/ton) incurred in fragmenting the rock mass volume are inferred to be some function of the data within 2), 3), 5), 6), 7), and 8)above;
14. the cost incurred by the subsequent loading of the fragmented rock mass volume are some function of the data within 8), 10), and 11) above.

Given hypothetical constraints:

1. Because of practical considerations pertaining to either to ground control or stemming ejection, there exists an upper limitation on the explosive mass that may be introduced into the rock mass volume via the drill hole to permit size reduction by blasting;
2. because of practical considerations pertaining to fragment loading, there exists a upper limitation on the volume of rock mass affected by the explosive mass.

Concluding hypothetical argument:

1. There exists some discrete value(s) for some variable(s) within the fragment descriptor set, such that while subject to the explosive mass and material handling constraints, and while subject to the physical nature of the rock mass, the total cost per ton incurred by drilling, blasting, and loading the rock mass volume will be minimized.

1.5 The Fragmentation and Rock Mass Descriptors - In Brief

The concluding argument above implies that a formulation for total excavation cost will involve sets of variables (descriptor sets) that describe the drill, the rock mass, the fragments, and the loading machine. The complete fragmentation descriptor set is described in Chapter 3 (Section 3.4.4) and consists of 20 discrete descriptors. A single descriptor from this set was selected to test the concluding argument; the screen size of the rock mass fragments. Undoubtedly total cost formulations will eventually be derived as multivariate functions that will include other additional fragment descriptors, such as fragment shape or fragment “ key factor ” (i.e. how the fragments are keyed or locked together). But as the developments presented within the subsequent Chapters show, the formulation of total cost per ton as a function of a single screen size descriptor is mathematically complex. But the same approaches and techniques can be used as guidelines for other researchers attempting to formulate rock mass size reduction cost as a multivariate function of fragmentation descriptors.

Information composing the rock mass descriptor set will consist of it's dimensions, strength, and structural features, as provided by the drill pattern, the drill penetration rate, and digital image analysis, respectively.

1.6 Analytical Tools Utilized in the Research

Two important tools were used to process the experimental excavation data: Digital image analysis (DIA) and regression analysis (RA). DIA was used to provide descriptors for: 1) The pre-blasted rock mass, and 2) the rock mass fragments that

resulted from the blast. RA was then used to determine functional relationships between these descriptors and productivity models for drilling, blasting, and loading. More complete explanations of the roles played by DIA and RA within the research are given below.

1.6.1 Digital Image Analysis

Digital image analysis was a fundamental tool for the research. The formulation of total excavation cost required determination of both the pre and post blast size distributions of the rock mass. This was accomplished with a sophisticated package of digital image analysis software.

The phrase “fragment size” used throughout this work is synonymous with the term “fragment screen size”; and fragment size distributions produced by a digital fragment delineation system are representative of the results produced by physically screening the rock fragments through a system of sieves, or filters, each having proportionately smaller aperture size, compared to the preceding filter.

Still images of fragment muckpiles were processed with the “SPLIT” image processing program developed at the University of Arizona Department of Mining and Geological Engineering [Kemeny, 1993]. SPLIT is composed of many specialized subroutines written for an digital image processing package originally developed by the National Institute of Health for medical research. Still images of exposed rock mass faces were processed with a special “scan line” subroutine developed by Kemeny to estimate the size distribution of the material within the rock mass bounded by faults and fractures.

1.6.2 Regression Analysis

Regression analysis of the site data was utilized to determine relationships between:

1. drill penetration rate and the strength of the rock mass;
2. rock mass and fragment size (as determined by DIA) and blasting;
3. loading machine production and fragment size.

1.7 The Research Objectives

In any mine, the physical nature of the rock mass volume (i.e. the “ground conditions”) are not constant. The ground conditions can change rapidly on the spatial scale. Typically a mine’s operating plan will account for changing ground conditions by assigning different categories to the ground, such as “weak” or “strong”. The true meanings of these terms can differ from mine to mine. For this work, the physical nature of the ground is described by its strength (as provided by the drill) and by its structural features (as provided by DIA). The size of the fragments produced by blasting the rock mass volume is a function of the ground conditions. In open pit mines, blasting engineers compensate for changing ground conditions by: 1) Changing the volume of rock mass affected by the blast, by altering the horizontal pattern between holes; and 2) changing the quantity of explosive loaded into the drill holes, either by altering the subdrill (below grade hole length) and/or by altering the stemming (length of inert material in the drill hole above the explosive). If the performance of loading machines is an explicit function of fragment size, then it follows that machine performance is also an implicit function of

blasting and ground condition variables.

The objectives of the research are to investigate how total excavation cost (drilling, blasting, and loading) changes subject to changing ground conditions. The goal is to produce a total excavation cost model that includes both rock mass volume and explosive mass per drill hole as control variables. Then given the ground conditions and the types of drilling and loading machines, the model will automatically determine the rock mass volume and explosive load associated with minimizing total excavation cost.

1.8 A Summary of the Work

The preliminary mathematical formulation for total excavation cost follows the hypothetical argument presented in Section 1.4 above, and is presented in Chapter 2. The final form of the total excavation cost formulation required the determination of certain constants and functions. The use of DIA and RA on the experimental data set to determine these constants and functions is described with examples in Chapter 3. The development of cost and productivity models for blasting, drilling, and loading machines are then presented in Chapters 4, 5, and 6 respectively. The final form of the total excavation cost model is then presented in Chapter 7, where the total estimated cost is minimized with respect to 2 variables: Powder column length and rock mass volume. Results and conclusions for modeled estimates of total excavation cost for different loading machines and different ground conditions are shown in Chapter 8. Chapter 9 then goes on to present recommended future work.

2. A MATHEMATICAL FORMULATION FOR TOTAL EXCAVATION COST

“ In the 15th century heavy artillery had reached a high level of perfection. In the 16th and 17th centuries the war industry made enormous demands upon the metallurgical industry. In the months of March and April 1652 alone, Cromwell required 335 cannon, and in December a further 1,500 guns of an aggregate weight of 2,230 tons, with 117,000 balls and 5,000 hand bombs in addition. Consequently it is clear why the problem of the most effective exploitation of mines became a matter of prime importance. First and foremost arises the problem set by the depth at which the ores lie. But the deeper the mines, the more difficult and dangerous work in them becomes. ”

B. Hessen (1939) --- *The Social and Economic Roots of Newton's Principia*

The work presented in this Chapter consists of the mathematical formulations for the dollar per rock mass ton costs of drilling and blasting (Section 2.1) and loading machines (Section 2.2). Taken together, these two terms compose the total cost per ton of excavation (Section 2.3).

The dependent variable selected to assess machine performance is fragment screen size. Given a rock mass of known strength (as determined by the penetration rate of a drill of known diameter) and structural features (as determined by image analysis), then the ultimate motivation is the development of an excavation cost model that can “ tune ” control variables such as explosive mass and rock mass volume (i.e. pattern size) to control the fragment screen size and hence loading machine cost per ton. Drilling cost per ton depends upon the volume of rock mass that is blocked out by the drill and subsequently affected by the blast. Thus explosive cost per ton will also depend upon rock mass volume, but the explosive cost must also include variables describing the strength

and structure of the rock mass. The total excavation cost is then the sum of the drilling, blasting, and loading cost terms. However, the full derivation of the total excavation cost model will not be possible until certain terms and constants within the preliminary mathematical formulation are determined via regression analysis performed upon the experimental data set. These constants and terms are developed for the fragmentation, loading machine, and drilling models in Chapters 4, 5, and 6 respectively. All of this work then converges in Chapter 7, where the total excavation cost model is completely developed.

2.1 The Dollar Cost per Ton of Blasting

Before a volume of rock mass can be blasted into fragments it must be perforated with a drill hole. The drilling time (hr) required to perforate a volume of rock mass is:

$$t_d = \frac{k_d}{V_{rm}} \quad (2.1)$$

where k_d is a drill machine constant ($yd^3 \cdot hr$) and V_{rm} is the rock mass volume (yd^3).

The drill constant is equivalent to:

$$k_d = \frac{V_{rm} (H + sd)}{\bar{r}_d} \quad (2.2)$$

where \bar{r}_d is the average drill penetration rate (ft/hr), H is the vertical dimension (bench height) of the rock mass volume (ft), and sd is the subdrill (ft). (Drilling and blasting terminology is presented in Chapter 4 within Figure 4.1). The production (ton/hr) of the drill is then:

$$P_d = \frac{\rho_b (V_{rm})^2}{k_d} = \frac{\rho_b V_{rm} \bar{r}_d}{H + sd} \quad (2.3)$$

where ρ_b is the bank density (tons/yd³) of the rock mass. The dollar per ton cost of the drill may now be expressed as:

$$C_d = \frac{a_d + b_d}{P_d} = \frac{k_d (a_d + b_d)}{\rho_b (V_{rm})^2} = \frac{(a_d + b_d)(H + sd)}{\rho_b V_{rm} \bar{r}_d} \quad (2.4)$$

where a_d and b_d represent the total costs (\$/hr) of owning (or leasing) and operating the drill, respectively. The operating cost term must be defined to include machine utilization and availability.

To determine the cost associated with the explosive mode of size reduction, it is necessary to define the following term:

$$F_{pv} = \frac{M_e}{V_{rm}} \quad (2.5)$$

where F_{pv} is the volumetric “ powder factor ” (lbs/yd³), and M_e is the mass of explosive (lbs) inserted into the drill hole. The mass specific powder factor is defined as:

$$F_{pm} = \frac{M_e}{M_{rm}} = \frac{M_e}{\rho_b V_{rm}} \quad (2.6)$$

where M_{rm} is the rock mass (tons) and ρ_b is the rock mass bank density (tons/yd³). A mass specific energy factor term (MJ/ton) can be defined as:

$$F_{em} = e_m F_{pm} = e_m \frac{M_e}{M_{rm}} = \frac{E_e}{\rho_b V_{rm}} = \frac{e_m M_e}{\rho_b V_{rm}} \quad (2.7)$$

where e_m is the mass specific energy of the explosive (MJ/lb), and E_e is the total

explosive energy content (MJ). Equation 1.1, which related the mass specific energy consumed by a size reducing process to some constant of material resistance and some function of reduction ratio is repeated here:

$$E_r = k_m f(R) \quad (2.8)$$

Currently, the form of the reduction ratio function for the explosive mode of size reduction is unknown, so:

$$E_{re} = k_{me} f(R) \quad (2.9)$$

where E_{re} denotes the energy expended by the explosive per ton of rock mass (MJ/ ton), and k_{me} relates the specific energy (MJ/ ton) actually consumed by the rock undergoing the form of size reduction represented by the function “ f ”. Presently the functional variables of the k_{me} term are also unknown. Equating Equations 2.7 and 2.9 and solving for M_e :

$$M_e = \frac{V_{rm} \rho_b k_{me} f(R)}{e_m} \quad (2.10)$$

The cost (\$/ton) of fragmenting the rock mass may now be defined as:

$$C_e = (a_e + b_e) \frac{M_e}{\rho_b V_{rm}} \quad (2.11)$$

where a_e and b_e now represent the total *dollar per explosive pound* costs of owning (or leasing) and operating the powder loading equipment, respectively. The following expression results from substituting the right hand side of Equation 2.10 for the M_e term in Equation 2.11:

$$C_e = (a_e + b_e) \left(\frac{k_{me} f(R)}{e_m} \right) \quad (2.12)$$

Volumes of rock mass are rarely monolithic; rather they are most often composed of discrete blocks or chunks of rock separated from each other by fracture surfaces. The reduction ratio R will be defined as the ratio of rock mass chunk to fragment screen size, or s_{rm}/s_f . Then the total dollar per ton cost of blasting a rock mass volume composed of characteristic chunk size s_{rm} (in) into fragments of characteristic size s_f (in) will be:

$$C_b = C_d + C_e = (a_d + b_d) \left(\frac{(H + sd)}{\rho_b V_{rm} \bar{r}_d} \right) + (a_e + b_e) \left(\frac{k_{me} f \left(\frac{s_{rm}}{s_f} \right)}{e_m} \right) \quad (2.13)$$

2.2 The Dollar Cost per Ton of Loading Machines

The average ton per hour production of a loading machine is:

$$\bar{P}_m = \frac{\bar{\rho}_h V_b \bar{F}_b}{\bar{t}_{tot}} \quad (2.14)$$

where V_b is the bucket volume (yd^3), and $\bar{\rho}_h$, \bar{t}_{tot} and \bar{F}_b are the hourly average values for the heaped muckpile density ($tons/yd^3$), total machine cycle time (hr), and bucket fill factor (a dimensionless constant ranging from 0 to over 1). The total cycle time can be defined as a sum of machine “ perfect cycle time ” and “ shear cycle time ”:

$$\bar{t}_{tot} = \bar{t}_p + \bar{t}_s \quad (2.15)$$

where the shear cycle time represents the time expended in shearing or ploughing fragments in the vicinity of the bucket's surface. \bar{t}_{tot} is a function of some set of descriptors

describing the muckpile fragments. If one descriptor is fragment screen size (“ s_f ”), then \bar{t}_{tot} must be defined by some function such that when $s_f \rightarrow 0$, $\bar{t}_{tot} \rightarrow \bar{t}_p$. Then when s_f approaches some critical value of screen size, $\bar{t}_{tot} \rightarrow \infty$. This critical size value will be defined as the bucket width (W_b). A function that describes the non-linear relationship between \bar{t}_{tot} and s_f is:

$$\bar{t}_{tot} = \frac{-k_m}{s_f - W_b} = \bar{t}_p + \bar{t}_s \quad (2.16)$$

where k_m (in \cdot hrs) is a machine constant. This function is only defined over the size

interval $0 \leq s_f < W_b$ since when $s_f = 0$, $\bar{t}_{tot} = \frac{k_m}{W_b} = \bar{t}_p$, and when $s_f \rightarrow W_b$, $\bar{t}_{tot} \rightarrow \infty$.

The average cost (\$/ton) of utilizing the machine to load fragments over the screen size range $0 \leq s_f < W_b$ is then:

$$\bar{C}_m = \frac{a_m + b_m}{\bar{P}_m} = \bar{t}_{tot} \left(\frac{a_m + b_m}{\bar{\rho}_h V_b \bar{F}_b} \right) = \frac{-k_m}{s_f - W_b} \left(\frac{a_m + b_m}{\bar{\rho}_h V_b \bar{F}_b} \right) \quad (2.17)$$

where a_m and b_m represent the total costs (\$/hr) of owning (or leasing) and operating the excavating machine, respectively. The operating cost term is defined analogous to that for the drill to include machine utilization and availability.

The denominator of Equation 2.17 above contains terms for the heaped density and bucket fill factor; clearly when $s_f \rightarrow 0$, $\rho_h \rightarrow \rho_b$ (where ρ_b is the material bank density) and $F_b \rightarrow 1$. The exact form of these limiting relationships depends upon the shape of the fragments. This topic is worthy of future research, but for the present development the heaped density and fill factor terms are assumed to be independent of fragment screen

size. Then Equation 2.17 can be manipulated into the following form:

$$\bar{C}_m = \frac{\bar{t}_p}{\left(1 - \frac{s_f}{W_b}\right)} \left(\frac{a_m + b_m}{\bar{\rho}_h V_b \bar{F}_b} \right) = \frac{\left(\frac{k_m}{W_b}\right)}{\left(1 - \frac{s_f}{W_b}\right)} \left(\frac{a_m + b_m}{\bar{\rho}_h V_b \bar{F}_b} \right) \quad (2.18)$$

2.3 The Equation for the Total Cost of Excavation

Summing Equations 2.13 and 2.18 results in a formulation for the total cost per ton of blasting rock mass volume V_m into fragments of screen size s_f and subsequently loading the fragments:

$$C_{tot} = (C_d + C_e) + \bar{C}_m = C_b + \bar{C}_m = (a_d + b_d) \frac{(H + sd)}{\rho_b V_{rm} \bar{r}_d} + (a_e + b_e) \left(\frac{k_{me} f\left(\frac{s_{rm}}{s_f}\right)}{e_m} \right) + \frac{\left(\frac{k_m}{W_b}\right)}{\left(1 - \frac{s_f}{W_b}\right)} \left(\frac{a_m + b_m}{\bar{\rho}_h V_b \bar{F}_b} \right) \quad (2.22)$$

Tables 2.1 through 2.5 below summarize the variables, constants, and function contained within Equation 2.22. As depicted in the table columns headed with the term “Derivation”, many of the terms will have to be developed via image analysis or regression analysis. These two analytical tools are described within the subsequent Chapter, which is entirely concerned with the experimental data set. Chapters 4, 5, and 6 are concerned with regression analysis performed upon the blasting, loading, and drilling subsets of the experimental data, respectively. The completed total excavation cost model is then developed within Chapter 7. Estimated cost results for different ground conditions are presented in Chapter 8.

Table 2.1 - Physical Variables within the Excavation Cost Equation

Symbol	Units	Description	Derivation of Variable	Derivation Source
V_{rm}	yd ³	rock mass volume	site data (drill data)	Appendix
H	ft	rock mass bench height	site data (drill data)	Appendix
sd	ft	sub-drill	site data (drill data)	Appendix
s_{rm}	in	characteristic screen size of rock mass "chunks" composing V_{rm}	Image Analysis	Chapter 3
s_f	in	characteristic fragment screen size	Image Analysis	Chapter 3
ρ_b	yd ³ /ton	bank density of the rock mass volume	site data (core test)	Appendix
$\bar{\rho}_h$	yd ³ /ton	average heaped density of the shot rock muckpile	Regression Analysis	Chapter 5
e_m	MJ/lb	mass specific energy of the explosive	site data " shot " records	Appendix

Table 2.2 - Machine Constants within the Excavation Cost Equation

Symbol	Units	Description	Derivation of Constant	Derivation Source
\bar{B}_f	none	average bucket fill factor	Regression Analysis	Chapter 5
k_m	in · hr	loading machine constant	Regression Analysis	Chapter 5
V_b	yd ³	struck bucket volume	site and handbook data	Appendix, References
W_b	in	bucket width	site and handbook data	Appendix, References
\bar{r}_d	ft/hr	average drill penetration rate	Regression Analysis	Chapter 6

Table 2.3 - Cost Constants within the Excavation Cost Equation

Symbol	Units	Description	Derivation of Constant	Derivation Source
$a_d + b_d$	\$/hr	drill owning and operating cost	handbook data, literature, expert opinions	Chapter 7
$a_m + b_m$	\$/hr	machine owning and operating cost	“	Chapter 7
$a_e + b_e$	\$/lb	powder rig owning and operating cost	“	Chapter 7

Table 2.4 - Physical Constants within the Excavation Cost Equation

Symbol	Units	Description	Derivation of Constant	Derivation Source
k_{me}	MJ/ton	explosive specific energy expended in size reduction	Regression Analysis	Chapter 4

Table 2.5 - Functions within the Excavation Cost Equation

Symbol	Units	Description	Derivation of Variable or Constant	Derivation Source
f	none	explosive size reduction function	Regression Analysis	Chapter 4

3. COLLECTION, PROCESSING, ANALYSIS, AND MODELING OF THE EXPERIMENTAL DATA

“ The tractors came over the roads and into the fields, great crawlers moving like insects, having the incredible strength of insects. They crawled over the ground, laying the track and rolling on it and picking it up. Diesel tractors, puttering while they stood idle; they thundered when they moved, and then settled down to a droning roar. Snub-nosed monsters, raising the dust and sticking their snouts into it, straight down the country, across the country, through fences, through dooryards, in and out of gullies in straight lines. They did not run on the ground, but on their own roadbeds. They ignored hills and gulches, water courses, fences, houses. ”

Steinbeck (1939) --- *The Grapes of Wrath*

3.1 The Scope of the Loading Machine Database

A research project funded by the Caterpillar Corporation was undertaken by the University of Arizona Department of Mining and Geological Engineering during the summer of 1995. The original purpose of the work consisted of performing mine site visits to collect data in an attempt to quantify the parameters that affect the performance of loading machines. The work resulted in a rich blasting and loading machine database which contains many different research topics. However, the scope of the original work contract never included any specific in-depth study of the data. This data was subsequently utilized for the excavation cost model that is the subject of this thesis.

3.2 Collection of the Experimental Data

The original raw data collected consisted of video imagery on 8 mm tape substrate,

field notes, and rock samples. The data was obtained at a total of 67 different sites; 62 of these sites were in 13 different open-pit gold and copper mines located in the western United States. The remaining five sites were in three different industrial rock or mineral quarries located in California.

The video data consists of machines loading from shot-rock muckpiles, and also includes images of the vertical faces of the unblasted rock mass in the vicinity of the muckpiles. The field note data consists of information characterizing the type, make, class, and dimensions of the mining machines used at the sites, and includes drilling and blasting data. The field notes also include the results of a visual mapping of rock mass structural features. The rock samples were gathered in order to perform basic laboratory tests that would characterize the strength and hardness of the rocks at the sites.

A preliminary investigation of the data showed that both the blasting patterns and fragment size distributions at the quarry sites differed considerably from the metal mining sites; this data was parsed from subsequent analysis in order to simplify and “normalize” the research towards “hard-rock” metal mining. In addition, hard-rock sites that consisted of fines (tailings, alluvial overburdens, sands, etc.) were excluded, simply because, due to their high proportion of fine material, they could not be reliably analyzed with the image processing software. (The limitations imposed by attempting to process fine particles with the image software are discussed in detail in Section 3.7.2.1.) The exclusion of the sites characterized by fine fragment material resulted in a reduced set of data.

3.3 Description of the Experimental Data

The reduced database includes performance data for a total of 52 open pit Gold and Copper mining sites. The loading machines at 12 of the sites are large (12 yd³) front end loaders. Seven of the sites utilize extra large (21.3 yd³) front end loaders. There are a total of 16 sites with medium, large and extra large cable shovels; the bucket capacities of the machines in these three size classes range from 19 to 22 yd³ , 34 to 41 yd³ , and 56 yd³ respectively. Muck at the remaining 15 sites was loaded with small, medium and large hydraulic shovels; the bucket capacities of the machines in these size classes were 13, 18 to 23.5, and 25 to 27 cubic yards, respectively.

Primarily due to the lack of competent test core, strength data exists for only 39 of these sites. Certain of the sites visited were blasted before shot records were kept, and therefore blast data (pattern, powder factor, etc.) exists for but 36 of these sites. 30 of the sites have both rock strength data and blast data; and rock mass cell still images exist for 20 of these 30 sites.

3.4 Experimental Data Processing

The video images of the loading machines were analyzed to obtain machine cycle time and production information. Video images of the site muckpiles were captured, scaled, and analyzed with particle delineation software to obtain fragment size distribution data. Still images of the rock mass cell faces were analyzed with a “ scanline ” subroutine to obtain pre-blast fracture distribution data. Laboratory strength tests were performed to obtain the geomechanical properties of the rocks at the different sites.

3.4.1 Sampling Theory

It is important to emphasize the difference between the terms “ population ” and “ sample ”. The population is the total set of all possible and potential observations. The sample is the set of discrete observations taken to represent the population. Therefore the nature of the population is estimated by the sample. For a number of sample observations of size n on the random variate x_i , the sample mean is an approximation of the population mean μ :

$$\bar{x} = \frac{1}{n} \sum_{i=1}^n x_i = \hat{\mu} \quad (3.1)$$

Where the $\hat{\mu}$ symbol denotes “ estimator ”. A measure of the spread of the observations about the mean is obtained by summing the squared deviations of the sample observations from the sample mean:

$$v = \sum_{i=1}^n (x_i - \bar{x})^2 \quad (3.2)$$

where v is called “ the sum of the squared deviations ” or else simply the “ variation ”.

The “ biased ” population variance is estimated as:

$$\hat{\sigma}_b^2 = \frac{1}{n} \sum_{i=1}^n (x_i - \bar{x})^2 = S^2 \quad (3.3)$$

The denominator of the above term is called the “ degrees of freedom ” (DOF). For biased sampling the DOF is always equivalent to the total observations. If the mean is considered as an observation, then the sampling is considered “ unbiased ” and the estimated variance of the population becomes:

$$\hat{\sigma}^2 = \frac{1}{(n-1)} \sum_{i=1}^n (x_i - \bar{x})^2 = s^2 \quad (3.4)$$

For this work the unbiased form of sample variance will be used extensively, unless otherwise noted. The population standard deviation can now be estimated with the sample standard deviation:

$$\hat{\sigma} = \sqrt{\frac{1}{(n-1)} \sum_{i=1}^n (x_i - \bar{x})^2} = s \quad (3.5)$$

A useful measure of the relative variability of different sample and populations is the “coefficient of variation” (COV). The COV for a population and for a sample are defined respectively as:

$$\gamma = \frac{\sigma}{\mu} \quad (3.6)$$

$$C = \frac{s}{\bar{x}} \quad (3.7)$$

Until information is obtained concerning how the observations on the population are distributed, the above terms summarize the practical extent of what may be inferred about the population from sampling. Distributions are discussed below in Section 3.7.

3.4.2 Cycle Timing Analysis

All of the excavating machines studied for this work were used to load large off road haul trucks. None of the machines were engaged in “load and haul” mode, whereby the machine would have to load and consequently haul material to a dumping point well

away from the loading location. Machine production (ton/hr) was determined by timing the number of excavation cycles required to load a truck of known tonnage capacity.

With the aid of a cycle timing program written on a personal computer, loading machine movement was observed on the video tape and categorized into one of the following nine cycle categories; load, swing, dump, and return times, truck wait time, clean-up time, move time, repair time, and unknown time.

One goal of this work is to predict machine production in terms of fragmentation, therefore only the first four cycle timing categories listed above are used to characterize machine production. The remaining categories are not related to fragmentation, but rather provide information concerning the utilization and availability of truck fleets, the rates at which loading machines move between loading sites, and machine reliability and maintenance.

The load cycle commenced when the bucket entered the muckpile, and ended when the bucket exited the muckpile. The swing cycle started at the end of the load cycle and finished when the bucket had been positioned over the bed of the haul truck to begin dumping. The dump cycle began at the termination of the swing cycle and was completed when all of the material within the bucket had been dumped into the bed of the haul truck. The return cycle is defined between the end of the dump cycle and the start of the load cycle. The machine cycle time is then defined as the total time required to complete one excavation cycle:

$$t_{tot} = t_l + t_s + t_d + t_r \quad (3.8)$$

where t_l , t_s , t_d and t_r are the load, swing, dump, and return times (seconds), respectively.

3.4.3 Machine Production

Machine productivity was defined on a per truck basis:

$$P_m = \left(\frac{3600 C_{truck}}{t_{truck}} \right) \quad (3.9)$$

where:

$$\begin{aligned} P_m &= \text{loading machine production (tons/hr);} \\ C_{truck} &= \text{rated truck capacity (tons);} \\ t_{truck} &= \text{truck load time (sec), defined over the total number of excavation} \\ &\quad \text{cycles " n " required to serve the truck of rated capacity } C_{truck} : \\ t_{truck} &= \sum_{i=1}^n (t_{tot})_i \end{aligned} \quad (3.10)$$

where t_{tot} is defined according to Equation 3.8 above.

The average total number of trucks filled at the front end loader sites studied was eight; the cable and hydraulic shovel sites were characterized by an average of 11 filled trucks. The total number of excavation cycles at the sites varied widely, and depended on such factors as machine type, bucket size, and truck capacity. The number used to characterize a machine's performance at a site was taken as the average site production (tons/hr), defined for the total number of truck cycles " n ":

$$\bar{P}_m = \frac{1}{n} \sum_{i=1}^n (P_m)_i \quad (3.11)$$

3.4.3.1 Idealizations Regarding Site Average Machine Production

The site average machine production value, as developed in the preceding section, does not account for variation in the:

1. bucket fill factor (thus the quantity of material loaded and carried per excavation cycle will vary);
2. truck fill factor (thus the quantity of material loaded and carried per truck cycle will vary);
3. proficiency and morale of the machine operators;
4. distance between the load and dump locations;
5. maneuvering space available for machine operation;
6. tractive condition of the surfaces upon which the machines operated;
7. climatic conditions within which the machines operated;
8. the mechanical condition (engine hours, tire wear, etc.) of the loading machines.

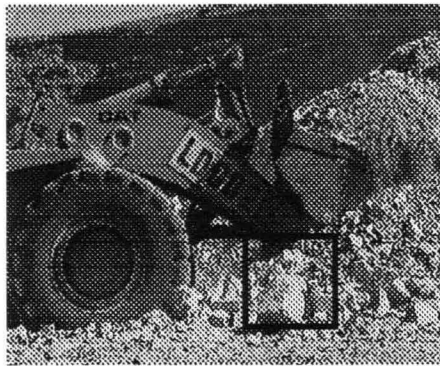
3.4.4 Determination of Rock Fragment Size Distribution

Still images of the fragment muckpiles were processed with the SPLIT image processing program developed at the University of Arizona Department of Mining and Geological Engineering. SPLIT is composed of many specialized subroutines written for an image processing package originally developed by the National Institute of Health for medical research. The methodology used by SPLIT to determine the distribution of fragment sizes is presented on Figure 3.1, and the following list outlines the procedure:

1. An image of the muckpile containing the rock fragments is captured together with an object of known dimension to permit determination of image scale (Plate A);

2. a subsequent “ zoom ” of the muckpile is captured, and the scale of this captured image is determined by cross-reference with an object in the image previously captured (Plate B);
3. the image of Plate B is delineated into discrete fragments and ellipses are fit to each delineated fragment by the N.I.H. image processing software (Plate C);
4. the shape data of the fragments is filtered through a statistical filtering function to determine the physical screen size of the fragments, and a cumulative fragment size distribution is produced for a user specified screen size (“ bin ”) increment (Plate D).

(A) Image Captured and Scaled



(B) Image of Scaled Fragments for Processing



“ Shape ” Output File
for all
Delineated Fragments

Statistical Filtering Function
Determines Fragment Screen Size

Fragment Size Distribution Output



(D) Data Processing Procedures on Ellipse Parameters

(C) Binary Image of Delineated Fragments with a best fitting Ellipse shown.

Figure 3.1 - Methodology for Determination of Fragment Size Distribution

3.4.4.1 The Fragment Shape Descriptors

Typically, thousands of fragments are delineated for each muckpile image set used to characterize a site. If relationships could be discovered between machine production, blasting, and certain variables defined to characterize the 2 dimensional shape of the fragments, then the use of time consuming fragment size processing subroutines could be avoided. A total of 16 descriptors were defined to represent fragment shape. These descriptors were later used for regression analysis performed to characterize machine production as a function of fragment descriptor. The fragment “ shape ” output file produced by the image software includes the following data for each delineated fragment “ i ” :

1. The perimeter (P_i) and surface area (A_i) of the fragment i ;
2. the lengths of the major axis (a_i) and minor axis (b_i) of the best fitting ellipse on the fragment i;
3. the included angle (θ_i) between the major axis of the best fitting ellipse and the image horizontal.

The fragment shape descriptors were defined to consist of the means (\bar{P} , \bar{A} , \bar{a} , \bar{b} , and $\bar{\theta}$ respectively) and standard deviations of each variable listed above. Two additional descriptors were defined to characterize the “ elongation ” and “ roughness ” of the fragments:

$$I_E = \frac{1}{n} \sum_{i=1}^n \left[1 - \left(\frac{b_i}{a_i} \right) \right] \quad (3.12)$$

$$I_R = \frac{1}{n} \sum_{i=1}^n \left\{ 1 - \frac{\left[\left(\frac{A_i}{P_i} \right)_{\text{frag}} \right]}{\left[\left(\frac{A_i}{P_i} \right)_{\text{ellipse}} \right]} \right\} \quad (3.13)$$

where I_E and I_R are dimensionless indices of elongation and roughness, respectively.

Finally, two parameter Weibull frequency distributions were fit to the observed distributions representing the major and minor ellipse axis. (Weibull frequency distributions are discussed in detail in Section 3.7.2) The scale and shape parameters of these Weibull distributions were also included in the fragment shape descriptor set.

3.4.4.2 The Expression for Apparent Screen Size

A detailed development of the statistical filter used for the computation of size distribution is given by Kemeny et al (1993), and will not be repeated here, except for an important expression used to determine a fragment's apparent screen size d_i ;

$$d_i = 1.649 b_i + 0.004 a_i \quad (3.14)$$

where b_i and a_i are the major and minor axis dimensions for the fragment's best fitting ellipse (Section 3.4.4.1 above). But subsequent to his 1993 work, a more accurate expression was developed for fragment screen size (Girdner et al, 1996); and this expression was used to produce the fragment size distributions used in this work:

$$d_i = 1.16 b_i \sqrt{\frac{(1.35 a_i)}{b_i}} \quad (3.15)$$

3.4.4.3 Idealizations Regarding Characterization of the Site Fragment Size Distribution

The machine loading sites are characterized by their fragmentation descriptor set. The variables composing this set consist of fragment shape data and the fragment size distribution derived from the shape data that resulted directly from the image analysis. After the video imagery for a particular site was reviewed, the tape-time locations of superior fragment images were noted down; these images were then subsequently captured, scaled, and processed. Upon the completion of this work, it was discovered that due to either severe dust conditions or the lack of reliable references with which to scale the images, a number of sites could be characterized by no more than a total of 3 discrete muckpile images. Therefore all of the sites were characterized by “ batch ” processing a total of 3 muckpile images. In such a batch processing mode, the computer analyzes the images sequentially, and the final shape and size distribution results are presented as averages, as if one discrete image, totally composed of the fragments contained within the three separate images, had been submitted. The following list summarizes the pertinent information that is not contained within the fragment descriptor set:

1. The fragment images were not sampled in random fashion, rather image quality and the availability of a reliable scale factor was the basis of image selection;
2. for any particular bin size, between-image variations in the fragment sizes observed to lie within the bin were always observed, and the image software characterized this variation with a “ bin coefficient of variation ”, equal to the ratio of the fragment size standard deviation to fragment size mean, for the fragments contained within the bin;
3. the fragment size distributions were derived by utilizing the average bin fragment size from (2) above, because attempting to utilize the bin standard deviation for the determination of size distribution proved problematic;

4. the fragments are derived from explosive blasting, and some blast theories (i.e. Livingston Crater Theory) predict a spatial distribution of fragment sizes, where fines are located close to the charge center and larger fragments are located some proportional function of distance away from the charge;
5. it is inferred that one predictor of loading machine performance is fragment size;
6. if (4) and (5) above are true, then loading machine performance should change according to some function of distance away from what was the former location of the charge;
7. the locations of the loading machines with respect to powder columns were never recorded.

3.4.5 Determination of Rock Mass Size Distribution

The rock mass that was blasted to produce the “ shot-rock ” fragments at the different sites was never monolithic; always these masses were composed of a network of smaller blocks or chunks separated from one another by joints and fractures. Still images of these fracture networks were analyzed with a specialized “ scan-line ” imaging subroutine running within the SPLIT image processing software to obtain information concerning the size distribution of the material bounded by the fractures. These size distributions were subsequently used to help produce an image based blasting model (Chapter 4). The methodology used by SPLIT to determine the distribution of rock mass size is presented on Figure 3.2, and the following list outlines the procedure:

1. A scaled image of an exposed face of the rock mass is submitted for filtering (Plate A);
2. the image is processed through specialized filters to remove shadows and accentuate fractural features (Plate B);
3. four scan lines are superimposed over the filtered image at principal directions (Plate C);

- the intersections of the scan lines and fractures are measured and subsequently counted and sorted to produce the rock mass size distribution (Plate D).

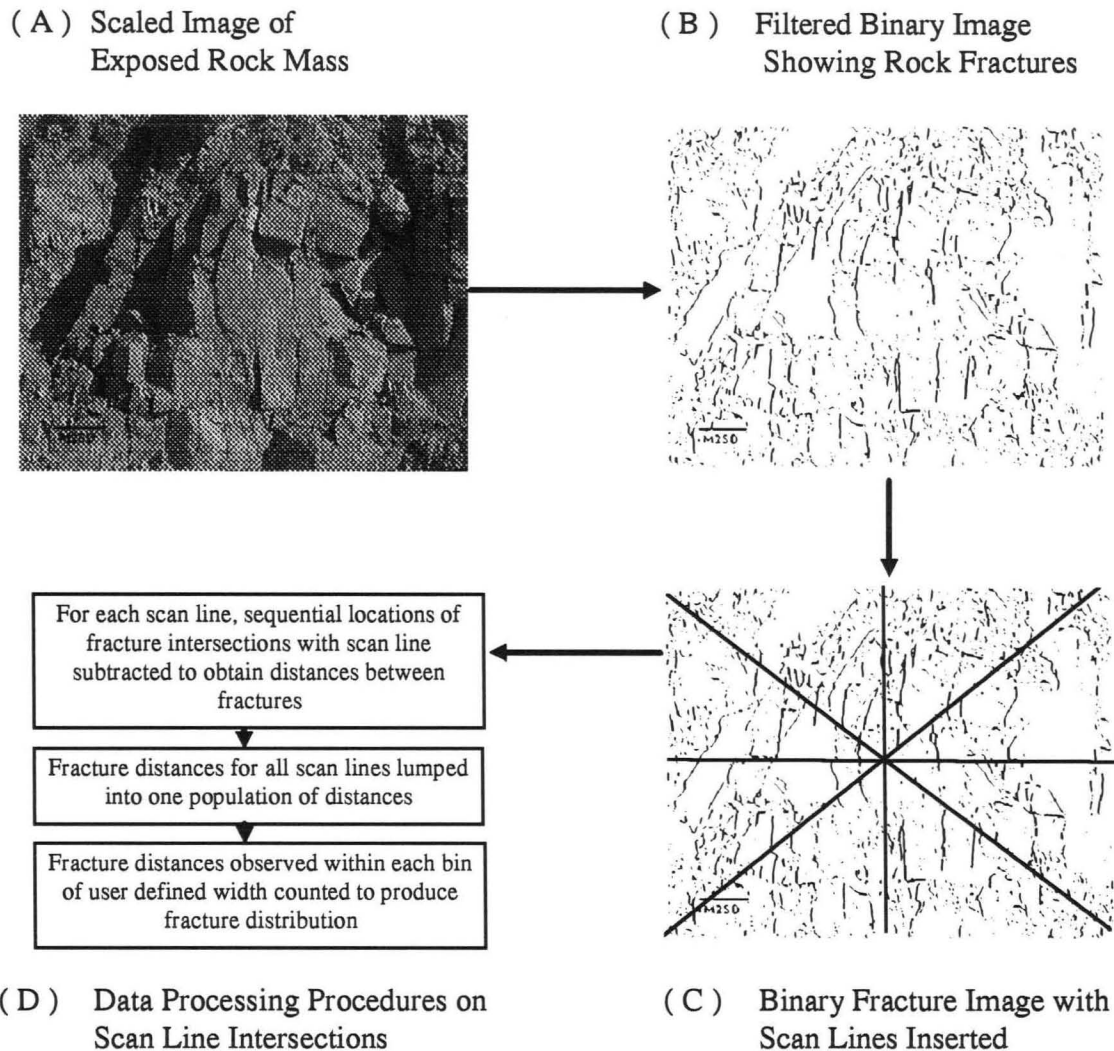


Figure 3.2 - Methodology for Determination of Rock Mass Chunk Size Distribution

3.4.5.1 Idealizations Regarding Characterization of the Site Rock Mass Size Distribution

- Because the principal reason of a site visit was to video tape loading machines, the site rock mass cell still images were never obtained before the rock mass was blasted into fragments; rather the site images were always obtained at a time scale roughly

- concurrent with loading operations at the nearest conveniently exposed rock mass face;
2. usually this face was located on the same bench adjacent to the machine loading site, but occasionally the image was obtained from other bench levels in the vicinity;
 3. the purpose for obtaining the rock mass image was to characterize the size distribution of the rock mass chunks that was blasted to produce the “ shot-rock ” fragments;
 4. thus implicit in (1), (2), and (3) above is an assumption that the rock mass chunks have low spatial variance;
 5. also implicit in the general methodology is an assumption that the fracture information obtained from one exposed face can be extended spatially throughout the entire rock mass volume which is subsequently blasted;
 6. of particular consequence for (5) above is the fact that the scan line program cannot determine the dip of the fracture features with respect to the exposed face;
 7. another consideration of major importance is the fact that the scan-line technique cannot distinguish “ natural ” joints and fractures from those imposed by previous blasts;
 8. blast imposed fractures may in fact extend only a short distance into the subject rock mass;
 9. there will exist many fine fractures upon the surface of the rock mass face that the imaging software cannot resolve.

3.5 Linear Regression Analysis

Linear regression analysis is concerned with establishing whether linear relationships exist between different sets of variables. The basis of linear regression is the method of least variation which is presented in the following section. The least variation method is readily extended towards both linear and non-linear multivariate regression. This basic tool enabled the development of the production and cost models presented within the subsequent Chapters.

3.5.1 The Method of Least Variation

The well known line equation $y = a + bx$ relates two equally numbered sets of x and y data. Because $y = f(x)$, y is called the dependent variable. It is sometimes advantageous to obtain an expression of the form:

$$\hat{y} = a + bx \quad (3.16)$$

where \hat{y} is an estimate of the dependent variable y . If y can be estimated accurately, then the advantage gained is the fact that y will not always have to be observed. The error of this approach can be assessed with the method of least variation, which is sometimes called the method of least squares. The sum of the squared deviations (i.e. the variation) for an entire n -sized set of observed and predicted y variables would be:

$$v = \sum_{i=1}^n [y_i - \hat{y}_i]^2 = \sum_{i=1}^n [y_i - (a + bx_i)]^2 \quad (3.17)$$

If \hat{y} is to be an accurate estimator of y , a and b must be chosen to minimize the variation. The partial derivatives of the variation with respect to the constants are equated to zero to achieve this necessary minimization:

$$\frac{\partial v}{\partial a} = \sum_{i=1}^n y_i - na - b \sum_{i=1}^n x_i = 0 \quad (3.18)$$

$$\frac{\partial v}{\partial b} = \sum_{i=1}^n x_i y_i - a \sum_{i=1}^n x_i - b \sum_{i=1}^n x_i^2 = 0 \quad (3.19)$$

If the x values of the sample $(x_1, y_1) \dots, (x_n, y_n)$ are not all equal, then there exists a unique solution for the two simultaneous equations above. The solution can be presented as [Kreyszig, 1988]:

$$a = \bar{y} - b\bar{x} \quad (\text{y axis intercept}) \quad (3.20)$$

$$b = \frac{\sum_{i=1}^n (x_i - \bar{x})(y_i - \bar{y})}{\sum_{i=1}^n (x_i - \bar{x})^2} \quad (\text{slope}) \quad (3.21)$$

where \bar{x} and \bar{y} are the sample means. If the line equation $y = a + bx$ is manipulated into $a = y - bx$ and equated to Equation 3.20 the geometric definition of slope can be obtained:

$$b = \frac{(y - \bar{y})}{(x - \bar{x})} \quad (3.22)$$

and therefore the regression line $\hat{y} = a + bx$ always passes through the point defined by \bar{x}, \bar{y} , which is sometimes called the “data centroid”.

An example of linear regression can be obtained by applying the method of least variation to determine the best fitting line relating the SPLIT derived fragment size distribution scale parameter to the production of large front end loaders. These loaders are of the same make and type, and they all possess buckets of equivalent width and volume. Figure 3.3 shows the layout of this trend line for large front end loaders operating at 13 different sites:

- The trend line passes through the data centroid, at 1819 tons/hr and 6.80 inches;
- the fragment size distribution scale parameters range from 2 to 22 inches, and the observed loader productions range from 2300 to 1400 tons/hr, respectively;
- the trend line predicts that large loader production will decrease 37.6 tons/hr per inch increase in fragment scale size;
- the loader operating at site Au7SG, situated at 22 inches of scale, exhibits about the same production as the loaders at sites Cu2SG and Au8SC situated at about 5.5 and 7 inches of scale, respectively;

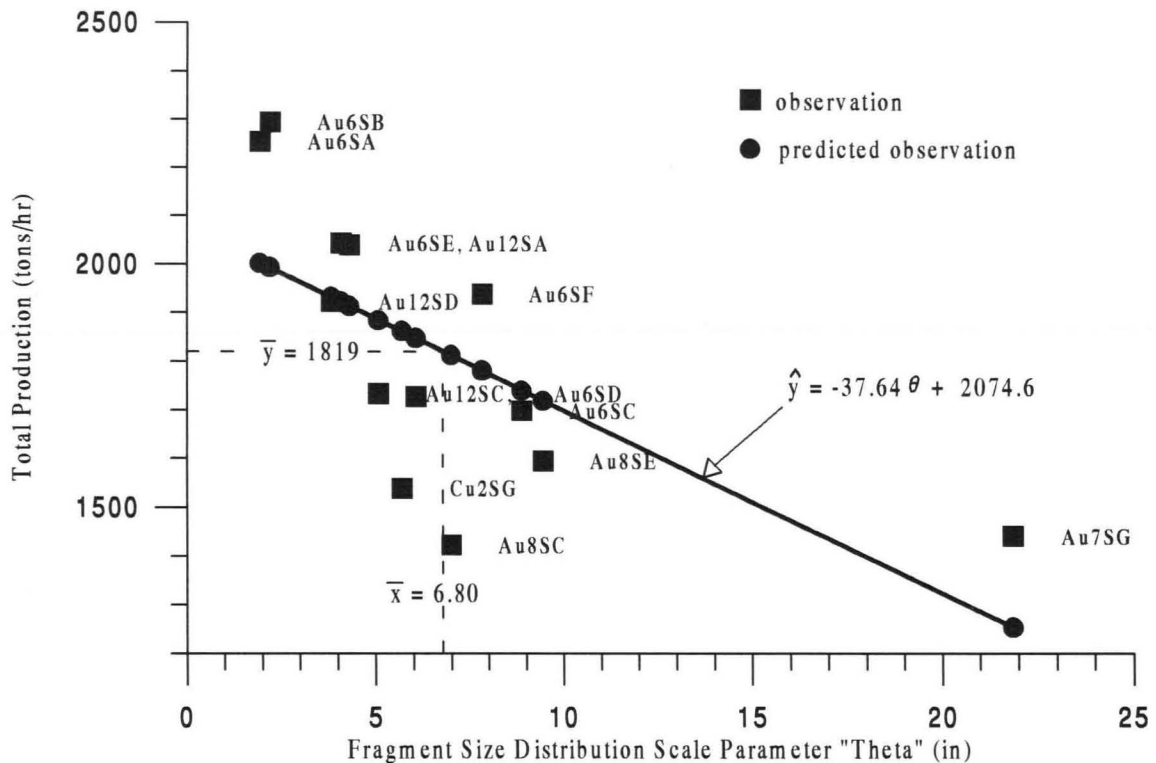


Figure 3.3 - Best Fitting Large Front End Loaders Production Trend Line for Fragment Scale Parameter Observations

- if the site Au7SG loader was parsed from the data, a much higher slope would result, i.e. predicted loader production would be much more sensitive to fragment scale size;
- if the loaders at sites Cu2SG and Au8SC were parsed, then the predicted production line would shift upwards for all of the remaining loaders.

In the next section a simple methodology for assessing the quality of the fit is addressed; then different regressions can be realistically compared.

3.5.2 Assessing the Quality of a Linear Regression

Figure 3.4 shows a hypothetical loader production observation y_i conveniently located near the data centroid:

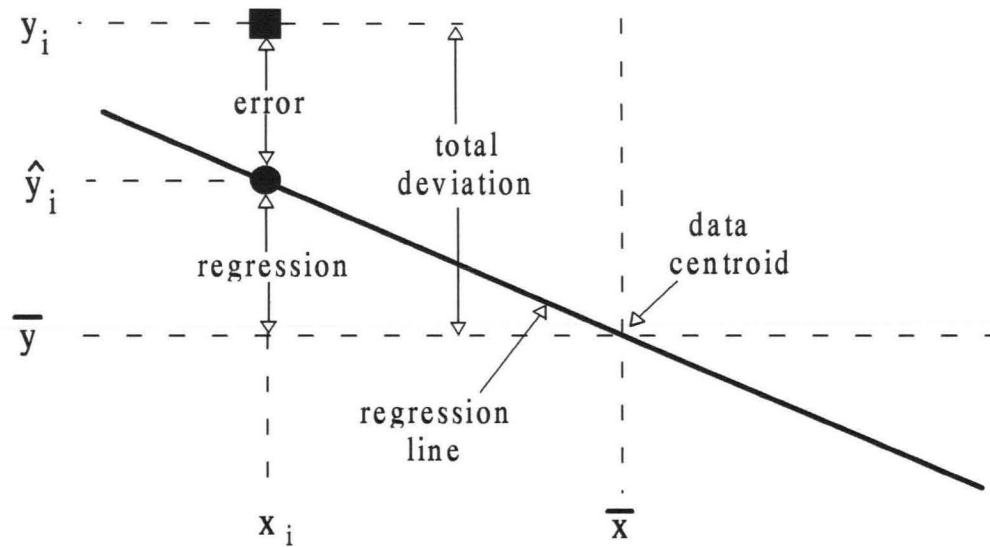


Figure 3.4 - Graphical Depiction of Residual, Regression, and Total Deviation Between an Observed and Predicted Value

The deviation between the observed value y_i and the estimated value \hat{y}_i is called the error. The deviation between the estimated value \hat{y}_i and the mean value \bar{y} is called the regression. The total deviation is the sum of these two terms. Extending these definitions to include all predicted and estimated observations, the variations can be defined as:

$$v_e = \sum_{i=1}^n [y_i - \hat{y}_i]^2 \quad (3.23)$$

$$v_r = \sum_{i=1}^n [\hat{y}_i - \bar{y}_i]^2 \quad (3.24)$$

$$v_{tot} = v_e + v_r = \sum_{i=1}^n [y_i - \bar{y}_i]^2 = \sum_{i=1}^n [y_i - \hat{y}_i]^2 + \sum_{i=1}^n [\hat{y}_i - \bar{y}_i]^2 \quad (3.25)$$

The quality of the fit upon an observations y_i could be assessed by forming proportions one of three ways, relating: 1) Regression deviation to total deviation; 2) error deviation to total deviation; or 3) regression deviation to error deviation. Extending this line of

reasoning to include the entire set of observed and predicted observations, the variation formulas previously presented could be utilized to obtain : 1) Ratio 1 = v_r/v_{tot} ; 2) Ratio 2 = v_e/v_{tot} ; and 3) Ratio 3 = v_r/v_e . The information contained within the three ratios above is redundant, and so typically only the first ratio is utilized to assess the accuracy of a regression. This ratio is called the “ squared correlation ” or sometimes simply “ R^2 ”. R^2 relates the proportion of total variation that can be explained by the linear regression function. The square root of R^2 is called the “ correlation coefficient ”. The correlation coefficient is the measure of linear correlation between the two variables; R values of 0 and 1 signify no linear correlation and perfect linear correlation, respectively. If an R^2 of 0.50 could be considered as average, then the corresponding R would be 0.707. An R^2 value of 0.44 was obtained for the large front end loader production regression, corresponding to an R of 0.66. Therefore:

- Only 44% of the total variation in observed total production for the large front end loaders can be explained by regressing against the scale parameter of the fragment size distributions;
- the remaining 56% of the total variation is caused by “ error ”.

Possible causes for the error include, but are not limited to, the items listed in Section 3.4.3.1 and 3.4.4.3 above. One way to increase the accuracy of the regression would be to parse “ outlier ” observations that contribute significant error. One authority of statistics states that “ A crude rule might be to consider a residual a possible outlier if is more than 1.5 or 2 standard deviations away from the zero mean. ” [Morrison, 1983]. The standard deviation of the sampled error can be readily calculated from Equation 3.5 as:

$$s_e = \sqrt{\frac{\sum_{i=1}^n [y_i - \hat{y}_i]^2}{n-2}} \quad (3.26)$$

where two degrees of freedom are subtracted from the denominator because two bits of information have been consumed determining the regression constants of the \hat{y} estimator.

Dividing each observed error deviation by s_e normalizes the error deviations (residuals) into units of s_e . The resulting residual scatterplot is shown on Figure 3.5.

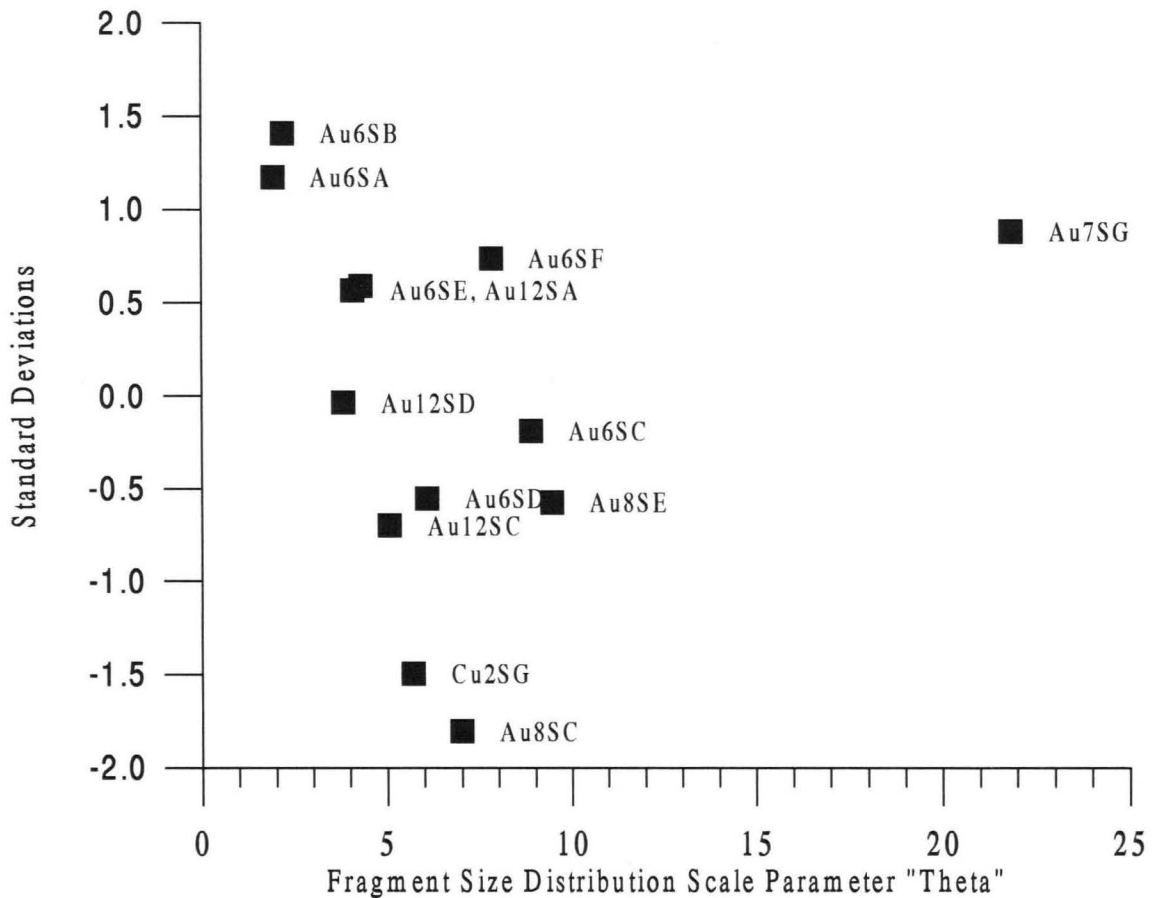


Figure 3.5 - A Residual Scatterplot for the Large Front End Loaders

Figure 3.5 shows that sites Cu2SG and Au8SC are both located between 1.5 and 2

standard deviations from zero. Thus by parsing these two observations, production would have a higher linear correlation to fragment scale size. But there exist a total of 19 other descriptors that characterize the fragments (Section 3.4.4). For example, higher R^2 values were obtained simply by utilizing the modal (most probable) size of the fragments (a closed form expression for the modal size is presented as Equation 3.34). Also, multivariate production models exhibiting much higher R^2 values than the current example were subsequently developed, but before this work is discussed, the following statements are necessary:

1. Linear regression is a data analysis technique concerned with composing the most accurate linear relationship between different sets of sample observations;
2. linear modeling is concerned with the most accurate linear relationship between different sets of populations;
3. moving from observations to populations requires inference;
4. inference involves error;
5. error is best described with statistics;
6. statistics requires theoretical frequency distributions.

3.6 Statistics and the Linear Model

The linear regression equation $\hat{y} = a + bx$ presented in the previous section is very similar to the form of an equation representing a linear model:

$$Y = \alpha + \beta X + E \quad (3.27)$$

where the model now relates the populations from which a set of observations $(x_1, y_1) \dots, (x_n, y_n)$ are sampled, and E represents the error population. It is advantageous to be

able to model the dependent Y population as some function \hat{Y} acting upon the X population. If the α and β model parameters are conveniently estimated with the regression parameters obtained from sampled data, then \hat{Y} becomes equal to $a + bX$, and the linear model is approximated as:

$$\varepsilon = Y - \hat{Y} \quad (3.28)$$

where ε is the sampled estimate of the population error. The estimated standard deviation of the error population becomes:

$$\hat{\sigma}_\varepsilon = \sqrt{\frac{\sum_{i=1}^n [y_i - \hat{Y}_i]^2}{n-2}} \quad (3.29)$$

The principal aim of an accurate linear population model is the appropriate selection of the α and β model parameters such that σ_ε will be minimized. But in the material above, the sample regression parameters a and b have already been utilized to estimate α and β . It is therefore inferred that $\alpha = a \pm f_1(\sigma_\varepsilon)$, and $\beta = b \pm f_2(\sigma_\varepsilon)$, where f_1 and f_2 are some functions defining the distribution of probability for the error population E . Linear modeling is vastly simplified if the error population is modeled according to the Normal frequency distribution.

3.7 Theoretical Frequency Distributions

“ There is, in principal, an infinite number of theoretical frequency distributions, many of which may under some conditions have frequency curves that look alike... there is no way to find a theoretical frequency distribution that is a unique representation of a set of actual observations. ” Koch and Link (1971) --- *Statistical Analysis of Geological Data*

A theoretical frequency distribution is a mathematical representation of an observed frequency distribution. The following theoretical frequency distributions were applied to the experimental data:

1. The Normal distribution was used to model sampling error and machine cycle time distributions;
2. the Weibull distribution was used to model the size distributions of rock mass and the fragment size distributions that resulted from blasting the rock mass;
3. the F distribution (Fisher-Snedecor form) was used to test hypothetical arguments for regression models, and for deciding whether different sets of sampling observations are part of the same population;
4. Student's t distribution was used to establish confidence intervals for population means and to test arguments for multivariate regression models.

The following sections contain examples of how the distributions were used in the data analysis. The first three distributions listed above utilize two different parameters to account for distributive scale/location and shape aspects; Student's t distribution utilizes only a single shape parameter. For the sake of brevity, parameter estimation techniques will not be included herein; except for a graphical technique for obtaining the Weibull parameters, presented in Section 3.7.2.2.

It is important to define the meaning of the following often misunderstood terms related to the dispersion of a frequency distribution about certain "central values" of its horizontal x-variate, or range:

- a) The " mean " is the arithmetic average of the observed range values;
- b) the " mode " is the range value at which there exists the most probable observation;
- c) the " median " value of the range has a 0.50 probability of being exceeded by any observation.

The mean, mode, and median values of the Normal distribution are equal. By utilizing the appropriate distribution parameters, all of the other distributions listed above can be made to approximate the symmetric “ bell ” shaped form of the Normal distribution. But it is important to stress that the best fitting models to certain observed frequency distributions set forth in the examples below are not Normal, rather they are unsymmetric, or “ skewed ”. For skewed distributions, the mean, median, and modal values can differ considerably.

3.7.1 The Normal Distribution

Machine cycle times were studied with different theoretical distributions, including the Normal, the Weibull, and the Gamma. The quality of the model “ fit ” was ranked by observing the sum of squared differences between the observed data and the theoretical model. Modeling observed cycle time data with Normal distributions always resulted in the lowest sum of squares values.

The frequency distribution (sometimes called the probability density function) for the Normal distribution is defined as [Shigley, 1977]:

$$f(x) = \frac{1}{\sigma \sqrt{2\pi}} \exp \left[\frac{-(x - \mu)^2}{2\sigma^2} \right] = \quad N : \mu , \sigma \quad (3.30)$$

where:

- x = the x-variate;
- μ = the location parameter (population mean);
- σ = the scale parameter (population standard deviation).

An analytic integration of Equation 3.30 is not possible; instead the cumulative distributions can be obtained by numerically integrating the observed or modeled frequency data as shown in the following example.

Figure 3.6 shows the forms of the observed and modeled frequency and cumulative frequency distributions for a population of 21 machine load cycle times for a large front end loader operating at site Au6SA (Gold Mine Six, Loading Site A). Estimators for the distribution parameters (μ and σ) were obtained from the proprietary machine data base. This same data showed that the bucket capacity of this machine was 11.7 yd³ (struck), and the heaped density of the blasted rock at the site averaged about 1.54 yd³/ton; thus 18 tons of shot rock would be removed from the site by each full bucket during the machine dig cycle. Referring to Figure 3.6:

- The continuous Normal model of the observed frequency (●) is considerably smoother than the “ spike-like ” frequency polygon representing the actual observed data (O);
- the mean, median, and modal values (read on the cumulative curves at the 50th percentile value) for the observed and modeled data are virtually identical and correspond to a load cycle time of 9.6 seconds;
- between the 50th and 95th percentile values (right hand scale) of load cycle time, there is little difference between the observed (◇) and modeled (◆)cumulative load cycle times;
- between the 10th and 50th percentile values, the cumulative model (◆) predicts lower load cycle times than those actually observed (◇), because of four extremely short load cycle time observations (O) occurring at 2, 3, 4, 5, and 6 seconds, respectively.

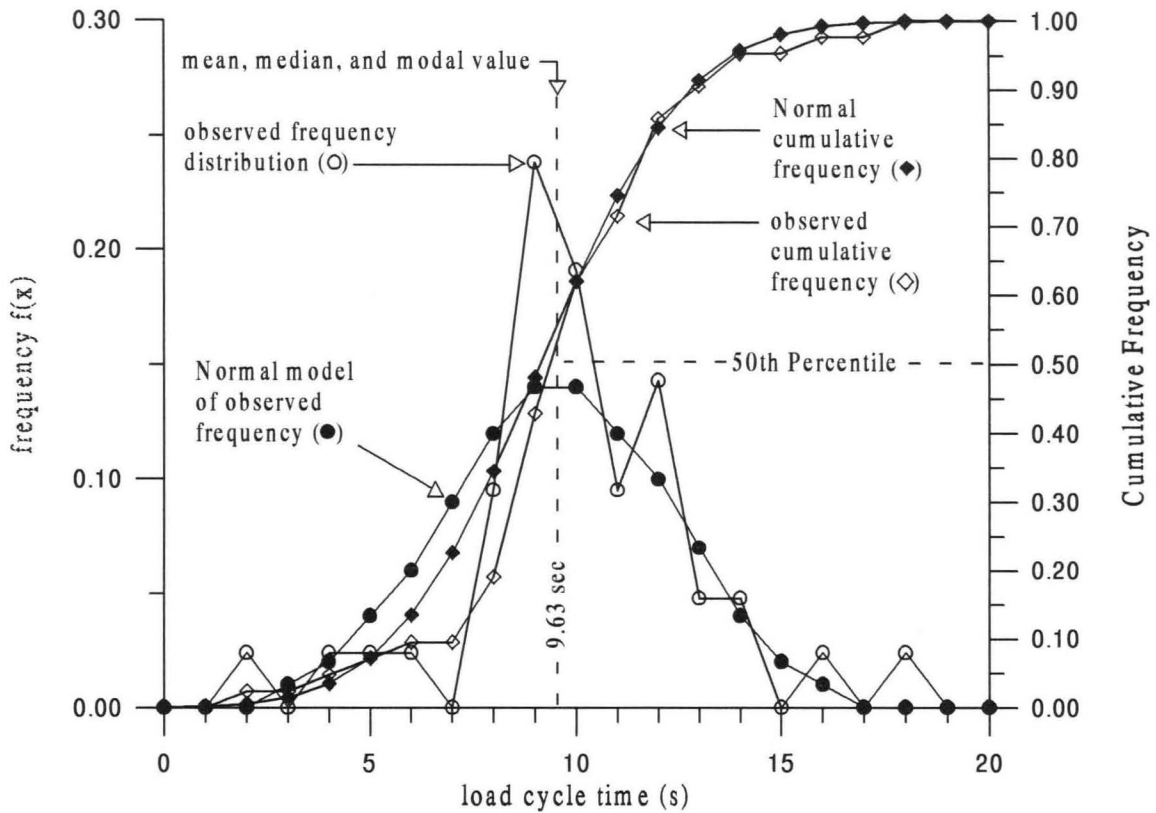


Figure 3.6 - Observed and Normal Models of Frequency Distributions for the Load Cycle Time of a Large Front End Loader Operating at Site Au6SA

Although short cycle times are particularly important for maximizing machine production, the cause of the observed short cycle times cannot be inferred from the frequency plots.

3.7.2 The Weibull Distribution

This distribution was used by the Swedish scientist Waloddi Weibull to model the strength-volume relationship for rocks [Weibull, 1939]. A cumulative form of the Weibull distribution was used by American researchers to model the size distributions of powdered coal [Rosin and Rammler, 1933]; the “Rosin-Rammler” distribution has

subsequently become a popular standard used to characterize particle sizes resulting from crushing, grinding, and milling processes. The distribution was by the Siberian Scientist V. Kuznetsov [Kuznetsov, 1973] as a tool in the analytical development of an expression for determining the mean fragment size that would result from blasting a rock mass. The distribution was first used to model complete rock fragment size distributions resulting from blasting by the English Mining Engineer C. Cunningham [Cunningham, 1983] , who expanded upon Kuznetsov's earlier work. (The work of Kuznetsov and Cunningham is covered in more complete detail in Chapter 4.)

The Weibull probability distribution function is [Evans et al., 1993]:

$$f(x) = \frac{n}{\theta} \left(\frac{x}{\theta} \right)^{n-1} \exp \left[- \left(\frac{x}{\theta} \right)^n \right] = W : n, \theta \quad (3.31)$$

where the x -variate can range from 0 to infinity; n = the distribution shape parameter

($n \geq 0$); and θ = the distribution scale parameter ($\theta \geq 0$). Analytic expressions for the

mean, median, and modal values of the Weibull probability distribution are:

$$\text{mean} = \theta \Gamma \left(1 + \frac{1}{n} \right) \quad (3.32)$$

$$\text{median} = \theta (\ln 2)^{1/n} \quad (3.33)$$

$$\text{mode} = \theta \left(\frac{n-1}{n} \right)^{1/n} \quad (3.34)$$

where Γ is the Gamma function. The cumulative form of the distribution can be obtained in closed form by integrating Equation 3.31 with respect to x :

$$F(x) = 1 - \exp \left[- \left(\frac{x}{\theta} \right)^n \right] \quad (3.35)$$

where $F(x)$ is the probability ($0 \leq P \leq 1$) that the x variate takes a value less than or equal to x . The distribution scale parameter θ is sometimes called the “characteristic” value [Evans et al., 1993]. If x is equated to θ in Equation 3.35, then:

$$F(x) = 1 - \exp(-1) = 0.632 \quad (3.36)$$

for any value of shape parameter (“ n ”) greater than zero. Thus the scale parameter value of the Weibull probability distribution is always approximately equivalent to the 63rd percentile value of the Weibull cumulative distribution. The scale parameter serves as a measure of the central tendency of the data, much like the mean value of the Normal distribution.

Figure 3.7 shows the observed fragment frequency distribution for Site Cu2SD, together with the form of the best fitting Weibull distribution model. Referring only to the form of the observed frequency distribution (O) on Figure 3.7:

- The x variate of the distribution represents fragment (screen) size (inches), and each curve symbol represents the frequency, or probability of observation, for fragment size;
- fragment sizes at this site range from about a half inch to 28 inches;
- the fragment sizes have been grouped into class widths, or “bin sizes” of width 0.50 inch;
- a “step-wise” shift in the observed fragment frequency occurs between the fragment class sizes of 7.5 and 8.0 inches.

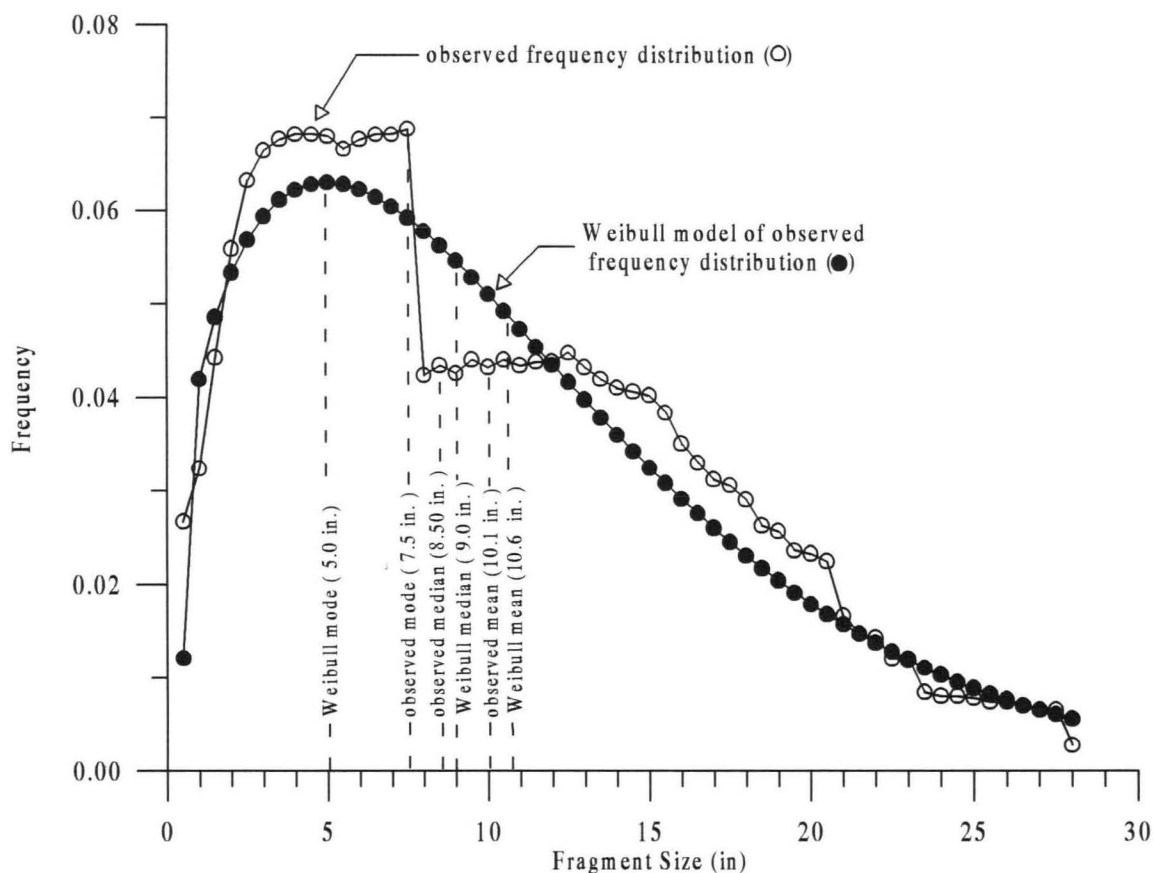


Figure 3.7 - Observed and Weibull Model Frequency Distributions for Fragment Size at Site Cu2SD

3.7.2.1 Step-wise Frequency Shifts in the Observed Frequency Data

Step-wise frequency shifts associated with a particular fragment size that is located in the lower region of the fragment size range are characteristic of all of the observed frequency distributions used to help characterize site fragment size for this thesis. These frequency shifts are a relic of the image processing software, and the reasons they occur are set forth in the following list. The words in parenthesis denote the specific jargon used by image processing personnel utilizing the SPLIT fragment delineation system:

1. The image processing software has a lower bound limit (called the “ cut-off ” size) at which it can resolve a fragment;
2. the resolution limit of the imagery changes according to the overall scale of the image, the intensity of the incident light source, and the focus of the image;
3. thus the cut-off size can vary between different images;
4. below the cut-off size, the computer does not know the exact nature of the fragment size distribution;
5. the invisible fragment material below the cut-off is called the “ fines ”;
6. a user input to the image processing software is a percent solid composition estimate (called “ % fines ”) of the material below the cut-off, i.e. what percent of this fragment material are fines from which the percent “ interstitial void ” can be determined;
7. the software then utilizes an interpolating function to obtain the form of the distribution below the cut-off fragment size;
8. the feedback used by the image processor to check the % fines estimate is not the form of a screen plot of the frequency distribution, but rather the form of a screen plot of the cumulative fragment size distribution;
9. a pronounced “ knee ” structure on this cumulative distribution curve indicates a gross error in the % fines or cut-off) estimate;
10. even a small knee on the cumulative distribution will shows up as a pronounced step on the frequency distribution.

The cumulative form of the fragment size distribution will be discussed subsequently; but first the Weibull model of the fragment size frequency distribution will again be discussed.

Referring back to Figure 3.7:

- The Weibull model of the observed frequency is skewed (tailed) towards the right; and therefore the mean, median, and modal values of this distribution will differ. The following table presents these values for both the observed and modeled distributions presented on Figure 3.7, and shows that the largest difference occurs at the mode, where

the observed fragment size is 2.5 inches larger than the modeled size.

Table 3.1 - Comparison of Results for Observed and Modeled Fragment Size Frequency Distribution for Site Cu2SD

Fragment Frequency Distribution	Modal Fragment Size (in)	Median Fragment Size (in)	Mean Fragment Size (in)
Observed	7.5	8.5	10.1
Weibull Model	5	9	10.6

Figure 3.8 includes some of the same information as Figure 3.7, but now includes the

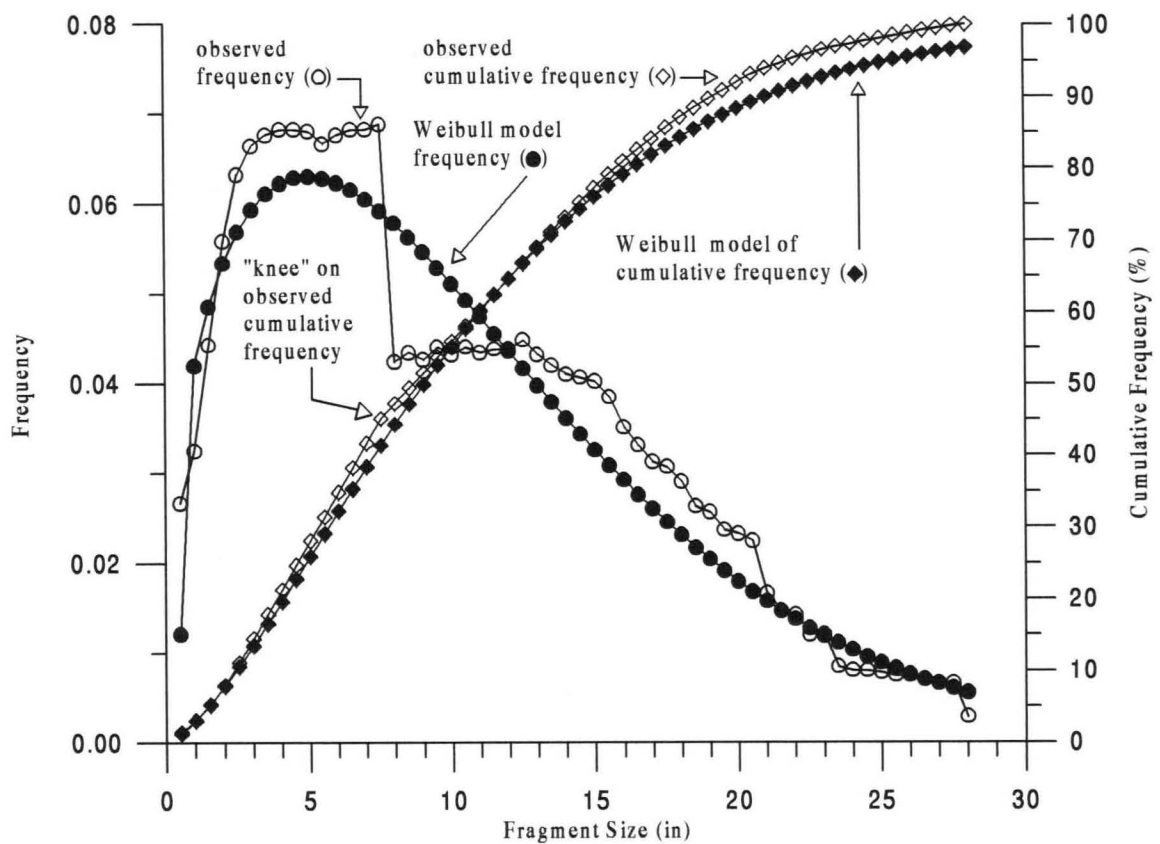


Figure 3.8 - Observed and Modeled Frequency and Cumulative Frequency Distributions for Fragment Size at Site Cu2SD

cumulative forms of the fragment size frequency distributions for both the observed data and the Weibull model. Referring to Figure 3.8:

- The observed cumulative frequency distribution exhibits a small “knee” structure corresponding to the step-wise frequency shift in the observed frequency distribution;
- the Weibull cumulative frequency model is a good approximation to the observed data for all cumulative frequency values below the 75th percentile;
- if the Weibull cumulative frequency model is used above the 75th percentile, larger than observed fragment sizes will result.

3.7.2.2 The Rosin-Rammler Particle Size Distribution

The traditional method for the determination of particle size is test sieving. Sieving consists of passing a mass composed of a range of particle sizes through a series of nested screens, each of incrementally smaller aperture size. After all the subject mass has passed into the nest, the mass trapped upon each of the screens is weighed; these weights can then be used to produce a plot of screen size versus mass percent. Equation 3.35 from the previous section, which described the cumulative form of the Weibull distribution, and defined the probability that the particle size variate takes a value less than or equal to x , is here repeated as:

$$F(x) = 1 - \exp \left[- \left(\frac{x}{\theta} \right)^n \right] \quad (3.37)$$

But for the test sieving methodology described above, the concern is not with particles that have passed a given screen size, but rather with the particles retained on the screens.

In classical statistics, this probability value is obtained with the “survival” function

[Evans et al, 1993]. For the Weibull distribution, the survival function defines the probability that the particle size takes a value greater than x is defined as:

$$S(x) = 1 - F(x) = \exp \left[- \left(\frac{x}{\theta} \right)^n \right] \quad (3.38)$$

Since the goal is to determine the percent mass retained, both sides of Equation 3.38 are multiplied by 100:

$$100 - 100 F(x) = 100 \exp \left[- \left(\frac{x}{\theta} \right)^n \right] \quad (3.39)$$

Rearranging and taking the Naperian logarithm of each side results in:

$$\ln \left(\frac{100}{100 - 100 F(x)} \right) = \left(\frac{x}{\theta} \right)^n \quad (3.40)$$

then taking the base 10 logarithm of each side results in:

$$\log \left(\ln \left(\frac{100}{100 - 100 F(x)} \right) \right) = n \log x + \log \left(\frac{1}{\theta} \right)^n \quad (3.41)$$

which has a linear form ($y = mx + b$); thus by plotting the left hand side of Equation 3.41 against the logarithm of particle size, the slope of the line, and hence the Weibull shape parameter (“ n ”), can be determined by graphical interpolation. The Weibull scale parameter readily determined by noting that when the left hand side of 3.41 is equated to zero, $\theta = x$. Figure 3.9 shows how the application of Equation 3.41 upon the observed fragment size data for site Cu2SD (previously presented in both frequency and cumulative frequency form on Figure 3.8) results in a line. Given that rock particles produced by blasting, crushing, and grinding can be characterized with the Weibull distribution, then

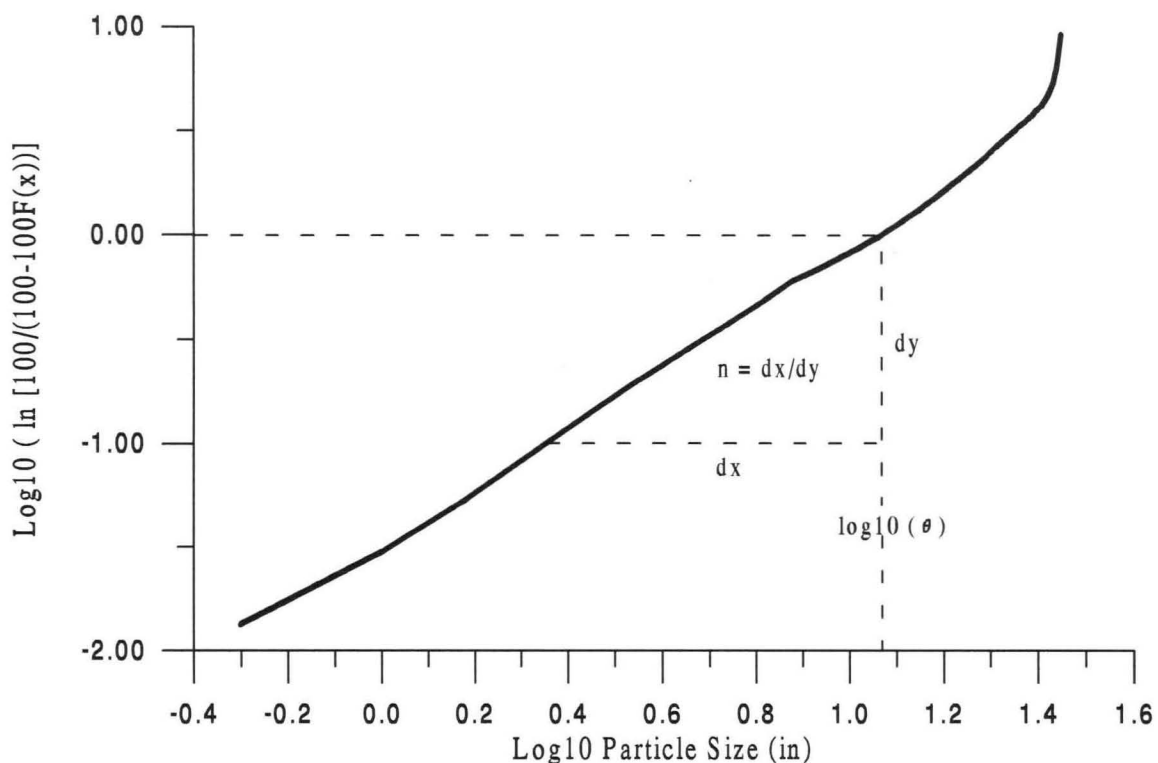


Figure 3.9 - Graphical Determination of Weibull Scale and Shape Parameters for Site Cu2SD

the following list explains the extreme usefulness of Equation 3.41 for test sieving purposes:

1. The Weibull cumulative distribution, when modified into the form represented by Equation 3.41, will plot as a line;
2. two points define a line;
3. therefore a sieving test consisting of a minimum of two sieves could be used to produce a particle size distribution;
4. thus a particle size distribution can be obtained via a sieving test much more quickly.

These simple observations suggest imaging algorithms that could produce size distributions at an extremely rapid rate; undoubtedly other researchers have investigated this possibility. In any event, the Rosin-Rammler Equation is often presented in the

following form [Wills, 1992]:

$$100 - P = 100 \exp(b x^n) \quad (3.42)$$

where P is the “ cumulative undersize ” (%), and b and n are “ constants ”. Following the same methodology used to reduce Equation 3.39, Equation 3.42 can be rewritten as:

$$\log \left(\ln \left(\frac{100}{100-P} \right) \right) = n \log x + \log b \quad (3.43)$$

Now comparing 3.43 to Equation 3.39 (repeated directly below as 3.44), the function P

$$\log \left(\ln \left(\frac{100}{100-100F(x)} \right) \right) = n \log x + \log \left(\frac{1}{\theta} \right)^n \quad (3.44)$$

describing the “ cumulative undersize ” is equivalent to the Weibull cumulative distribution function F expressed in % units (100 F(x)). Furthermore, the Rosin-Rammler constant “ b ” can be expressed as a function of the Weibull scale and shape parameters. Thus the Rosin-Rammler distribution is merely a disguised form of the Weibull cumulative frequency distribution.

3.7.3 The F Distribution (Fisher-Snedecor Form)

The probability density of the F distribution is given by [Evans et al., 1993]:

$$f(x) = \frac{\Gamma \left[\frac{(\nu + \omega)}{2} \right] (\nu / \omega)^{(\nu/2)} x^{(\nu-2)/2}}{\Gamma \left(\frac{\nu}{2} \right) \Gamma \left(\frac{\omega}{2} \right) \left[1 + \left(\frac{\nu}{\omega} \right) x \right]^{(\nu+\omega)/2}} = \mathbf{F: \nu, \omega} \quad (3.45)$$

where:

Γ = the Gamma function;
 ν, ω = shape parameters typically referred to as “degrees of freedom”.

The F distribution function is complicated, but it can be easily programmed into a personal computer to investigate the following relationship for two independent samples of normally distributed observations [Evans et al., 1993]:

$$\frac{\frac{n_1 S_1^2}{(n_1 - 1)\sigma_1^2}}{\frac{n_2 S_2^2}{(n_2 - 1)\sigma_2^2}} \sim F : n_1, n_2 \quad (3.46)$$

where n_1, n_2, S_1^2, S_2^2 , and σ_1^2, σ_2^2 are the number of observations for the two sample groups, the biased variances of the sample groups, and the variances of the sample populations, respectively. If the population variances of the two sample groups are equal, then the above relationship can be reduced to:

$$\frac{s_1^2}{s_2^2} \sim F : n_1, n_2 \quad (3.47)$$

and the ratios of two independent unbiased sample variances taken from the same population have a probability density distributed as an F function. This relationship is one of the most useful in all statistics [Kock and Link, 1971] and is the basis of analysis of variance (ANOVA). The following example outlines the use of ANOVA towards an investigation of rock strength sample data.

3.7.3.1 The Analysis of Rock Strength Variance

The rocks at a total of 39 sites can be characterized with uniaxial compressive strength. 22 of these strengths represent samples obtained at Gold mining sites; the remaining 17 represent rock strengths at sites within Copper mines. The experimental strength data is presented on Table A2 within the Appendix. Rock mass strength is a fundamental parameter of the fragmentation modeling that will be subsequently presented in Chapter 4. The models were developed by regression analysis (Section 3.5), and regression analysis is principally concerned about relationships between average values. Thus before the model was developed, a “ fuzzy ” research hypothesis was formulated as: “ Are the rocks at Copper mines from the same strength population as the rocks at Gold mines? ” If not, then separate fragmentation models will have to be developed. From the rock strength data of Table A2, a sample mean of 14,071 p.s.i. is readily calculated for the Gold mine sites, and 10,849 p.s.i. for the Copper mining sites, so the rocks at Gold mines exhibit about 30% more average strength than the rocks at Copper mines. But the sample sizes are not equal. To determine whether these strengths are in fact from the same population, a research model is formulated as follows:

1. Hypothesis: The two population means for rock strength are equal for Gold and Copper mining sites; $H : \mu_{Au} = \mu_{Cu}$.
2. Alternate hypothesis: $AH: \mu_{Au} \neq \mu_{Cu}$.
3. Assumptions: Two groups of randomly selected strength samples obtained from normally distributed populations.
4. Risk Level: (Probability of rejecting a true hypothesis H) --- to be subsequently determined.

ANOVA is utilized to address this problem by: 1) Assuming all of the rock strength

observations are from the same population; 2) obtaining two independent estimates of rock strength population variance; 3) forming the ratio of the two population variances; and 4) computing the F probability distribution function value corresponding to the variance ratio value. The methodology of steps 2 through 4 are outlined below.

Obtaining independent estimates of population variance first involves the determination of the total variation of the two groups of observations representing the population. The total variation may be defined as:

$$V_{\text{tot}} = \sum_{i=1}^{n_1} (x_i - \bar{x}_g)^2 + \sum_{i=1}^{n_2} (x_i - \bar{x}_g)^2 = \sum_{j,i} (x_{ji} - \bar{x}_g)^2 \quad (3.48)$$

where the subscript j denotes the group, and i denotes the observation within the group; \bar{x}_g represents the “grand mean” (arithmetic average) of the observations within the two sample groups:

$$\bar{x}_g = \frac{\sum_{i=1}^{n_1+n_2} x_i}{n_1 + n_2} = \frac{n_1 \bar{x}_1 + n_2 \bar{x}_2}{n_1 + n_2} \quad (3.49)$$

The right hand side of 3.48 is equivalent to:

$$\sum_{j,i} (x_{ji} - \bar{x}_g)^2 = \sum_{j,i} (x_{ji} - \bar{x}_j)^2 + \sum_{j,i} (\bar{x}_j - \bar{x}_g)^2 \quad (3.50)$$

expanding the terms on the right hand side of the above equality results in:

$$\sum_{j,i} (x_{ji} - \bar{x}_g)^2 = \left[\sum_{i=1}^{n_1} (x_i - \bar{x}_1)^2 + \sum_{i=1}^{n_2} (x_i - \bar{x}_2)^2 \right] + \left[n_1 (\bar{x}_1 - \bar{x}_g)^2 + n_2 (\bar{x}_2 - \bar{x}_g)^2 \right] \quad (3.51)$$

The first quantity on the right hand side of the above equality is called the “within group variation” (or the “within group sum of squares”) and the final quantity is the “between

group variation ” (or the “ between group sum of squares ”). The total variation of the observations within the two sample groups (Equation 3.48) can now be expressed as :

$$V_{\text{tot}} = V_w + V_b \quad (3.52)$$

Transforming the above expressions into unbiased variance form (Section 3.4.1) results in:

$$\frac{\sum_{j,i} (x_{ji} - \bar{x}_g)^2}{(n_1 + n_2 - 1)} = \frac{\left[\sum_{i=1}^{n_1} (x_i - \bar{x}_1)^2 + \sum_{i=1}^{n_2} (x_i - \bar{x}_2)^2 \right]}{(n_1 + n_2 - 2)} + \frac{\left[n_1 (\bar{x}_1 - \bar{x}_g)^2 + n_2 (\bar{x}_2 - \bar{x}_g)^2 \right]}{(j-1)} \quad (3.53)$$

where the denominators of the terms on the right of the equality are called the “ within group degrees of freedom ” and the “ between group degrees of freedom ” respectively.

The previous equation can be expressed as the following simplified representation:

$$s_{\text{tot}}^2 = s_w^2 + s_b^2 \quad (3.54)$$

The variances to the right of the above equality can now be divided and the variance ratio relationship (Equation 3.47) can be utilized:

$$\frac{s_b^2}{s_w^2} \sim F : j - 1, n_1 + n_2 - 2 = F : 1, 37 \quad (3.55)$$

and the between to within group variance ratio of the two sample groups representing 22 Gold sites and 17 Copper sites is distributed as an F probability function with 1 and 37 degrees of freedom. Figure 3.10 shows the graphical layout to explain how the F distribution is used to assess the risk associated with the hypothesis that the population

means of Gold and Copper site rock strength are equal.

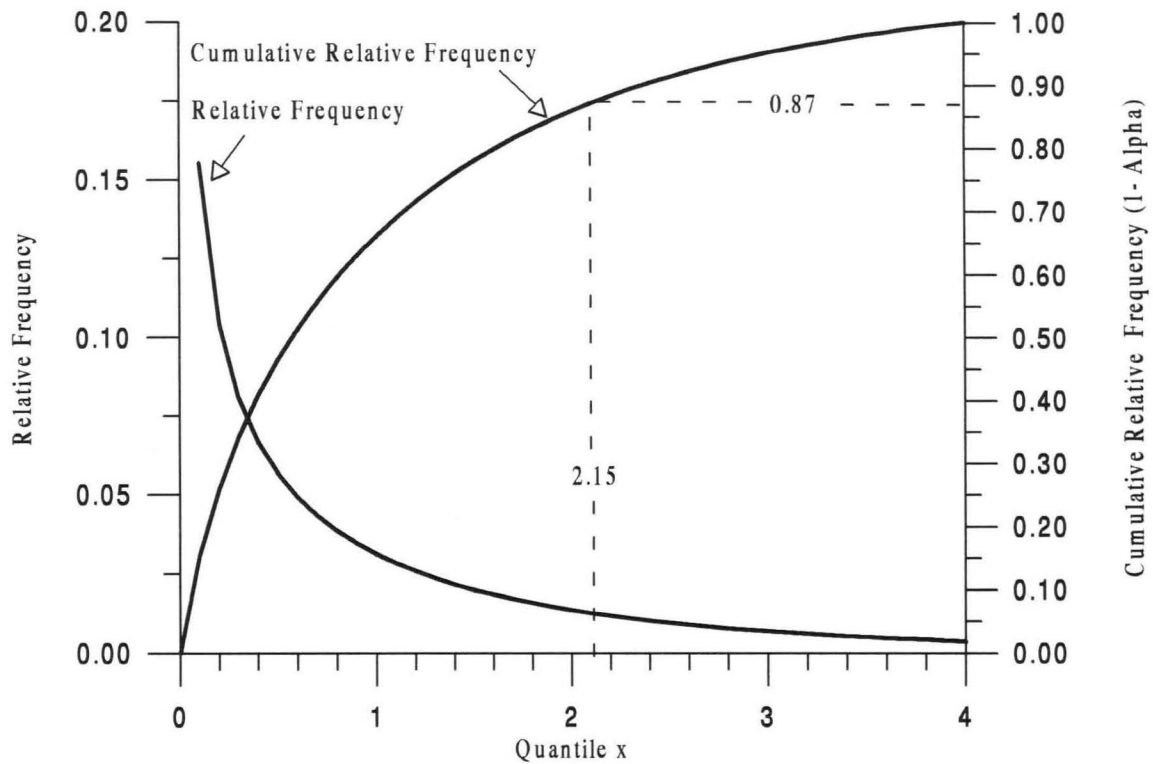


Figure 3.10 - F distributions with 1 and 37 degrees of freedom for the Graphical Determination of Risk Level for Analysis of Variance on Site Rock Strengths

The relative frequency values shown were obtained by utilizing Equation 3.45 with 1 and 37 degrees of freedom; the frequency curve was subsequently numerically integrated to obtain the cumulative probability values. Equation 3.47 was utilized to determine an F-ratio value of 2.15 for the data. Now referring to Figure 3.10:

- 2.15 corresponds to cumulative frequency of 0.87, or an α (risk level) of 0.13, or 13 %;
- so 87% of the time, the variance ratio of population rock strength will be less than or equal to a value of 2.15;

- this corresponds to an 87% certainty that the hypothesis H: $\mu_{Au} = \mu_{Cu}$ is the correct decision;
- the risk of incorrectly deciding for the alternate hypothesis AH: $\mu_{Au} \neq \mu_{Cu}$ of unequal means is 13%.

This result is peculiar in consideration of the fact that Gold and Copper deposits are hosted by different types of rock. The Gold mines are predominantly Carlin type replacement deposits, where the ore is hosted in silica flooded carbonate rich rocks that were originally limestones; certain other of the Gold mines appear to be of epithermal vein type, where the ore occurs in silica rich veins and silica flooded stockworks cutting through piles of older volcanic rocks. The Copper mines are always massive porphyry type, where the ore occurs either directly within massive acidic intrusives or older rocks invaded by the intrusives, or both. But rock strength (as determined via drill penetration rates as presented in Chapter 6) is only one of the variables utilized by the fragmentation model (Chapter 4); the other required variable is the pre-blasted rock mass chunk size, determined via image analysis as presented in Section 3.4.5 above. When ANOVA is applied to the rock mass chunk size scale parameters observed at the Gold and Copper mines (Table A1 Appendix) , there exists a 76% probability that the average rock mass chunk size scale parameters for mines excavating rock containing the two different types of commodity are from the same population. Then for the time being, ANOVA shows that the average strength and chunk sizes of the rock mass at Gold and Copper mines will not require partitioning into two separate populations for the purposes of accurately modeling fragmentation.

3.7.4 Student's t Distribution

The probability density of Student's t distribution is given by [Evans et al., 1993]:

$$f(x) = \frac{\{\Gamma[(v+1)/2]\}}{\sqrt{(\pi v)} \Gamma(v/2) [1+(x^2/v)]^{(v+1)/2}} = t : v \quad (3.56)$$

where v is a shape parameter referred to as the degrees of freedom. The t distribution is another sampling distribution, and it possesses a useful relationship for a random sample of normally distributed observations [Evans et al, 1993]:

$$t : n-1 \sim \frac{\bar{x} - \mu}{S/\sqrt{n-1}} \quad (3.57)$$

where \bar{x} and S are the mean and biased standard deviation of the sample of size n , and μ is the population mean. Thus a population mean estimated from n observations is distributed as a t probability function with $n - 1$ degrees of freedom. 3.57 can be rearranged as:

$$\mu \sim \bar{x} - \frac{S(t:n-1)}{\sqrt{n-1}} \quad (3.58)$$

and the t distribution can be utilized to determine a "one sided" confidence interval associated with the mean population value; by an argument based upon the symmetry of the distribution a two-sided confidence interval for the population mean can be determined, as in:

$$\mu \sim \bar{x} \pm \frac{S(t:n-1)}{\sqrt{n-1}} \quad (3.59)$$

As an example, the t - distribution is utilized to estimate a two sided confidence interval

about the grand population mean for the rock strength observations discussed in the previous section. From Table A2 (Appendix), the mean and the biased standard deviation for the 39 rock strength samples can be determined as 13,022 p.s.i. and 8,144 p.s.i. respectively. If a 90% confidence level is chosen for the estimate of the mean population strength, then cumulative relative frequency limits that bound 90 % of the area below the frequency distribution must be selected. Conveniently selecting the area bounded by the 5th and 95th percentile cumulative values, as shown on Figure 3.11:

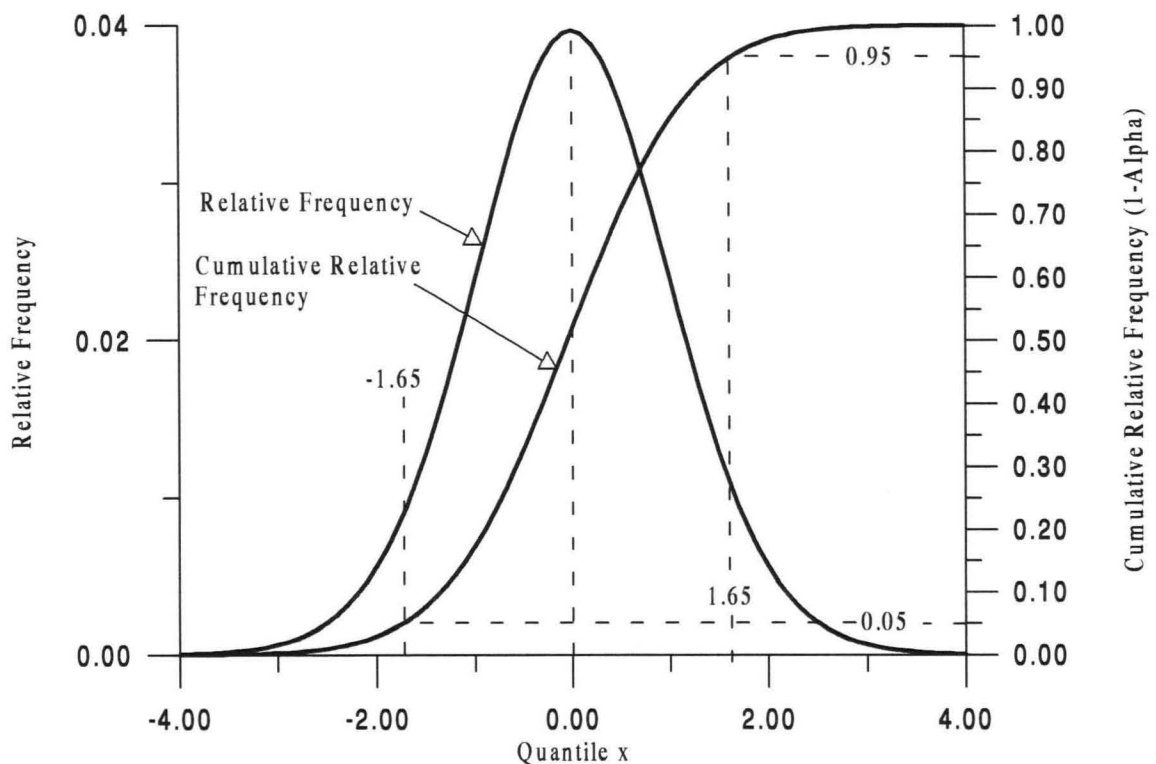


Figure 3.11 - t Distributions with 38 Degrees of Freedom for Graphical Determination of Confidence Intervals for Rock Strength Population Mean

- 95% of the time, the x variate will be less than or equal to 1.65;

- 5% of the time, the x variate will be less than or equal to -1.65;
- thus 90% of the time, the x variate will be > -1.65 and ≤ 1.65 ;

This corresponds to 90% certainty that the population mean of rock strength (p.s.i.) for all open pit Gold and Copper mines is somewhere within the interval defined by 3.59:

$$\mu = 13,022 \pm \frac{8,144(1.65)}{\sqrt{38}} = 13,022 \pm 2,179 \quad (3.60)$$

One other important property of the t distribution is used to determine confidence and prediction intervals for regression analysis. For two sets of normally distributed observations [Evans et al, 1993]:

$$t : n_1 + n_2 - 1 \sim \frac{(\bar{x}_1 - \bar{x}_2) - (\mu_1 - \mu_2)}{\sqrt{\frac{n_1 S_1^2 + n_2 S_2^2}{n_1 + n_2 - 2} + \frac{1}{n_1} + \frac{1}{n_2}}} \quad (3.61)$$

A large number of regressions are presented within the following chapters. Occasionally estimated variables determined via regression had to be recombined into functional expressions. The following sections show how the accuracy of an individual regression is represented, and how the error of functional expressions containing more than one estimated variable was assessed.

3.8 Representation of Regression Analysis Results

Typically, a regression will be presented with certain terms and statistics representing the accuracy of the regression. For example, Equation 7.36 from Chapter 7 estimates stemming (ft) from multiple variates consisting of the drill diameter ϕ (inches)

and above grade energy E_{ag} (MJ) as:

$$\hat{stm} = 4.983 (\phi) - 0.00761(E_{ag}) - 20.760 \quad [R^2 = 0.953, \text{Sig. F} = 0.000] \quad (3.62)$$

$$\quad [0.0000] \quad [0.0001] \quad [0.0000]$$

The meaning of the squared correlation (R^2) was presented in Section 3.5.2 above.

“ Sig. F ” is the F distribution probability value that the estimated stemming values are not related in linear fashion to the observed values. The values within the square brackets below the variates and constant are the individual t distribution probability values for the terms directly above; for example the 0.0001 below E_{ag} indicates that the probability that the predicted E_{ag} value is not linearly related to the observed E_{ag} value is 0.01%.

3.9 Uncertainty Analysis

In certain instances, particularly for the machine modeling work performed for Chapter 5, a number of different estimated variables (originally developed through regression analysis) had to be subsequently recombined into functional expressions; for example as in:

$$P = P(x, y, z) \quad (3.63)$$

where P is some function acting upon the independent variates x, y, and z. Then the standard deviation of the value predicted by the functional expression was estimated with the following method [Holman, 1978]:

$$\sigma_P = \left[\left(\frac{\partial P}{\partial x} \sigma_x \right)^2 + \left(\frac{\partial P}{\partial y} \sigma_y \right)^2 + \left(\frac{\partial P}{\partial z} \sigma_z \right)^2 \right]^{1/2} \quad (3.64)$$

where σ_x , σ_y , and σ_z are the standard deviations (Equation 3.5) of the x, y, and z variates, respectively.

A considerable body of regression analysis had to be performed to develop a model for rock mass fragmentation; this work is the subject of the very next Chapter.

4. ROCK MASS FRAGMENTATION MODELS

“ 151. Resources Control

a. In establishing requirements for resources control, priorities must be assigned to specific items to be denied the insurgent. Restrictions on certain items may be injurious to the attitude of the population, such as the control of fertilizer in a primarily agrarian area. Two methods may be employed in controlling materials -

- (1) *Price Regulation.*
- (2) *Rationing.*

b. Additional controls must be employed for materials that can be used as expedients in manufacturing improvised explosives. Adequate control of these items will depend upon properly trained security personnel positioned at the production and distribution facilities for these sensitive items.

c. The use of resources control measures is sensitive and must be carried out with utmost discretion. Infringement upon the rights of the local population, through violence or needless oppression, will lose the population to the insurgent. Local law enforcement agencies should be closely supervised at all times during the operation. ”

United States Department of the Army (1965)
Field Manual FM 31-20 : Special Forces Operational Techniques

There are two goals for the work presented in this Chapter:

1. Establishing an accurate image-based model for rock mass fragmentation;
2. the determination of a specific energy index term for the explosive mode of rock mass size reduction.

The image-based model can then be utilized to predict and design rock mass fragmentation, and the specific energy index term can be used for the excavation cost modeling outlined in Chapter 2. The following list summarizes the path of the research.

The section references contain the detailed information:

1. The terminology of open-cast explosive blasting is presented (Section 4.1);
2. a hypothetical substance is utilized to gain insights into fragmentation (Section 4.2);
3. a prominent theory for the prediction of the average fragment size resulting from blasting a rock mass with explosive is reviewed (Section 4.3);
4. a contemporary state of the art model that is based upon the aforementioned mean fragment size theory for predicting the distribution of fragment sizes resulting from blasting is reviewed (Section 4.4);
5. fragmentation distributions predicted by the state of the art model are compared to distributions obtained via the SPLIT imaging system, and the compared parameter values were found to be at high variance (Section 4.5);
6. higher accuracy fragmentation models are developed that are in better agreement with the results obtained from the SPLIT imaging system (Sections 4.6 and 4.7);
7. the development of the specific energy index term for the explosive mode of rock mass size reduction is summarized (Section 4.8);
8. two different estimators for fragment size distribution scale parameter are developed (Section 4.9);
9. a formulation for the cost of the explosive mode of size reduction is presented (Section 4.10).

4.1 Open-Pit Blasting Terminology

Before fragmentation is discussed, a brief preview of the terms used to describe open pit blasting will be necessary. Figure 4.1 presents an oblique view containing the principal dimensional terms, together with terms describing certain problematic features. On Figure 4.1 fragments created by a previous blast on the same bench level have been removed, leaving an exposed bench face. Bore holes have been drilled and loaded to become blast holes for the subsequent bench blast. To simplify the presentation, only a single row of three blast holes are shown. The principal dimensional terms are defined as

follows:

- The bench height is the vertical height from the bench toe to the bench crest;
- the spacing is the horizontal distance between adjacent blast holes, taken parallel to the bench crest;
- the burden is the horizontal dimension from the blast hole centers to the bench toe;
- the lengths of the stemming and powder column compose the total length of the blast hole;
- the subdrill is the vertical dimension between the bottom of the blast hole and the bench toe;
- the face slope is the angle between the bench face and the vertical.

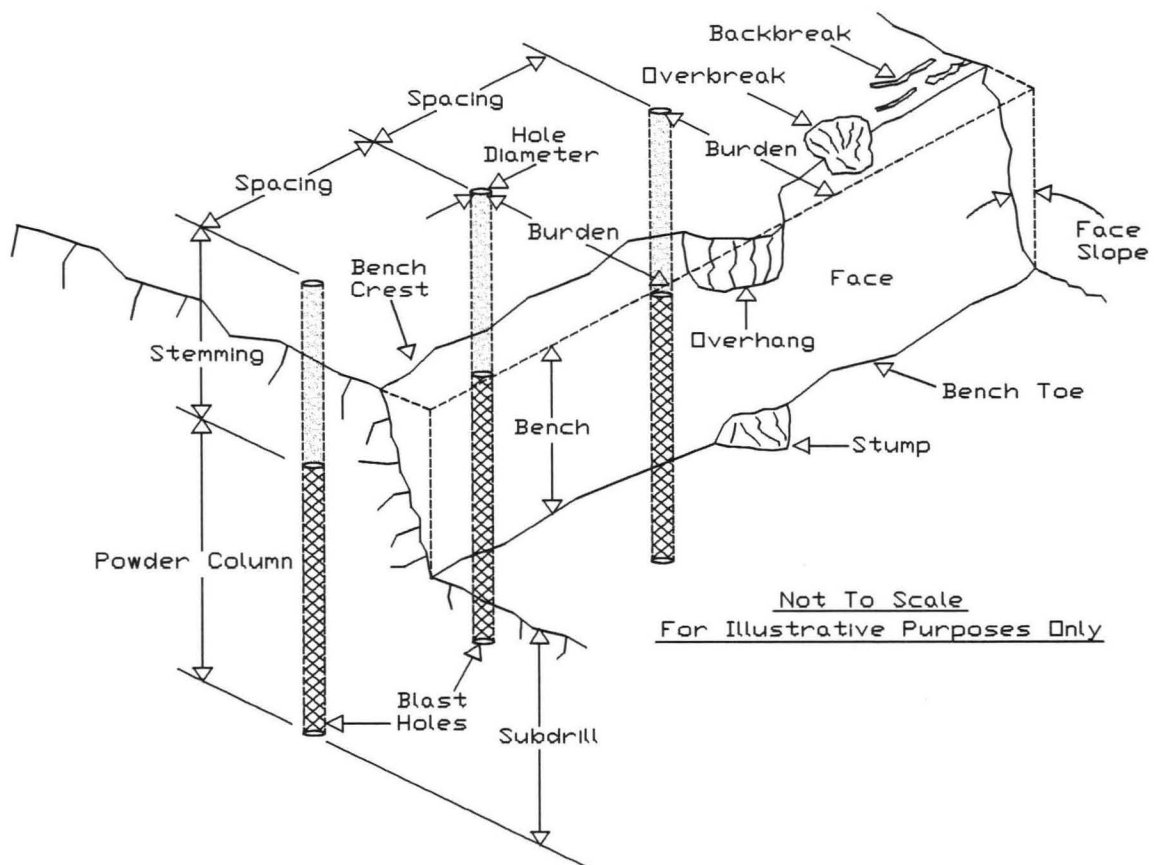


Figure 4.1 - Open Pit Blasting Terminology

Before the physical features presented on Figure 4.1 can be explained, the “powder factor” term needs to be defined. The powder factor relates the explosive mass per blast hole to the quantity of rock subsequently affected by the detonation of the explosive. In North America, explosive mass is expressed in pound units, and rock volume assumes units of cubic yards. Outside of North America, the term “specific charge” is used in place of powder factor, and the units change to kilograms and cubic meters. In either event, powder factor or specific charge is defined as:

$$F_{pv} = \frac{M_e}{V_{rm}} \quad (4.1)$$

where M_e is the explosive mass per blast hole, and V_{rm} is the rock mass volume. The “v” subscript on the F_{pv} term denotes that the explosive mass is specific to rock volume, as opposed to rock weight. The rock mass volume is typically determined as equivalent to the quantity (burden x spacing x bench height).

Stumps, overhangs, overbreak and backbreak are problematic physical features of open-cast blasting. Typical causes and effects of these features as depicted on Figure 4.1 are:

- Insufficient subdrill distance and/or powder factor can cause hard stumps which can damage tires and inhibit the mobility and efficiency of loading machines;
- insufficient stemming and/or powder factor can cause overhangs which produce hazardous working conditions below the bench face;
- excessive powder factor can cause overbreak and backbreak, which produce hazardous working conditions above and below the bench face and also adversely affect slope stability.

4.2 The Blastonium Construct

Explosive fragmentation is not well understood. This section defines a hypothetical substance (Blastonium) to gain insights into how a brittle mass fragments. The explosive induced size reduction of this substance was then subsequently compared to that predicted by the prominent existing theory.

Explosives reduce the size of mass by creating new surface area. The physics of the area creation process are not clear; currently up to 9 different theories attempt to explain the fragmentation process [Atlas Powder Company, 1987]. The resistance of rock mass to the explosive mode of size reduction appears to be a multivariate function of the:

1. Energy content of the explosive;
2. spatially distribution of the explosive within the rock mass volume;
3. strength-volume relationship of the rock mass;
4. size and spatial distribution of pre-existing flaws and fractures within the rock mass volume;
5. spatial distribution of density within the rock mass;
6. magnitude and direction of the local gravity vector.

The roles played by gravity and mass density variation within explosive fragmentation are problematic. Apparently rock mass fragmentation can occur in two separate time episodes: 1) Directly after detonation, as the chemical energy of the explosive is transformed into kinetic energy and mass is accelerated against the direction of the gravity vector, and 2) after the potential energy of the system is reconverted back into kinetic energy, as mass is re-accelerated in the direction of the gravity vector and

brought to rest.

The fragmentation of a brittle mass characterized by a uniform distribution of equally sized flaws and a variable strength-volume relationship is presented in the hypothetical construct below. Explosives are idealized to be perfectly distributed within this substance, and moreover the distributed masses of explosive are theorized to all have simultaneous detonation initiation (timing). The effects of gravity and mass density are neglected.

Consider a hypothetical brittle substance called Blastonium. Atoms of this substance always arrange a cubic space lattice, and the space lattices always form perfectly cubic crystals. The strength of Blastonium is defined such that when 1 kilogram of T.N.T. is detonated at the geometric center of a 1 m^3 crystal, then exactly three fracture planes are formed at right angles to one another. The fracture planes propagate from the center out through the crystal moving perpendicular to the outside surfaces such that all of the energy of the T.N.T. is totally expended when the three fracture planes breach the outer surface. Figure 4.2 shows the 3 fracture planes (depicted as dashed lines) resulting from the detonation. The total fracture surface area created would be 3 m^2 , and therefore the fracture area factor with respect to powder mass (F_{ap}) for Blastonium is defined to be a constant $3 \text{ (m}^2/\text{kg)}$. Detonating 1 kg of T.N.T. in a Blastonium cube of size 1 meter results in exactly 8 smaller crystals, each of side $1/2$ meter and volume $1/8 \text{ m}^3$. The volumetric powder factor for this first stage detonation is $1 \text{ (kg/m}^3 \text{)}$. Explosive can now be introduced into the centers of each of the 8 cubes formed by the first stage blast. The per cube volume is now $1/8 \text{ m}^3$, so using the stage 1 powder factor results in a load of $1/8$

kg per cube. This mass of T.N.T. will now have to form a total of $3/4 \text{ m}^2$ of surface area inside each cube. But since cracking Blastonium consumes exactly 3 m^2 of surface area per kilogram of T.N.T. , the $1/8 \text{ kg}$. per cube load will only form $3/8 \text{ m}^2$. So an assumption of constant powder factor with respect to volume results in a fracture area deficit of $3/8 \text{ m}^2$ for the 2nd stage blast.

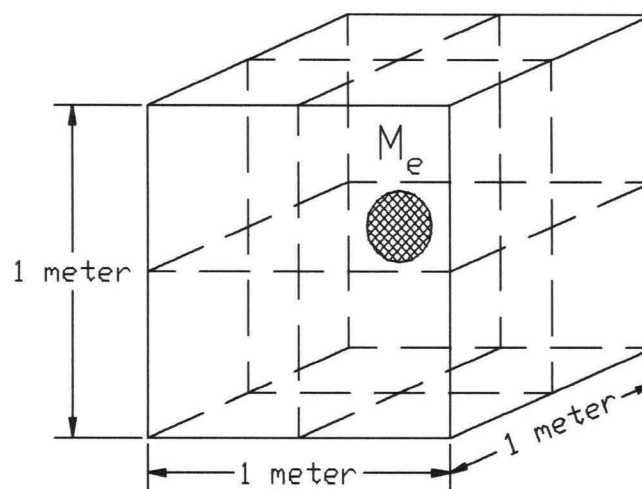


Figure 4.2 - The 1 meter Cube of Blastonium before the Stage 1 Detonation

To create the correct amount of surface area the load is doubled to $1/4 \text{ kg}$. per cube; this corresponds to a powder factor of $2 \text{ (kg/m}^3 \text{)}$. After the explosive in each of the eight cubes of size $1/2 \text{ meter}$ is detonated, a total of 64 cubes of side $1/4 \text{ meter}$ and volume $1/64 \text{ m}^3$ are formed. Each of these cubes requires $3/16 \text{ m}^2$ of fracture area; now loading for the constant area factor of $3 \text{ (m}^2/\text{kg)}$, each cube will require $1/16 \text{ kg}$ of T.N.T., corresponding to a powder factor of $4 \text{ (kg/m}^3 \text{)}$. In theory this cube cracking process can be continued on down to the level of individual molecular lattices; but already the pertinent sequences have formed and conclusions may be drawn. Table 4.1 below

summarizes the results of 4 stages of reduction creating 4,096 cubes from the original 1 meter cube. Alternately the 4096 cubes could have also been produced by a single stage blast by evenly distributing a total of 4 kg of explosive within 512 even portions of the original Blastonium volume, and then detonating all of the explosive at the same time. Many different conclusions may be drawn from the information within Table 4.1. Perhaps the most important is to reiterate that for Blastonium, the per stage area factor with respect to volume doubles for each increasing stage of detonation, and this then requires that the powder load be doubled. The information in Table 4.1 can also be utilized to form an expression for “ average ” fragment size. This expression can then be compared to empirically derived expressions for the determination of average fragment size, which are presented in subsequent sections of this Chapter.

Table 4.1 - The Size Reduction of Cubic Blastonium

stage of size reduction	1	2	3	4
cube size L (m)	1/2	1/4	1/8	1/16
total cubes formed	8	64	512	4096
volume per cube (m ³)	1/8	1/64	1/512	1/4096
total area to form cubes A _f (m ²)	3	6	12	24
total fracture area A _f ^{tot} (m ²)	3	9	21	45
mass T.N.T. M _e (kg)	1	2	4	8
total mass T.N.T. M _e ^{tot} (kg)	1	3	7	15
per stage powder factor with respect to volume F _{pv} (kg/m ³)	1	2	4	8
per stage area factor with respect to volume F _{av} (1/m)	3	6	12	24
per stage area factor with respect to powder F _{ap} (m ² /kg)	3	3	3	3

From the L , M_e , and M_e^{tot} entries in Table 4.1, a formulation for “average” fragment size (m) can be expressed as:

$$\bar{L} = \frac{L}{\frac{M_e^{\text{tot}}}{M_e} + 1} \quad (4.2)$$

and for which if $M_e^{\text{tot}} = M_e$, then:

$$\bar{L} = \frac{L}{2} \quad (4.3)$$

To determine the average cube size that would result from doubling the mass of T.N.T. distributed within the Blastonium, $M_e^{\text{tot}} = 2M_e$, and:

$$\bar{L}' = \frac{L}{3} \quad (4.4)$$

The percent decrease in average fragment size from doubling the explosive mass may now be expressed as:

$$\frac{\Delta \bar{L}}{\bar{L}} = \frac{\bar{L} - \bar{L}'}{\bar{L}} = \frac{\frac{L}{2} - \frac{L}{3}}{\frac{L}{2}} = \frac{1}{3} = 0.33 \approx 33 \% \quad (4.5)$$

4.3 The Kuznetsov Mean Fragment Size Theory

In the early 1970's, the Siberian mining engineer V. Kuznetsov published a functional expression for determining the mean size of the fragments that result when explosives are detonated within a rock mass. Kuznetsov determined the form of his expression via regression analysis upon data obtained from laboratory tests, mines, and

underground nuclear explosions. Therefore his expression was validated over a wide scale of blasts; the values of the rock test volumes used in the blasts differed by about four orders of magnitude. The form of the Kuznetsov Equation is [Kuznetsov, 1972]:

$$\bar{x} = A \frac{V_{rm}^{0.80}}{M_e^{0.63}} \quad (4.6)$$

where:

- \bar{x} = mean fragment size (cm);
- A = rock mass “hardness” parameter;
- V_{rm} = rock mass volume (m^3);
- M_e = equivalent mass of TNT applied to rock volume (kg).

Kuznetsov's hardness parameter attempts to account not only for the physical strength of the rock, but also what he termed the “fissuring” present within the rock volume prior to the blast. To validate his equation, Kuznetsov proposed that his hardness parameter would have to have a total range of 12 units. Table 4.2 summarizes the range of hardness parameters published by Kuznetsov:

Table 4.2 - The Kuznetsov Hardness Parameter and Associated Rock Physical Characteristics

Rock Physical Characteristics	Kuznetsov Hardness Parameter
“ extremely weak rock ”	1
“ medium hard rock ”	7
“ hard, but highly fissured rock ”	10
“ very hard, weakly fissured rock ”	13

Kuznetsov's attempt to quantify both the strength and structural features of the pre-blasted rock mass with a single parametric value is summarized by the following reservations he expressed:

1. There appeared to be no concise relationship between the rock's physical measure of hardness and the mean fragment size of the blasted product;
2. there was no clear association between the average fragment size and the spatial orientation of joints and fractures within the pre-blasted rock.

In addition, Kuznetsov noted that the applicability of his expression for the mean fragment size (Equation 4.6) was “ doubtful ” if:

3. a small number of fragments resulted from a blast;
4. a rock mass was repeatedly broken by blasting;
5. a rock mass was composed of different types of rocks.

The theoretical nature of Kuznetov's Equation is summarized in list items (1) and (4) above. Because the “ hardness ” and flaw density of rock mass can quickly change on the spatial-volumetric scale, it is virtually impossible to obtain physically identical test volumes for experimentation. But it will be useful to determine the percent decrease in average fragment size predicted by the Kuznetsov Equation resulting from a doubling of explosive mass for a rock mass of constant “ hardness ” and volume. When the explosive mass is doubled the average rock fragment size (Equation 4.6) becomes:

$$\bar{x}' = A \frac{V_{rm}^{0.80}}{(2M_e)^{0.63}} = A \frac{V_{rm}^{0.80}}{1.54 M_e^{0.63}} \quad (4.7)$$

And the percent decrease in average fragment size becomes:

$$\frac{\Delta \bar{x}}{\bar{x}} = \frac{\bar{x} - \bar{x}'}{\bar{x}} = \frac{A \frac{V_{rm}^{0.80}}{M_e^{0.63}}}{A \frac{V_{rm}^{0.80}}{M_e^{0.63}}} \left(1 - \frac{1}{1.54} \right) = 0.35 \approx 35 \% \quad (4.8)$$

This result is comparable to the 33 % decrease obtained for Blastonium (Section 4.2), for which the explosive was theorized to have perfectly uniform distribution. But curiously the form of Kuznetsov's equation does not account for the spatial distribution of explosive. The underground thermo-nuclear blasts cited by Kuznetsov are examples of explosive mass concentrated down into a point source. The mining blasts he studied were evidently a Russian ANFO type explosive contained within vertical drillholes. The details of the laboratory blasts cited by Kuznetsov are unknown; but for the time being it will be concluded that the mean fragment size resulting from blasting rock mass is independent of the spatial distribution of explosive.

The uniformity, or size consistency, of the fragment sizes produced by a blast does not appear to be independent of the spatial distribution of the explosive. This topic is covered in Section 4.6.4.

4.4 The Kuz-Ram Fragmentation Model

“ Cunningham realized that the Rosin-Rammler Curve had been generally recognized as a reasonable description of fragmentation for both crushed or blasted rock. One point on that curve, the mean size, could be determined with the Kuznetsov Equation. ”

Konya and Walter (1990) --- *Surface Blast Design*

Claude Cunningham, an English mining engineer who worked in Africa, made significant contributions to the field of explosive induced fragmentation. These contributions have subsequently become known as the “ Kuz-Ram ” model, because the model is based upon the Kuznetsov mean fragment size theory and the Rosin-Rammler

particle size distribution. The principal characteristics of the Kuz-Ram model are set forth on the following list, and the material presented within the referenced sections contains the detailed aspects of the information:

1. The form of the basic Kuznetsov equation was altered such that it would incorporate both " powder factor " and " weight strength " terms commonly utilized throughout the explosive industry of the Western world (Section 4.4.1);
2. the rock mass " hardness " term proposed by Kuznetsov is replaced by a more extensive term describing the " blastability " of the rock mass (Section 4.4.2);
3. the provision of analytic expressions to help estimate the shape and scale of the fragment size distributions resulting from blasting (Section 4.4.3).

4.4.1 The Kuznetsov Equation in Powder Factor Form

Cunningham put the Kuznetsov Equation into a form that would incorporate the powder factor term, and made a further simplification to allow for the use of explosives other than Tri-Nitro-Toluene [Cunningham, 1983]:

$$\bar{x} = A (F_{pv})^{-0.8} M_e^{1/6} \left(\frac{115}{E} \right)^{19/30} \quad (4.9)$$

where:

- \bar{x} = the mean fragment size (cm);
- A = the "hardness factor" (cm/m³)
- M_e = mass explosive used per blasthole (kg).
- E = relative weight strength of explosive used in blast (dimensionless).
[relative weight strength of T.N.T. = 115, ANFO \cong 100]
- F_{pv} = volumetric powder factor (kg/m³)

4.4.2 The Rock Mass Blastability Factor

Cunningham's research suggested that the simple rock hardness factor proposed by Kuznetsov was inadequate for modeling fragmentation. Adapting a rating system devised by P.A. Lilly [Lilly, 1986], Cunningham proposed that the following expression

be adopted to replace the Kuznetsov rock factor. In addition to hardness, the expression also considers the density, mechanical strength, elastic properties, and the pre-blast structure (joints and fractures) of the rock mass [Cunningham, 1987]:

$$A = 0.06 (RMD + JF + RDI + HF) \quad (4.10)$$

where:

RMD	=	the rock mass descriptor	-	Powdery/Friable	=	10
		“	-	Vert. Jointed	=	JF
		“	-	Massive	=	50

$$JF = JPS + JPA$$

JPS	=	Vertical Joint Spacing	-	0.1 m	=	10
		“	-	0.1 to MS	=	20
		“	-	MS to DP	=	50

(Where MS is oversize (m), and DP is drilling pattern size (m) , assuming $DP > MS$)

JPA	=	Joint Plane Angle	-	Dip out of face	=	20
		“	-	Strike Prp. face	=	30
		“	-	Dip into face	=	40

$$RDI = \text{Rock Density Influence} : RDI = 25(RD-50)$$

(Where RD = Rock Density (t/m^3))

$$HF = \text{Hardness Factor} : \begin{aligned} \text{If } E < 50 \text{ GPa, } HF &= E/3 \\ \text{If } E > 50 \text{ GPa, } HF &= UCS/5 \text{ (MPa)} \end{aligned}$$

4.4.3 Estimators for the Parameters of the Weibull Distribution

Cunningham's most significant contribution to the science of fragmentation was the formulation of predictors for determination of the shape and scale parameters for the fragment size distributions resulting from explosive blasting. The basis of the Kuz-Ram model is the Rosin-Rammler size distribution, the popular size distribution utilized throughout mining science for describing a range of particle sizes. The information

already presented in Section 3.7.2.2 demonstrated that the Rosin-Rammler distribution is identical to the Weibull distribution, the cumulative form of which is repeated below as:

$$F(x) = 1 - \exp \left[- \left(\frac{x}{\theta} \right)^n \right] \quad (4.11)$$

where:

$F(x)$ = fractional volume percent passing ($0 \leq F(x) \leq 1.0$);
 x = fragment size;
 n, θ = distribution parameters defining the distribution shape and scale, respectively.

Cunningham's development of the Kuz-Ram model appears to be based upon an approximation that the mean fragment size will occur at the 50th percentile value, or the median value, of the Weibull cumulative frequency distribution. But as the information presented in Section 3.7.2 demonstrated, fragment size distributions always appear skewed to the right (tailed to the right), and for such skewed distributions, the mean size will be greater than the median size. But by substituting the mean fragment size (\bar{x}) from Equation 4.9 for fragment size (x) in Equation 4.11, and equating $F(x)$ to 0.5 (the 50th percentile, or median value) and solving for the scale parameter, Cunningham obtained:

$$\theta = \frac{\bar{x}}{(0.693)^{1/n}} \quad (4.12)$$

Therefore the mean fragment size can be determined with Equations 4.10 and 4.9, and the distribution scale parameter (θ) can be determined, provided the shape parameter (n) is known. Using regression analysis performed upon data derived from blasting operations,

Cunningham proposed the following complex expression for the shape parameter

[Cunningham, 1987]:

$$n = \left(2.2 - 14 \frac{B}{D} \right) \sqrt{\frac{1 + \frac{S}{B}}{2}} \left(1 - \frac{W}{B} \right) \left(\frac{\text{abs}(BCL - CCL)}{L} + 0.1 \right)^{0.1} \left(\frac{L}{H} \right) \quad (4.13)$$

where:

D	=	Hole diameter (mm);
B	=	burden (m);
S	=	spacing (m);
BCL	=	bottom charge length (m);
CCL	=	column charge length (m);
L	=	total charge length, or powder column (m);
W	=	standard deviation of drilling accuracy (m);
H	=	bench height (m).

The BCL and CCL terms above account for two different types of explosive within the drill hole.

4.5 Weibull Distribution Parameter Comparisons: SPLIT Vs. Kuz-Ram

To investigate the applicability of the Kuz-Ram model as a predictive tool for estimating the scale and shape parameters (Equation 4.11) of the fragment size distributions resulting from blasting, the Kuz-Ram estimators for distribution shape and scale were compared to the size distributions sampled with the SPLIT system for fragment delineation.

A crucial aspect of the Kuz-Ram model is the determination of the rock mass blastability factor, presented in Section 4.4.2. These factors were not determined from field observation, but rather from visually observing scaled rock mass cell still images some time after the video tapes were recorded. The blast, strength, and cell image data

used to characterize these 20 sites are included in Table A1 of the Appendix. On all of the subsequent plots, the shorter alphabetic labels (cross referenced to actual mining sites within Table A1) are used to prevent plot label “clustering” and facilitate the identification of the different mining sites.

Relationships between the fragment size Weibull distribution parameters determined by the SPLIT system and predicted by the Kuz-Ram model are shown on Figures 4.3 and 4.4, which compare the scale and shape parameters, respectively. The 95% prediction intervals are included in the form of upper and lower dashed-line limits; in conjunction they form a 95% prediction band for any future observation on the Y variable (SPLIT) for any new X variable (Kuz-Ram) value. The Equations of the best fitting lines shown on Figures 4.3 and 4.4 are respectively:

$$\theta_{\text{SPLIT}} = 0.0389 (\theta_{\text{KR}}) + 3.419 \quad [R^2 = 0.321, \text{Sig. F} = 0.009] \quad (4.14)$$

$$n_{\text{SPLIT}} = -0.075 (n_{\text{KR}}) + 1.571 \quad [R^2 = 0.007, \text{Sig. F} = 0.727] \quad (4.15)$$

where θ_{SPLIT} , n_{SPLIT} and θ_{KR} , n_{KR} are the scale and shape parameters for the Weibull distributions describing the distribution of fragment size, as determined by the SPLIT system and the Kuz-Ram model, respectively. The R^2 values and F statistics shown for these two equations alone are sufficient to form a conclusion; instead the regression accuracy will be interpreted by simply visually observing the plots. Figure 4.3 shows that:

- The scale parameters for the sites predicted by the Kuz-Ram model range from 10 to 90 inches, and the scale parameters derived from the SPLIT system range from 2 to 8 inches;
- the total width of the 95% prediction band is about 6 inches.

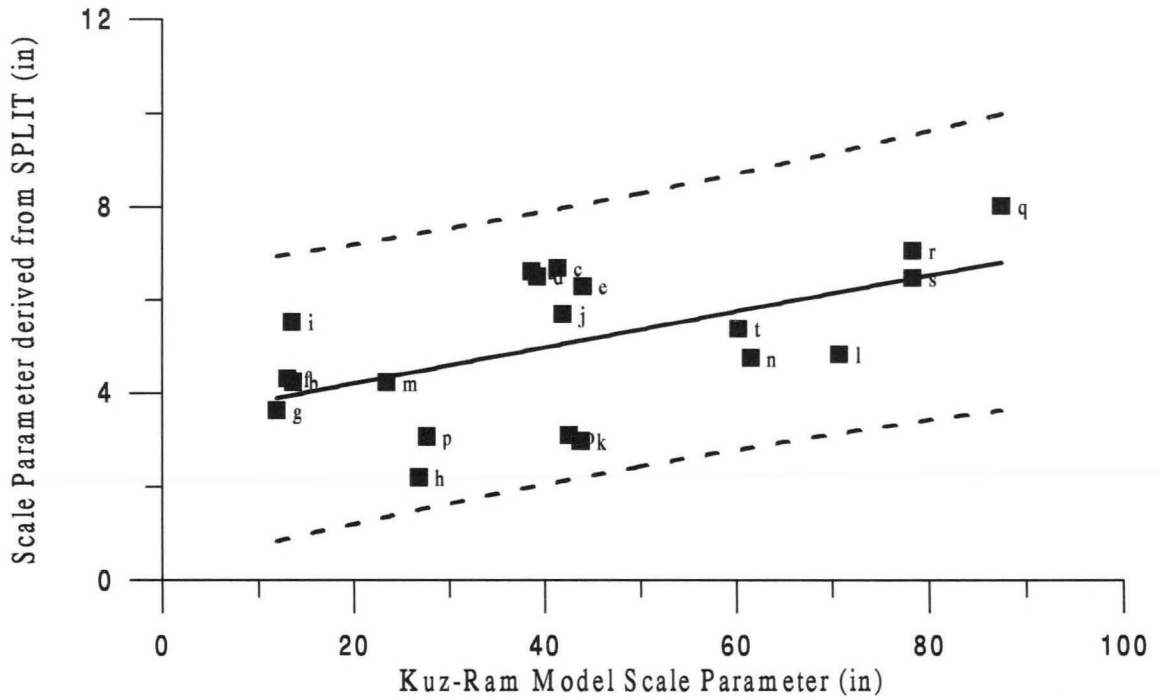


Figure 4.3 - Comparison of Fragment Size Distribution Scale Parameters: SPLIT Vs. Kuz-Ram

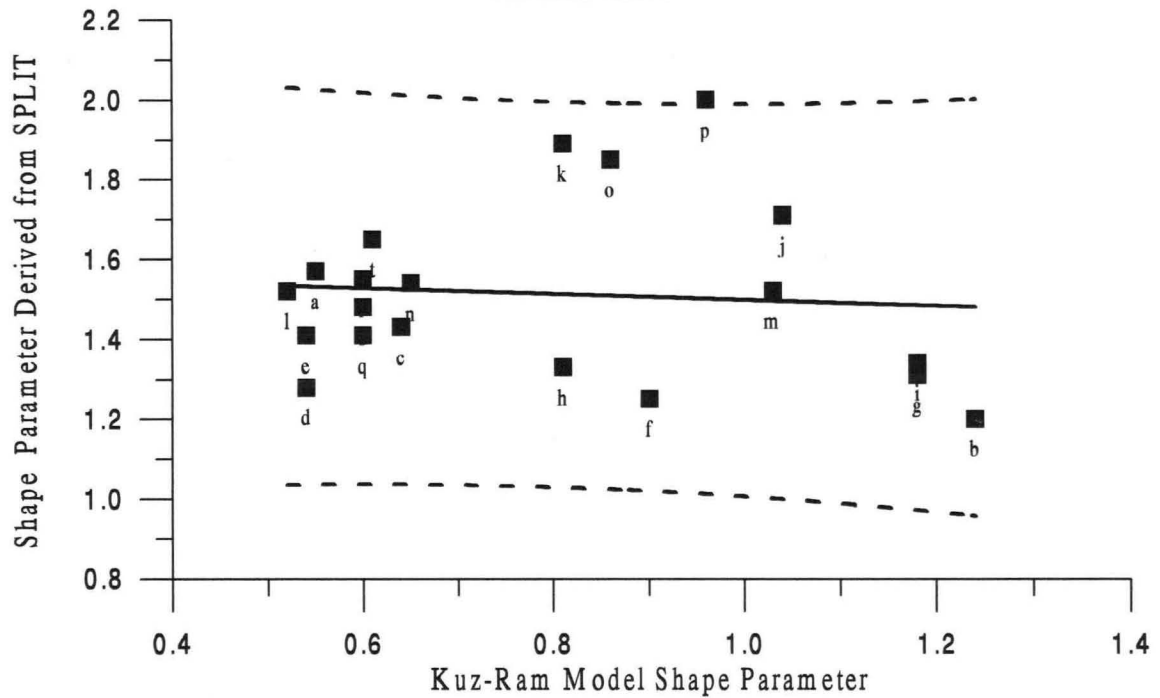


Figure 4.4 - Comparison of Fragment Size Distribution Shape Parameters: SPLIT Vs. Kuz-Ram

Figure 4.4 shows that:

- The shape parameters for the sites predicted by the Kuz-Ram model range from 0.5 to 1.25, and the scale parameters derived from the SPLIT system range from 1.2 to 2.0;
- the total width of the 95% prediction band is about 1 complete unit of shape parameter.

Conclusions: Fragment size distribution scale and shape parameters, as estimated by the Kuz-Ram model, do not appear to be accurately correlated to those sampled by the SPLIT imaging software; therefore the SPLIT software, used in conjunction with the Kuz-Ram model, probably cannot be used for designing and predicting rock mass fragmentation.

4.6 A New Model for the Explosive Induced Fragmentation of Rock Mass

The general nature of rock mass size reduction via explosives is presented on the frequency plots presented on Figure 4.5, where the average rock mass cell “chunk” size frequency distribution is plotted along with the corresponding average fragment size distribution which results from blasting the rock mass. The “chunk” size distribution is a hypothetical construct meant to represent:

1. A careful disassembly of the rock mass volume into its constituent mass chunks that are bounded by pre-existing fracture surfaces;
2. moving these mass chunks through a large screening system to obtain the size distribution.

The plots were produced by utilizing the average Weibull distribution scale and shape parameter values for both the rock mass chunks and fragments at the 20 sites listed in Table A1 (Appendix). Referring to Figure 4.5:

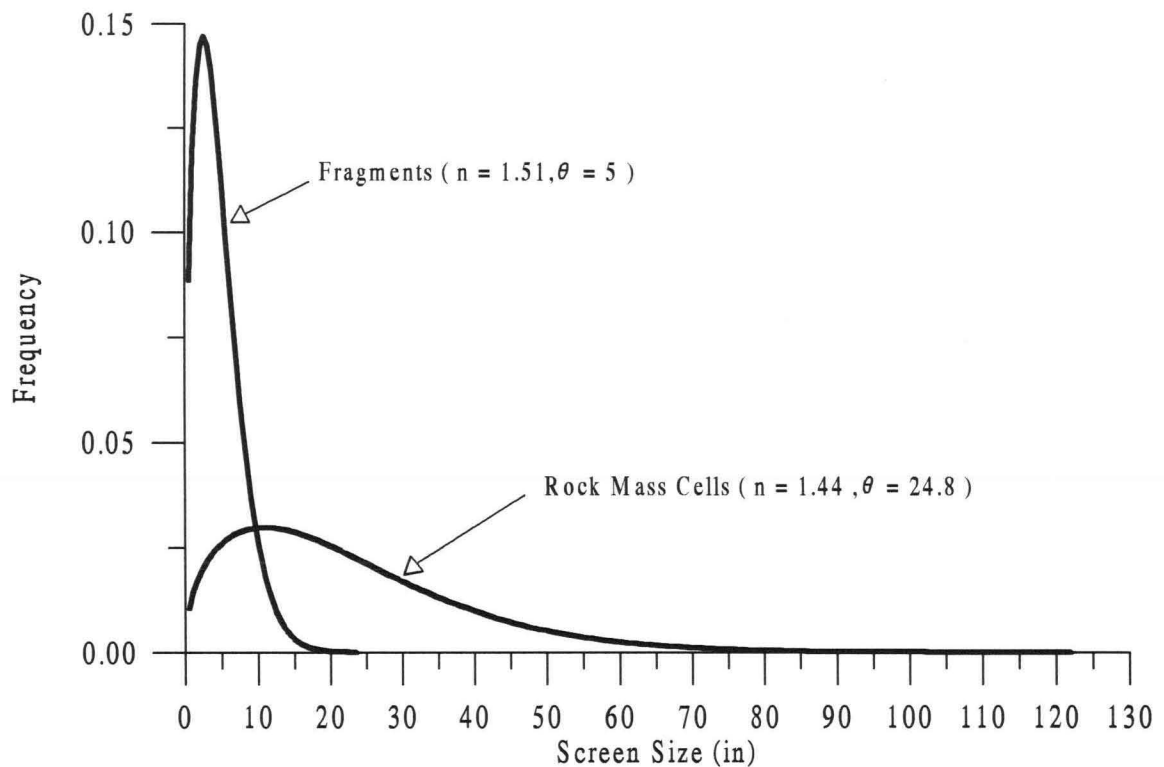


Figure 4.5 - Average Weibull Frequency Distributions of Size for the Rock Mass Cells and Fragments Composing the Experimental Data Set

- Even though the average shape parameters (“ n ”) of the two curves are similar, the average scale parameters (“ θ ”) are significantly different, and thus the use of shape parameter as a predictor of fragmentation will be meaningful only within the context of scale parameter;
- the modal sizes (the most probable values taken at the curve peaks) of the pre-blast rock mass cell chunks and post blast fragments are about 12.5 and 2.5 inches, respectively;
- on average, the total size range of the chunks composing the rock mass cells is about 120 inches, and the range of the fragment sizes produced by blasting a cell is about 24 inches;
- therefore on average, the blasts performed upon the rock mass cells to produce the fragments reduce the modal sizes by a factor of 5 and reduces the size range by a factor of about 5.

The cumulative forms of the distributions are obtained by integrating with respect to screen size, and these are presented below in linear form on Figure 4.6. Both axis have been transformed via the techniques already presented in Section 3.7.2.2;

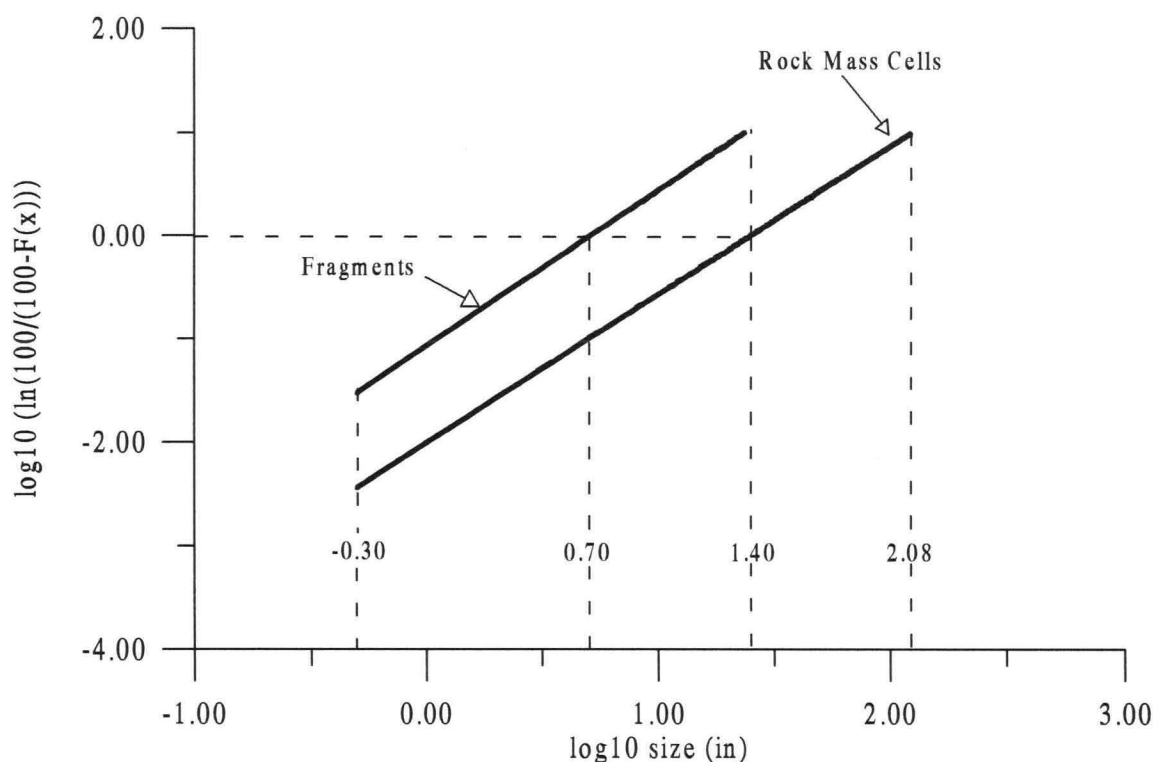


Figure 4.6 - Average Rosin-Rammler Size Distributions for the Rock Mass Cells and Fragments Composing the Experimental Data Set

and information presented in this same section showed that the shape parameter is equivalent to the slope of the line, and furthermore that regardless of shape parameter value, the base 10 log of the distribution scale parameter can be obtained at the X intercept of $Y = 0$. Figure 4.6 shows some of the same information as that presented on Figure 4.5, except now the minimal difference between the shape parameters (i.e. the line slopes) is much more distinct. On average, the process of blasting a mass of rock into

fragments has three principal characteristics:

- The total size range is reduced by about five (obtained from $\text{invlog}_{10} ((2.08 + 0.30) - (1.40 + 0.30))$);
- a very small increase in shape parameter, and hence uniformity of size (obtained from visual observation of line slopes);
- a decrease in scale parameter of about five ($\text{invlog}_{10} (1.4 - 0.7)$).

These results suggest that an empirical model for the prediction of fragmentation from blasting will have to be principally concerned with some function of reduction ratio, where such ratio is concerned with either range size, modal size, or scale size. Scale size is the logical candidate because it is a parameter of the Weibull distribution. But before the development of such a model can proceed, the relationships between rock strength, rock volume, and time must be investigated. Evidently, certain of these relationships were previously investigated by Waloddi Weibull.

4.6.1 A Proposed Time Domain Form of Weibull's Strength - Volume Relationship

An expression that relates the strength of a brittle mass to the mass volume is

[Weibull, 1939]:

$$m \log_{10} \left(\frac{S_1}{S_2} \right) = \log_{10} \left(\frac{V_2}{V_1} \right) \quad (4.16)$$

where S_1 is the strength of the brittle mass at volume V_1 , S_2 is the strength at volume V_2 , and m is a material constant. Because Weibull showed that an inverse relationship exists between rock mass strength and volume, the units of the material constant will have to assume a negative value.

For the purpose at hand, it is desirable to obtain the strength of the rock mass volume, or rather the resistance of the rock mass to the explosive mode of size reduction. Fortunately, uniaxial compressive strength (UCS) data exists for many of the rocks at the blast sites. Conveniently S_1 can then be taken as the rock mass test core UCS value, V_1 as the test core volume, and V_2 as the rock mass volume. Clearly the explosive mode of size reduction is much different than that used to obtain the uniaxial compressive strength of a test core, primarily because of time scale differences. The test cores were subjected to a standardized compressive strain rate of 0.0003 in/sec, and the time to core failure averaged about 4 minutes. If the time period of the explosive event (shock wave and mass heave) is approximated as about 4 sec, then the scale difference of time duration averages about 60. Therefore it is proposed that for the purposes of estimating the fragmentation resistance of a rock mass, a factor be included on both sides of Equation 4.16 to transform Weibull's relationship into the time domain:

$$t^m \log_{10} \left(\frac{S_1}{S_2} \right) = t \log_{10} \left(\frac{V_2}{V_1} \right) \quad (4.17)$$

4.6.2 A Proposed Relationship between Explosive Energy and Size Reduction

Conveniently a product of strength and volume is energy. Equation 4.17 can be solved for the product of the two known quantities of strength and volume (S_1 (MPa) and V_2 (m³) respectively):

$$K_1 \left(S_1^{mt} V_2^{-t} \right) = K_1 \left(S_2^{mt} V_1^{-t} \right) = K_2 \quad (4.18)$$

where K_1 is a dimensional constant necessary to express K_2 in units of energy (here MJ).

Equation 4.18 can be multiplied by a dimensionless function of reduction ratio:

$$K_1 S_1^{mt} V_2^{-t} f(R) = K_1 S_2^{mt} V_1^{-t} f(R) = K_2 f(R) \quad (4.19)$$

where R is defined as the ratio of some characteristic dimension representing the rock mass chunk and fragment screen size respectively:

$$R = \frac{x_{rm}}{x_f} \quad (4.20)$$

The energy expended (E_e (MJ)) in an explosive size reduction process can now be equated to the left hand side of Equation 4.19, following the substitution of Equation 4.20 for the reduction ratio R :

$$E_e = K_1 S_1^{mt} V_2^{-t} f\left(\frac{x_{rm}}{x_f}\right) = K_2 f\left(\frac{x_{rm}}{x_f}\right) = K_w f\left(\frac{x_{rm}}{x_f}\right) \quad (4.21)$$

where the strength-volume energy product term (K_w) may as well be called the “ Weibull Blast Index ”. K_w (MJ) is theorized to be a constant over certain ranges of both strength and volume for rock mass.

Despite the crudity of the above derivations, it can simply be concluded that if Equation 4.21 has a physical basis, then regression analysis performed upon empirical data will result in accurate determinations for the material and timing constants, as well as the form of the function acting upon the dimensionless reduction ratio.

4.6.3 Validation of the Weibull Blasting Index Fragmentation Model

A series of multivariate non-linear regressions were used upon the blast data for

the 20 sites to produce the following Equation:

$$\hat{E}_{ag} = 0.185 S^{0.141} V_{rm}^{0.891} \left(\frac{\theta_{rm}}{\theta_f} \right) = \hat{K}_w \left(\frac{\theta_{rm}}{\theta_f} \right) \quad [R^2 = 0.826] \quad (4.22)$$

where:

- \hat{E}_{ag} = the estimated above grade (excluding the subdrill) explosive energy (MJ);
- V_{rm} = the rock mass volume (m^3);
- S = the uniaxial compressive strength of a core bored from a fragment of the rock mass volume subsequent to the explosive event (MPa);
- θ_{rm}, θ_f = the Weibull scale parameters of the rock mass chunk and fragment screen size distributions, respectively (in);
- \hat{K}_w = the estimated “ Weibull Blast Index ” (MJ).

Back-solving Equation 4.22 for fragment size results in an estimated fragment screen size distribution scale parameter of :

$$\hat{\theta}_f = \hat{K}_w \frac{\theta_{rm}}{\hat{E}_{ag}} \quad (4.23)$$

then when $\hat{\theta}_f$ is linearly regressed back against the scale parameter observed with the SPLIT system, a squared correlation (R^2) of 0.51 results. Equation 4.23 predicts the following percent decrease in scale parameter for a doubling of explosive energy:

$$\frac{\Delta \hat{\theta}_f}{\hat{\theta}_f} = \frac{\hat{K}_w \frac{\hat{\theta}_{rm}}{\hat{E}_{ag}}}{\hat{K}_w \frac{\hat{\theta}_{rm}}{\hat{E}_{ag}}} \left(1 - \frac{1}{2} \right) = 0.50 = 50\% \quad (4.24)$$

which is inconsistent with the 35% result obtained for Kuznetsov's mean size equation (Equation 4.8). For Equation 4.24 above, the assumption that $\bar{x} \approx \theta_f$ was utilized;

which seems entirely reasonable for a differential expression.

Conclusions: The 50% reduction result predicted by Equation 4.24 above is excessive when compared to the prominent existing theory. Evidently the Equation 4.21 requirement for inclusion of a dimensionless function of size ratio should be altered into a non-dimensionless ratio of size functions, as in:

$$E_e = K_3 S_1^{mt} V_2^{-t} \frac{f_1(x_{rm})}{f_2(x_f)} = K_w^f \frac{f_1(x_{rm})}{f_2(x_f)} \quad (4.25)$$

where the K_3 term is a new dimensional constant necessary to convert all of the other terms on its immediate right into energy, and where the K_w^f term now differs from the previous K_w .

A pure physical derivation of Equation 4.25 will not be attempted, but it may prove challenging to researchers elsewhere. If f_1 and f_2 are chosen as power functions, then Equation 4.25 can be expressed as:

$$E_e = C_1 S^{C_2} V_{rm}^{C_3} \frac{(x_{rm})^{C_4}}{(x_f)^{C_5}} = K_w^f \frac{(x_{rm})^{C_4}}{(x_f)^{C_5}} \quad (4.26)$$

and solved for the characteristic fragment screen size dimension as:

$$x_f = \frac{1}{C_1^{C_5}} S^{\frac{C_2}{C_5}} V_{rm}^{\frac{C_3}{C_5}} \frac{(x_{rm})^{\frac{C_4}{C_5}}}{(E_e)^{\frac{1}{C_5}}} = \left(K_w^f\right)^{\frac{1}{C_5}} \frac{(x_{rm})^{\frac{C_4}{C_5}}}{(E_e)^{\frac{1}{C_5}}} \quad (4.27)$$

Utilizing the rock mass chunk and fragment screen size distribution scale parameters (expressed in inch units) and the above grade energy (MJ) to perform a regression such

as that indicated by Equation 4.27 results in:

$$\hat{\theta}_f = 3.358 \frac{S^{0.077} V_{rm}^{0.385} \theta_{rm}^{0.152}}{E_{ag}^{0.472}} = \hat{K}_w^f 0.472 \frac{\theta_{rm}^{0.152}}{E_{ag}^{0.472}} \quad [R^2 = 0.57] \quad (4.28)$$

and back-solving for above grade energy results in:

$$\hat{E}_{ag} = 13.0 S^{0.163} V_{rm}^{0.815} \left(\frac{\theta_{rm}^{0.321}}{\theta_f^{2.118}} \right) = \hat{K}_w^f \frac{\theta_{rm}^{0.321}}{\theta_f^{2.118}} \quad (4.29)$$

which clearly cannot be manipulated into a dimensionless function of reduction ratio,

analogous to the form of Equation 4.21 above, because the units of the \hat{K}_w^f term are not

pure Mega-Joules, but rather MJ- in^{1.79}. Equation 4.28 now predicts the following

percent decrease in scale parameter for doubling of explosive mass:

$$\frac{\Delta \hat{\theta}_f}{\hat{\theta}_f} = \frac{\hat{K}_w^f 0.472 \frac{\theta_{rm}^{0.152}}{E_{ag}^{0.472}}}{\hat{K}_w^f 0.472 \frac{\theta_{rm}^{0.152}}{E_{ag}^{0.472}}} \left(1 - \frac{1}{(2)^{0.472}} \right) = 0.28 = 28\% \quad (4.30)$$

which appears more consistent with the 35% result predicted from the Kuznetsov theory.

Figure 4.7 shows the results of plotting the site scale parameters predicted by Equation

4.28 (hereafter referred to as the “ Weibull Index ” model) against those derived from

the SPLIT delineation software. The equation of the line including the pertinent statistics

are:

$$\theta_f^{SPLIT} = 0.981 (\theta_f^{WI}) + 0.098 \quad [R^2 = 0.572, \text{Sig. F} = 0.0001] \quad (4.31)$$

On Figure 4.7:

- The scale parameters for the sites predicted by the Weibull Index model range from 3.25 to 7 inches, and the scale parameters derived from the SPLIT system range from 2 to 8 inches;
- the total width of the 95% prediction band is about 5 inches.

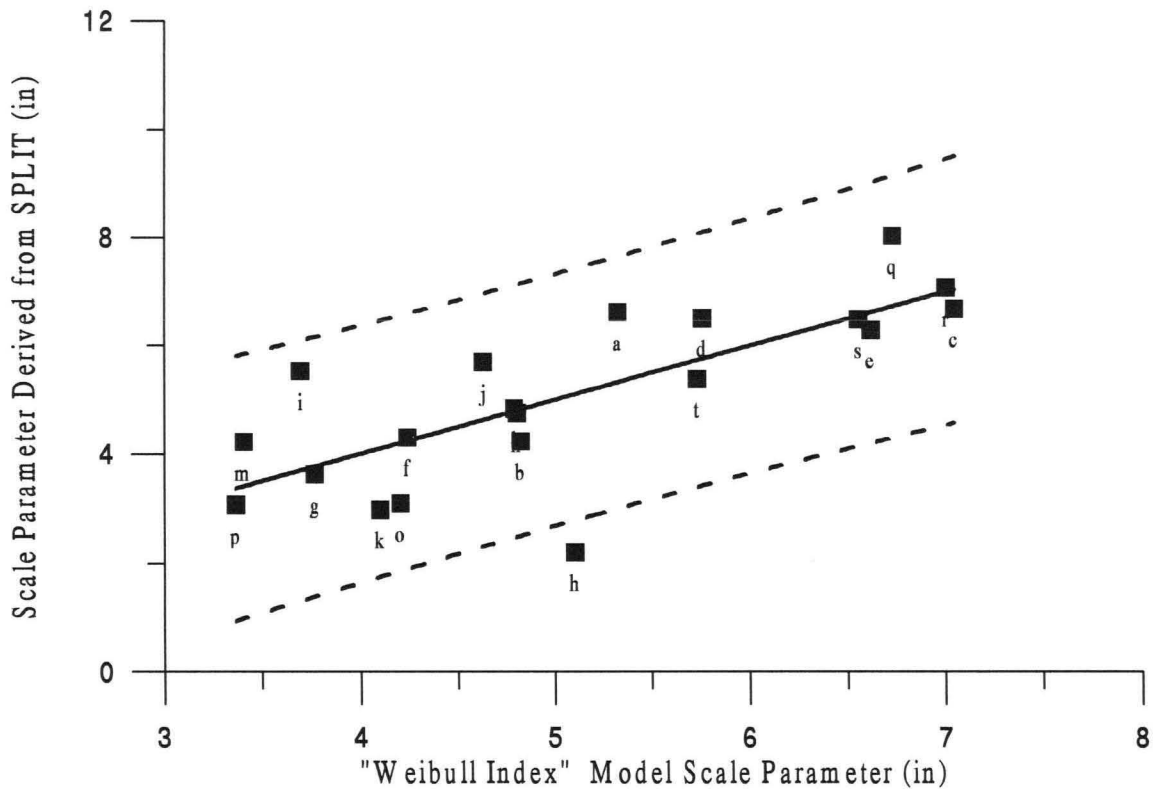


Figure 4.7 - Comparison of Fragment Size Distribution Scale Parameters: SPLIT Vs. Weibull Model

Conclusion: If Figure 4.7 is compared to Figure 4.3, it is apparent that the Weibull distribution fragment scale parameters predicted by the “ Weibull Index ” model are more accurate than those predicted by the Kuz-Ram model. This result is particularly important in consideration of the fact that rock mass fracture observations for the “ Weibull Index ” model were derived from the SPLIT image software, whereas the Kuz-Ram model relies upon a rather subjective visual interpretation of the rock’s fractures.

4.6.4 The Uniformity of Fragment Size Distributions

For the open-pit bench blasts studied for this work, the explosive is distributed within the rock volume simply as a cylindrical column within a drill hole. Some preliminary linear regression studies hinted that both cylinder diameter (hole diameter) and the ratio of bench height to explosive cylinder length (powder column length) were correlated to the uniformity (i.e. the consistency) of fragment size. Uniformity also appeared to be correlated to above grade explosive energy. Because above grade explosive energy can be expressed as a function of hole diameter, further regression analysis work was centered around a non-linear expression of the following form:

$$n = C_1 (E_{ag})^{C_2} + C_3 \left(\frac{H}{L} \right)^{C_4} \quad (4.32)$$

where C_1 through C_4 are constants, H is the bench height (m), and L is the length of the powder column (m). A regression of the form represented by Equation 4.32 performed on the site drill and blast data (Table A1 Appendix) resulted in:

$$\hat{n} = 2.830 \times 10^{-9} (E_{ag})^{2.58} + 1.17 \left(\frac{H}{L} \right)^{0.20} \quad (4.33)$$

a model which is anti-intuitive because at constant bench height H , fragment uniformity is predicted to decrease as powder column length L increases. Exactly the opposite would seem logical, i.e. that as explosive became more vertically distributed through the rock mass over the bench height, the fragments would become more uniform in size. When the shape parameter derived from the SPLIT system is regressed against that predicted by Equation 4.33:

$$n_{\text{SPLIT}} = -0.413 (\hat{n}) + 1.31 \quad [R^2 = 0.838, \text{Sig. } F = 0.000] \quad (4.34)$$

The relationships between the scale parameters determined by the SPLIT system and predicted by the Equation 4.33 model are presented on Figure 4.8, which shows that:

- The shape parameters for the sites predicted by the uniformity model (Equation 4.33) range from 1.25 to 1.8, and the scale parameters derived from the SPLIT system range from 1.2 to 2.0;
- the total width of the 95% prediction band is about 0.4 units of shape parameter.

Conclusions: When Figure 4.8 is compared to Figure 4.4, it is evident that the Weibull distribution fragment shape parameters predicted by the Equation 4.33 uniformity model are much more accurate than those predicted by the Kuz-Ram model.

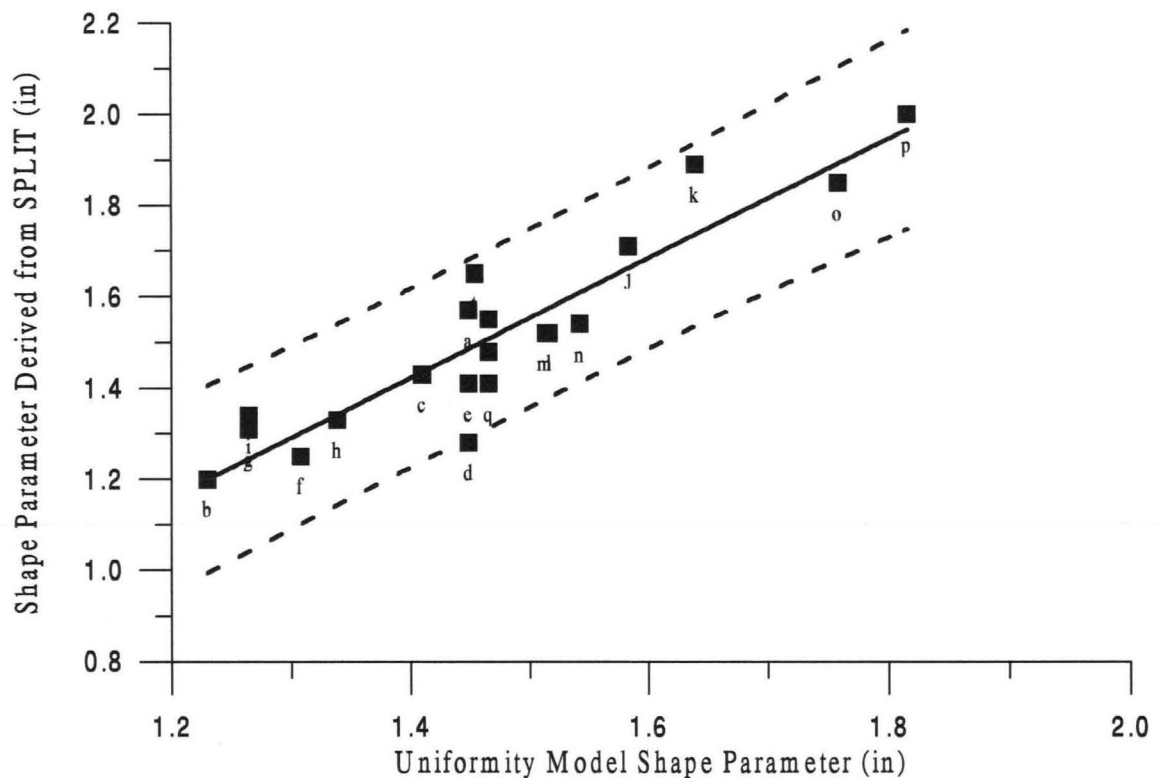


Figure 4.8 - Comparison of Fragment Size Distribution Shape Parameters: SPLIT Vs. Uniformity Model

4.7 The Equivalence of the Kuznetsov Hardness Parameter

Attention is now re-directed back onto the form of Kuznetsov's relationship for mean fragment size (Equation 4.6), repeated below as:

$$\bar{x} = A \frac{V_{rm}^{0.80}}{M_e^{0.63}} \quad (4.35)$$

where:

- \bar{x} = mean fragment size (cm);
- A = rock mass "hardness" parameter;
- V_{rm} = rock mass volume (m^3);
- M_e = equivalent mass of TNT applied to rock volume (kg).

It will be instructive to determine how well Kuznetsov's relationship models the observed data, without utilizing Cunningham's expression for rock mass blastability (Equation 4.10). Because \bar{x} , V_{rm} , and M_e are known by observation, the average rock mass hardness parameter "A" can be obtained via a non-linear regression as:

$$\hat{\bar{x}} = A \frac{V_{rm}^{0.80}}{(0.87 M_e^{tot})^{0.63}} \quad (4.36)$$

where M_e^{tot} represents the total ANFO mass (kg) used in the blasts, and $0.87 M_e^{tot}$ represents the equivalent mass of T.N.T. obtained by forming the ratio of explosive weight strengths ($0.87 = 100/115$) for ANFO and T.N.T. Performing the Equation 4.36 regression results in an average "A" value of 1.973 for the 20 data sites, and a standard deviation of 0.198. Assuming that the error associated with estimating "A" is normally distributed, then approximately 95% of the "A" population values can be expected to lie

within plus or minus two standard deviations of the mean value, or:

$$\bar{A} - 2\sigma \leq \bar{A} \leq \bar{A} + 2\sigma = 1.58 \leq 1.973 \leq 2.37 \quad (4.37)$$

Then the total range of A values is only about 0.80, which is 15 times less than the 12 unit total range proposed by Kuznetsov (Table 4.2, Section 4.3). Figure 4.9 below shows the graphical relationship between the mean fragment sizes as observed by the SPLIT system at the different sites, and the modeled mean sizes obtained with the average hardness parameter of 1.973 inserted into Equation 4.35 above. The equation of the “best fitting” solid line shown on Figure 4.9 is:

$$\bar{x}_{\text{Split}} = 0.017 \hat{x}_{\text{Kuz}} + 11.58 \quad [R^2 = 0.00025, \text{Sig. F} = 0.947] \quad (4.38)$$

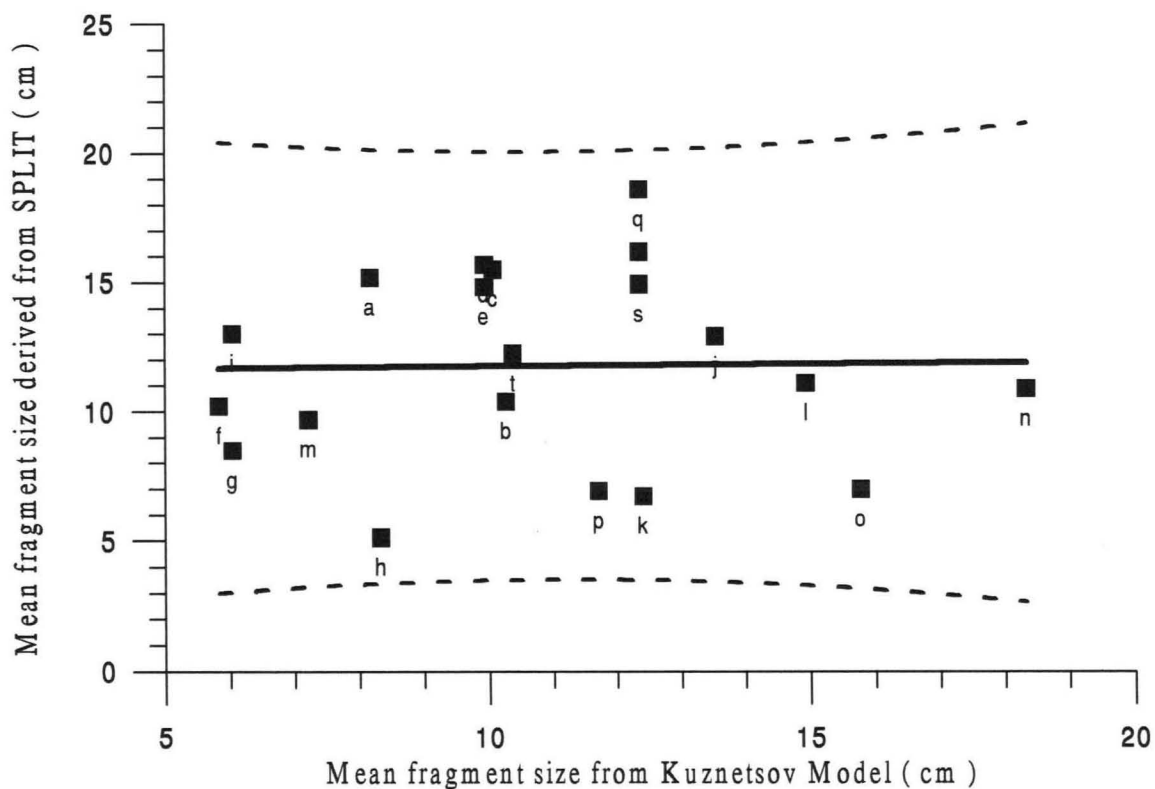


Figure 4.9 - Comparison of Mean Fragment Sizes : SPLIT Vs. Kuznetsov Model

Conclusions: Figure 4.9 indicates that the slope of the best fitting trend line is approximately zero (i.e. zero correlation) and the width of the 95% confidence interval is about 17 centimeters. The average fragment sizes observed by the SPLIT system and those predicted by the Kuznetsov Equation are at high variance.

Before Kuznetsov's Equation is put away, it will be instrumental to allow Kuznetsov's volume and explosive mass exponents to "float" in a regression such as:

$$\bar{x} = C_1 \frac{V_{rm}^{C_2}}{(0.87 M_e^{ag})^{C_3}} \quad (4.39)$$

for which the T.N.T. equivalent of explosive mass is now obtained for the above grade ANFO within the drill hole. Performing the indicated regression results in:

$$\hat{\bar{x}} = 11.32 \frac{V_{rm}^{0.350}}{(0.87 M_e^{ag})^{0.474}} \quad (4.40)$$

and the regression output results indicate that the standard deviation of \bar{A} is 3.40 units.

The 95% confidence interval for \bar{A} now becomes:

$$\bar{A} - 2\sigma \leq \bar{A} \leq \bar{A} + 2\sigma = 4.52 \leq 11.32 \leq 18.13 \quad (4.41)$$

the range of which totals 13.6, which now very closely matches the 12 unit range proposed by Kuznetsov (Table 4.2, Section 4.3). Figure 4.10 shows the relationship between the mean fragment sizes as observed by the SPLIT system at the different sites, and the modeled mean sizes predicted by Equation 4.40 above. The equation of the solid trend line shown on Figure 4.10 is:

$$\bar{x}_{Split} = 0.972 \hat{\bar{x}}_{Kuz} + 0.345 \quad [R^2 = 0.554, \text{Sig. F} = 0.002] \quad (4.42)$$

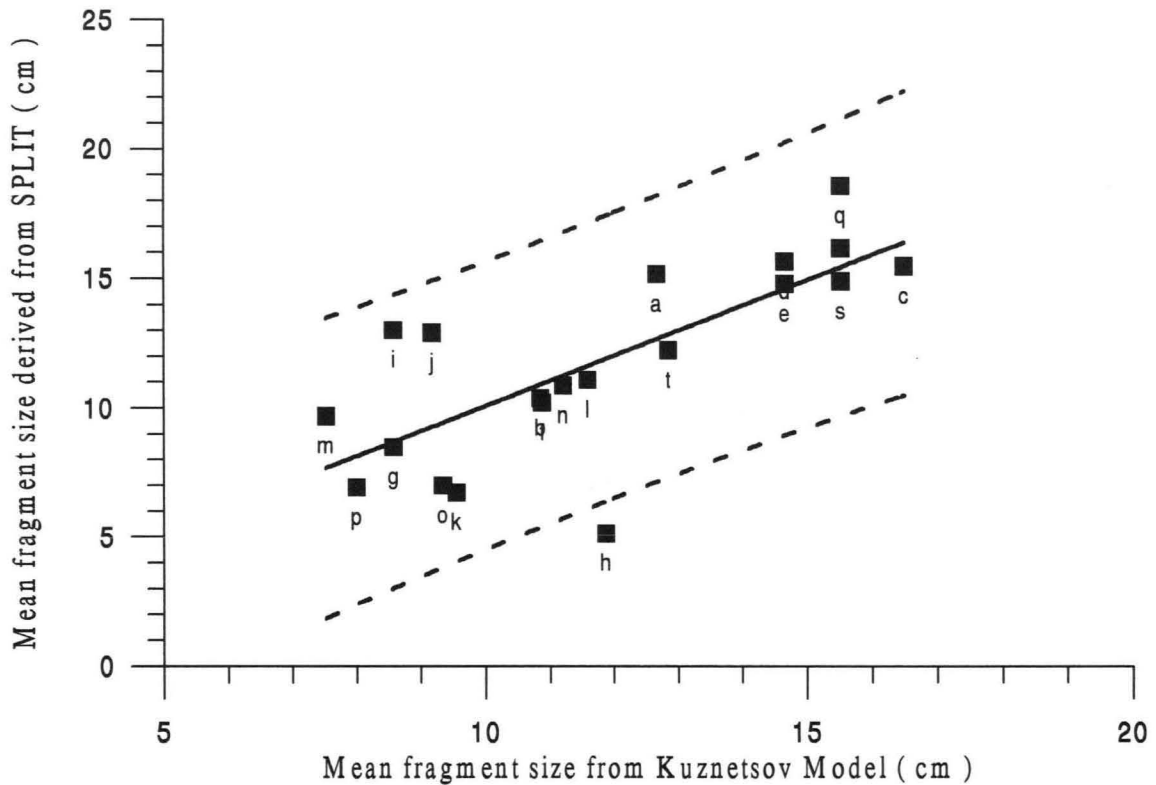


Figure 4.10 - Comparison of Mean Fragment Sizes : SPLIT Vs. Kuznetsov Model

Conclusions: Comparing Figure 4.10 to Figure 4.9, it can readily be concluded that Kuznetsov's original rock mass volume and explosive mass exponents (Equation 4.36) should change to the values represented within Equation 4.40, or else Kuznetsov's Equation is not applicable to the results of the SPLIT software.

This " tweaking " of Kuznetsov's exponents has other important implications. One important example is that Kuznetsov's hardness parameter may now be derived as a function involving the pre-blast rock mass cell imagery. Equation 4.28 for the fragment screen size distribution scale parameter is here repeated:

$$\hat{\theta}_f = 3.358 \frac{S^{0.077} V_{rm}^{0.385} \theta_{rm}^{0.152}}{E_{ag}^{0.472}} = \hat{K}_w^f{}^{0.472} \frac{\theta_{rm}^{0.152}}{E_{ag}^{0.472}} \quad (4.43)$$

and what may as well be called the “ Kuz-SPLIT ” Equation is represented by Equation 4.40, which is repeated below:

$$\hat{\bar{x}} = A \frac{V_{rm}^{0.350}}{(0.87 M_e^{ag})^{0.474}} = 11.32 \frac{V_{rm}^{0.350}}{(0.87 M_e^{ag})^{0.474}} \quad (4.44)$$

Realizing that the scale parameter serves a purpose similar to the mean in that they are both measures of central tendency, it is now proposed to determine an expression for the mean fragment screen size (cm) with the following regression:

$$\bar{x}_f = C_1 S^{C_2} \bar{x}_{rm}^{C_3} \left[\frac{V_{rm}^{0.350}}{(0.87 M_e^{ag})^{0.474}} \right] \quad (4.45)$$

where the exponent values acting on rock mass volume and explosive mass are held equivalent to those values observed in Equation 4.44, and \bar{x}_{rm} now represents the average rock mass chunk size (cm) derived from image analysis of the pre-blasted bench face. Performing the indicated regression results in:

$$\hat{\bar{x}}_f = 0.571 S^{0.043} \bar{x}_{rm}^{0.123} \left[\frac{V_{rm}^{0.350}}{(0.87 M_e^{ag})^{0.474}} \right] \quad (4.46)$$

The equation of the best fitting trend line between the mean fragment sizes observed with the SPLIT system and those predicted by Equation 4.46 is:

$$\bar{x}_{Split} = 0.969 \hat{\bar{x}}_f + 0.400 \quad [R^2 = 0.569, \text{Sig. F} = 0.0001] \quad (4.47)$$

which is virtually equivalent to Equation 4.42 above. Now Equations 4.44 and 4.46 can be equated resulting in a formulation for the Kuznetsov rock mass “hardness” term:

$$A = 0.571 S^{0.043} \bar{x}_{rm}^{0.123} \quad (4.48)$$

which aside from rock mass strength, now also includes a SPLIT derived term for the rock mass “fissuring” alluded to by Kuznetsov.

4.8 A Summary of Results for the Determination of the Rock Mass Specific Energy Term

An accurate k_{me} term is necessary to accurately perform explosive cost modeling.

The initial research activity for the determination of k_{me} was concerned with regression analysis performed around the form of Equation 1.2 from Chapter 1, here repeated as:

$$E_{re} = k_{me} f(R) \quad (4.49)$$

where E_{re} denotes the reductive energy expended by the explosive per ton of rock mass (MJ/ ton), R was the ratio of some characteristic dimensions representing the screen sizes of the rock mass “chunks” and muckpile fragments, and k_{me} relates the specific energy (MJ/ ton) consumed by the rock mass undergoing the form of size reduction represented by the function “ f ”. The results showed that the form of Equation 4.49 should probably be altered to include a ratio of functions:

$$E_{re} = k_{me} \frac{f_1(x_{rm})}{f_2(x_f)} \quad (4.50)$$

where x_{rm} and x_f are some characteristic rock mass chunk and fragment screen size, respectively. Further regression analysis then culminated in Equation 4.29

(Section 4.6.3) which was:

$$\hat{E}_{ag} = 13.0 S^{0.163} V_{rm}^{0.815} \left(\frac{\theta_{rm}^{0.321}}{\theta_f^{2.118}} \right) = \hat{K}_w^f \frac{\theta_{rm}^{0.321}}{\theta_f^{2.118}} \quad (4.51)$$

where E_{ag} was the estimated above grade energy (MJ); S was the rock strength (MPa); V_{rm} was the rock mass volume (m^3); θ_{rm} and θ_f were the 63rd percentile values of screen size for the rock mass and fragments, respectively (in), and \hat{K}_w^f was the estimated metric “ Weibull Blast Index ” (MJ- in^{1.79}). The strength and volume terms within Equation 4.51 were developed in metric units for purposes of realistic comparison with the results of the Kuz-Ram metric model. But the cost equations of Chapter 2 assume cubic yards as the fundamental unit of rock mass volume. The strength and volume terms on the right hand side of Equation 4.51 above can be expressed in English units as:

$$\hat{E}_{ag} = 4.54 S^{0.163} V_{rm}^{0.815} \left(\frac{\theta_{rm}^{0.321}}{\theta_f^{2.118}} \right) = \hat{K}_w^{fE} \frac{\theta_{rm}^{0.321}}{\theta_f^{2.118}} = 0.35 \hat{K}_w^f \frac{\theta_{rm}^{0.321}}{\theta_f^{2.118}} \quad (4.52)$$

where S and V_{rm} now assume units of lbf/in² and yd³ respectively. Then pursuant to the development of Section 2.1 and Equation 4.50 above, the k_{me} term (MJ - in^{1.79} /ton) can be estimated as:

$$\hat{k}_{me} = \frac{\hat{K}_w^{fE}}{\rho_b V_{rm}} \quad (4.53)$$

where ρ_b is the bank density (ton/yd³) of the rock mass volume V_{rm} (yd³). Thus formulated, the estimated k_{me} term of the above equation represents the resistance of the rock mass to the explosive mode of size reduction, where the “size reduction” must be

expressed as a ratio of functions acting upon the 63rd percentile screen size values of the pre-blast rock mass chunks and post-blast fragments.

4.9 Estimators for Fragment Screen Size Distribution Scale Parameters

The previous Chapter showed how shot-rock muckpiles can be characterized by a 2 parameter Weibull distribution. In the next Chapter, machine production will be developed as a function of such a distribution. In Section 4.6.5 of the current Chapter, an estimator for the distribution shape parameter was presented. Therefore to completely characterize the fragment size distribution, an estimator for the distribution scale parameter is necessary. This can be accomplished by simply back-solving Equation 4.52 above for fragment scale parameter resulting in an estimator of :

$$\hat{\theta}_f = 2.05 S^{0.077} V_{rm}^{0.385} \frac{\theta_{rm}^{0.152}}{E_{ag}^{0.472}} = \left(\hat{K}_w^{fE} \right)^{0.472} \frac{\theta_{rm}^{0.152}}{E_{ag}^{0.472}} \quad (4.54)$$

But the above expression can be transformed into a basic “Kuznetsov” form by rearranging terms:

$$\hat{\theta}_f = 2.05 S^{0.077} \theta_{rm}^{0.152} \frac{V_{rm}^{0.385}}{E_{ag}^{0.472}} = A_{\theta} \frac{V_{rm}^{0.385}}{E_{ag}^{0.472}} \quad (4.55)$$

where the subscript on the rock mass constant A_{θ} denotes that the rock mass chunk screen size scale parameter was utilized to determine the hardness parameter. The two equations above have different interpretations:

1. The \hat{K}_w^{fE} term in Equation 4.54 is theorized as constant over certain ranges of S and V_{rm} ;

2. the A_{θ} term of Equation 4.55 is theorized as constant over certain ranges of S and θ_{rm} ;
3. S and θ_{rm} are functions of V_{rm} ;
4. thus θ_f is related to V_{rm} explicitly by Equation 4.55 and implicitly by Equation 4.54.

4.10 The Estimated Cost of the Explosive Mode of Size Reduction

In Section 2.1, Equation 2.1 was developed to express the dollar per ton cost of blasting rock mass as:

$$C_e = (a_e + b_e) \left(\frac{k_{me} f(R)}{e_m} \right) \quad (4.56)$$

where $a_e + b_e$ were the costs of owning and operating the powder loading equipment (\$/lb), k_{me} was the specific energy (MJ/ton) consumed by the rock mass undergoing the functional form (f) of dimensionless size reduction (R), and e_m was the mass specific energy of the explosive (MJ/lb). The results of the previous Section demonstrated that C_e will have to be estimated as:

$$\hat{C}_e = (a_e + b_e) \left[\frac{\hat{k}_{me} \left(\frac{\theta_{rm}^{0.321}}{\theta_f^{2.118}} \right)}{e_m} \right] \quad (4.57)$$

where \hat{k}_{me} (Equation 4.53) has units of MJ - in^{1.79} /ton, and θ_{rm} and θ_f were the 63rd percentile values of the Weibull screen size distributions representing the rock mass and fragments respectively. The next Chapter is primarily concerned with estimating the cost of loading machines, and the work presented in Chapter 6 estimates the cost of the

drilling machine. The cost of the explosive mode of size reduction will be discussed yet again in the total excavation cost model developed in Chapter 7.

5. PRODUCTION AND COST ESTIMATORS FOR LOADING MACHINES

“ There are several kinds of shovels as regards quality, shapes and lengths of handle, and shape of blade. Handles are long or short and the end may be pointed or square. The blade may be round, half round, or square, and the shape of the blade may vary from flat to that of a scoop. The material to be handled, the place in which the shovel is to be used, the kind of work, etc., will govern the choice. ”

Wilson, Cunningham, and Butler (1934) --- *Arizona Lode Gold Mines and Gold Mining*

The goal of this chapter is the derivation of production and cost estimators for shot-rock loading machines. One dependent variable for the estimators is taken as the 100th percentile value of the fragment screen size distribution. The following list summarizes the work:

1. Machine production is derived as a function of perfect cycle time and shear cycle time (Section 5.1);
2. total machine cycle time trends are considered at different ranges of screen size (Section 5.2);
3. estimators for total machine production are derived (Section 5.3);
4. the effect of shear cycle time upon estimated total machine production is investigated (Section 5.4);
5. the machine cost estimator is developed (Section 5.5).

5.1 Machine Production and Total Cycle Time

In Section 3.4.3, production (tons/hr) was defined on a per truck basis as:

$$P_m = \left(\frac{3600 \rho_h V_t F_t}{t_{\text{truck}}} \right) = \left(\frac{3600 C_{\text{truck}}}{t_{\text{truck}}} \right) \quad (5.1)$$

where ρ_h is the heaped muckpile density (ton/yd³), V_t is the volume of the truck bed (yd³), F_t is the truck fill factor (dimensionless), C_{truck} is rated capacity (tons) of the truck, and t_{truck} is the truck load time (s) observed from the video imagery. Average machine production for a site is then defined as:

$$\bar{P}_m = \frac{1}{n} \sum_{i=1}^n (P_m)_i \quad (5.2)$$

where n is the total number of trucks filled by the machine. Average machine production was also defined in Section 3.4.3 as:

$$\bar{P}_m = \frac{\bar{\rho}_h V_b \bar{F}_b}{\bar{t}_{tot}} \quad (5.3)$$

where V_b is the struck bucket volume (yd³), and $\bar{\rho}_h$, \bar{t}_{tot} and \bar{F}_b are the hourly average values for the heaped muckpile density (tons/yd³), total machine cycle time (hr), and bucket fill factor. V_b and \bar{t}_{tot} are known from observation, but because $\bar{\rho}_h$ and \bar{F}_b are unknown, their product is treated as a constant:

$$\bar{P}_m = \bar{C}_\rho^F \frac{V_b}{\bar{t}_{tot}} \quad (5.4)$$

and the values of \bar{C}_ρ^F (tons/yd³) at the various machine loading sites are obtained by regression. The total average machine cycle time term of Equation 5.3 above was defined (Section 2.2) to be:

$$\bar{t}_{tot} = \frac{-\bar{k}_m}{s_f - W_b} = \bar{t}_p + \bar{t}_s \quad (5.5)$$

where \bar{k}_m (in · hrs) is the average machine constant, W_b (in) is bucket width, s_f (in)

is fragment screen size (in), \bar{t}_p (hr) is the “ perfect ” cycle time, and \bar{t}_s is the “ shear ” cycle time (hr), or the time expended in shearing or ploughing fragments with the bucket. The function represented by Equation 5.5 was defined only over the size interval $0 \leq s_f < W_b$. Perfect cycle time is defined at $s_f = 0$, or $\bar{t}_{tot} = \frac{\bar{k}_m}{W_b} = \bar{t}_p$. Above $s_f = 0$, shear cycle time adds to perfect cycle time until $s_f \rightarrow W_b$, and $\bar{t}_{tot} \rightarrow \infty$.

5.2 Total Cycle Time and Fragment Screen Size Considerations

Loading machine performance was assessed at the 100th percentile values of the fragment screen size distributions. For instance if the 100th percentile screen size value at a site is 20 inches, then there exists a 100 percent probability that the screen sizes of all of the fragments are less than or equal to 20 inches. Then as long as the loading machine bucket width is greater than 20 inches, all of the fragments can be loaded with 100 percent certainty. If the bucket width is less than 20 inches, then the total machine cycle time is undefined for fragments beyond 20 inches of screen size (Equation 5.5 above), and certain fragments contained within the distribution are never loaded.

The cumulative form of the Weibull distribution was presented in Section 3.7.2 as:

$$F(x) = 1 - \exp \left[- \left(\frac{x}{\theta} \right)^n \right] \quad (5.6)$$

where $F(x)$ is the probability ($0 \leq P \leq 1$) that the variate takes a value less than or equal to x , and θ and n are the scale and shape parameters of the distribution, respectively.

The distribution parameters for the fragment screen sizes at a loading site are estimated as discussed in Section 3.7.2; and thus the screen size (x) associated with any percentile value can be determined with Equation 5.6. However, at the 100th percentile value, $F(x) = 1.0$ in Equation 5.6, and:

$$\exp \left[- \left(\frac{x}{\theta} \right)^n \right] = 0 \quad (5.7)$$

for which $x = 0$ for both θ and $n > 0$. For the machine production modeling, this problem was overcome simply by approximating the 100th percentile value as $F(x) = 0.999$. Then the screen size approximating the 100th percentile can be obtained by back-solving for x as:

$$x_f^{100} \cong \theta (6.90)^{1/n} \quad (5.8)$$

Now taking $s_f = x_f^{100}$, and because \bar{t}_{tot} , and W_b are also known from observation, k_m values for the various machines can be determined via regression analysis.

Figure 5.1 shows some results for the large (11.7 yd³) front end loader population. The average total machine cycle time is expressed in minutes. The observed 100th percentile values (■) of fragment screen size range from 5 to 85 inches. A solid trend line has been fit over the range of the observed data, and a dashed line represents the trend of the average modeled total cycle time curve (obtained with Equation 5.5 above) within the range of observed data. The modeled time curve exhibits much more sensitivity (greater slope) than does the observed data trend line. The difference in sensitivity between the two trends is perhaps best explained by expanding the screen size range out

towards the W_b term (bucket width) of Equation 5.5. Figure 5.2 shows the results of such a total cycle time extrapolation for the large front end loaders; i.e. the probable machine behavior if production at sites with larger 100th percentile sizes could have been sampled.

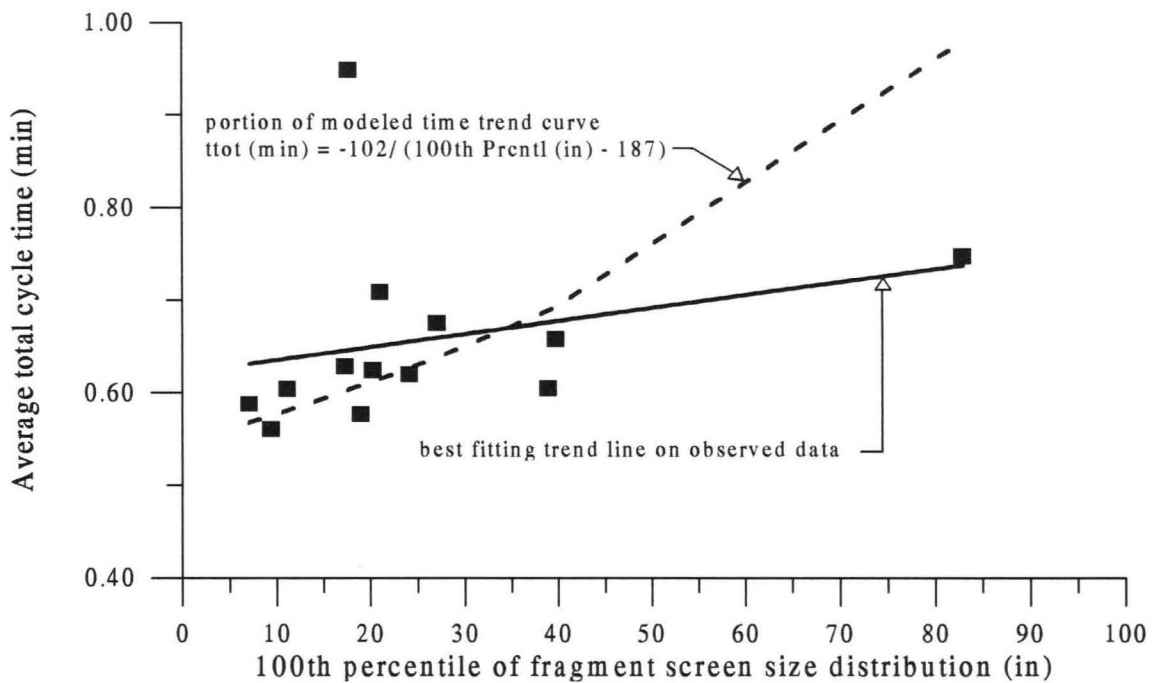


Figure 5.1 - The Observed and Modeled Average Total Cycle Times for Large Front End Loaders Over the Range of the Observed Data

On Figure 5.2, both the non-linear modeled time trend and the best fitting trend line (both on the observed data) have been projected out towards the bucket width (W_b) of the loaders. Beyond a screen size of about 40 inches, the modeled trend rapidly diverges above and away from the projection of the observed trend. As 100th percentile fragment size approaches the bucket width term W_b (which is 187 inches for these large front end loaders) the total cycle time approaches infinity, and the production will approach zero

(Equation 5.4) simply because certain fragments will never be loaded into the bucket.

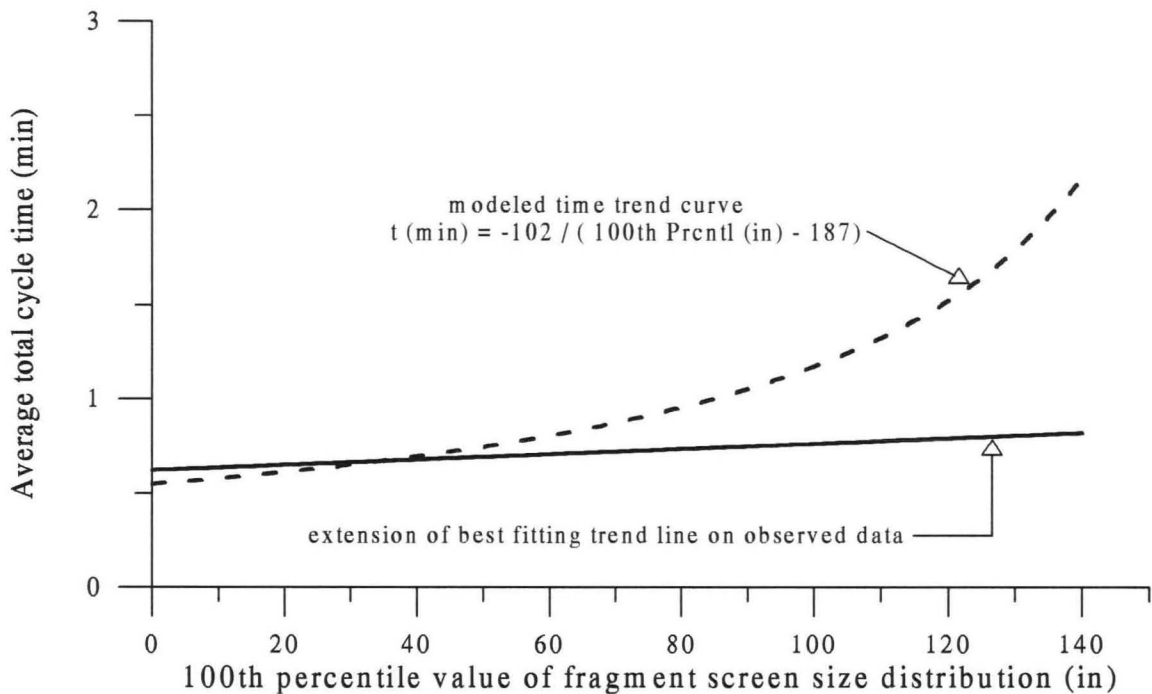


Figure 5.2 - The Observed and Modeled Average Total Cycle Times for Large Front End Loaders Extended Out Towards the Bucket Width

5.3 Machine Production Estimators

If Equation 5.5 above is substituted into Equation 5.4, then an expression for average machine production (tons/hr) as a function of fragment screen size results:

$$\hat{P}_m = \left(\frac{\hat{C}_p^F}{-\hat{k}_m} \right) V_b (s_f - W_b) \quad (5.9)$$

where the “bar” symbols (—) atop the variates indicate averages, and the “hat” symbols (^) indicate estimators. “Perfect production” is defined at $s_f = 0$:

$$\hat{P}_{mp} = \left(\frac{\hat{C}_p^F}{\hat{k}_m} \right) V_b W_b \quad (5.10)$$

To facilitate the analysis, machines of the same type were classified into different ranks according to bucket volume range. Then 5.10 above becomes:

$$\hat{P}_{mp} = \left(\frac{\hat{C}_p^F}{\hat{k}_m} \right) \bar{V}_b \bar{W}_b \quad (5.11)$$

The estimated standard deviation of the average production was assessed with the uncertainty analysis technique presented in Section 3.9:

$$\hat{\sigma}_{\hat{P}_{mp}} = \left[\left(\frac{\partial \hat{P}_{mp}}{\partial \hat{C}_p^F} \hat{\sigma}_{\hat{C}_p^F} \right)^2 + \left(\frac{\partial \hat{P}_{mp}}{\partial \hat{k}_m} \hat{\sigma}_{\hat{k}_m} \right)^2 + \left(\frac{\partial \hat{P}_{mp}}{\partial \bar{V}_b} \hat{\sigma}_{\bar{V}_b} \right)^2 + \left(\frac{\partial \hat{P}_{mp}}{\partial \bar{W}_b} \hat{\sigma}_{\bar{W}_b} \right)^2 \right]^{1/2} \quad (5.12)$$

The estimated coefficient of variation for the average estimated perfect machine production (tons/hr) is:

$$\hat{\gamma}_{\hat{P}_{mp}} = \frac{\hat{\sigma}_{\hat{P}_{mp}}}{\hat{P}_{mp}} \quad (5.13)$$

Table 5.1 presents some results of the machine regression analysis. The numbers in square brackets are the standard deviations of the values directly above them. The average perfect cycle time terms for the machines were estimated as:

$$\hat{t}_p = \frac{\hat{k}_m}{\bar{W}_b} \quad (5.14)$$

and converted to minutes to facilitate entry into the table. The standard errors of the perfect cycle time terms were assessed in a manner similar to that used for Equation 5.11 above.

Table 5.1 - Perfect Machine Production for Different Types and Classes of Loading Machines

Machine Class and Type	\hat{C}_p^F (tons per yd ³)	\hat{k}_m Machine Cnstnt. (in - hrs)	\bar{V}_b Struck Bckt. Vol. (yd ³)	\bar{W}_b Bckt Width (in)	\hat{t}_p Perfect Cycle Time (min)	$\hat{\gamma}_{\hat{t}_p}$ Perfect Cycle Time COV	\hat{P}_{mp} Perfect Prod. (tons per hr)	$\hat{\gamma}_{\hat{P}_{mp}}$ Pefect Prod. COV
large front end loaders (11.7 yd ³)	1.660 [0.052] ¹	1.700 [0.092]	11.7 [0]	187 [0]	0.545 [0.029]	0.054	2136 [67]	0.031
extra-large front end loaders (21.3 yd ³)	1.530 [0.054]	2.477 [0.163]	21.3 [0]	222 [0]	0.669 [0.044]	0.065	2920 [103]	0.035
medium cable shovels (19 to 22 yd ³)	1.673 [0.053]	0.809 [0.044]	20.6 [1.58]	108 [0]	0.449 [0.024]	0.054	4600 [382]	0.083
large cable shovels (34 to 41 yd ³)	1.280 [0.131]	0.921 [0.044]	37.8 [3.50]	156 [16.42]	0.354 [0.073]	0.208	8195 [1423]	0.174
extra-large cable shovels (56 yd ³)	1.430 [0.027]	1.54 [0.017]	56 [0]	192 [0]	0.481 [0.005]	0.011	9984 [188]	0.019
medium hydraulic shovels (18 to 23.5 yd ³)	1.206 [0.065]	1.002 [0.058]	21 [2.03]	151.5 [16.20]	0.396 [0.048]	0.021	3829 [589]	0.154
large hydraulic shovels (25 to 27 yd ³)	1.205 [0.063]	0.905 [0.077]	25.8 [1.09]	134 [28.56]	0.405 [0.092]	0.229	4603 [1028]	0.224

Note 1: Numbers in square brackets are standard deviations.

The principal results of Table 5.1 will be interpreted comparatively on bar charts.

Figure 5.3 presents the estimated perfect cycle averages for the six different ranks of loading machines, and Figure 5.4 presents the perfect productions. Referring first to Figure 5.3:

- Large and extra large front end loaders (LFEL and XLFEL, respectively) exhibit the longest average perfect cycle time, followed by cable shovels (suffixes CS) and then hydraulic shovels (suffixes HS) respectively.

Now referring to Figure 5.4:

- Front end loaders exhibit the lowest perfect production, followed by the hydraulic shovels and cable shovels, respectively.

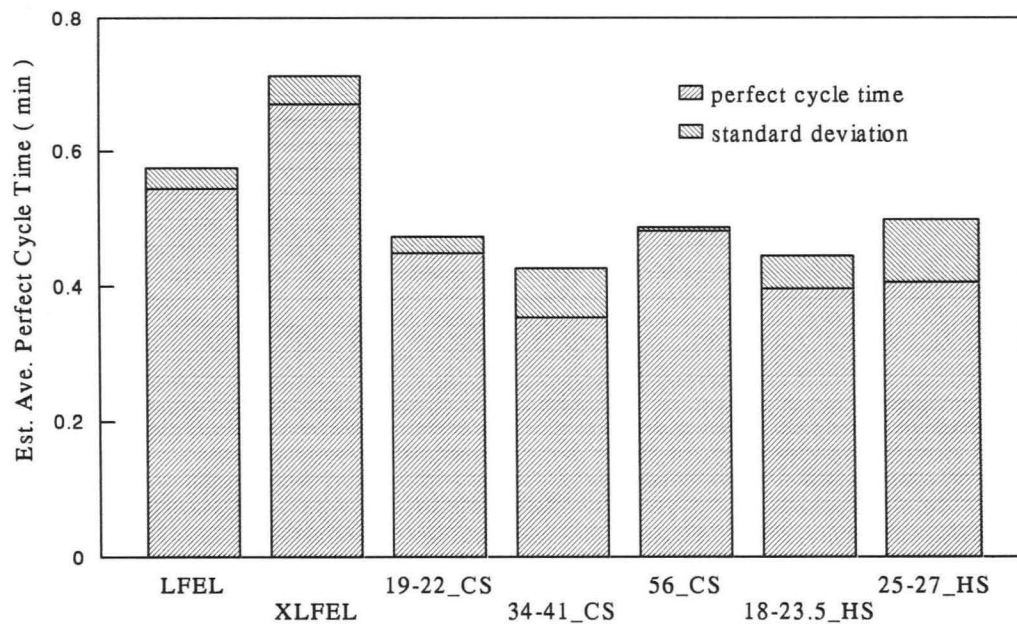


Figure 5.3 - Estimated Average Perfect Cycle Times for the Different Machine Ranks

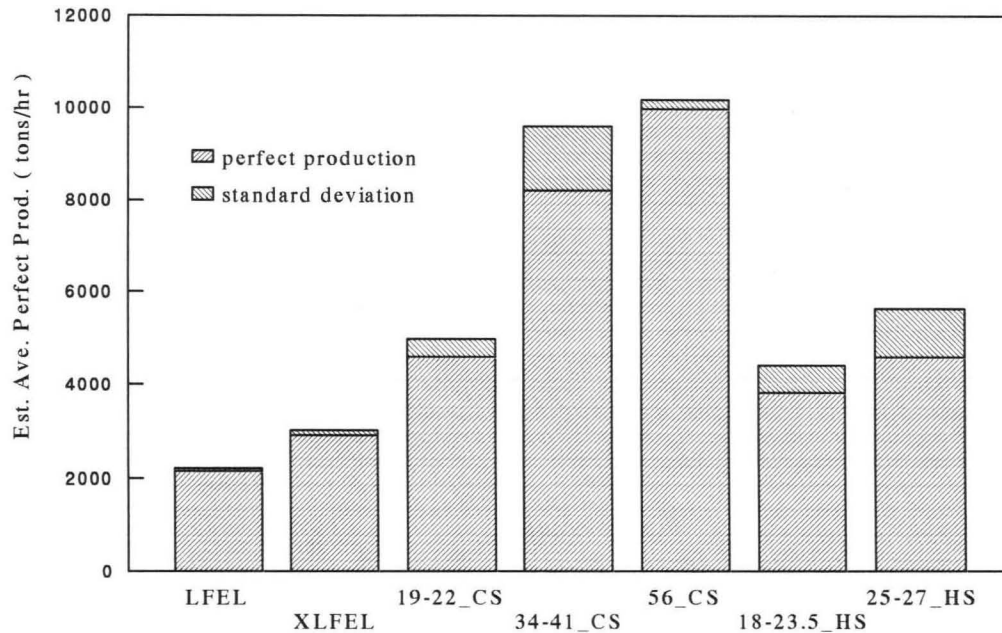


Figure 5.4 - Estimated Average Perfect Productions for the Different Machine Ranks

5.4 Shear Cycle Time and Machine Production

Now the influence of the shear cycle time (Equation 5.5) can be added to the perfect cycle time for the different machine ranks. The resulting estimated averages of the total cycle time for the different machine ranks are presented over a very large 100th percentile size range fragment size scale on Figure 5.5:

- Below 100th percentile screen size values of about 50 inches, the total average estimated cycle time for all machine ranks appears about the same;
- all of the total average estimated cycle times for the different machine ranks diverge sharply upwards near certain screen size values, signifying that the 100th percentile fragment size is approaching the average bucket width for the particular machine rank.

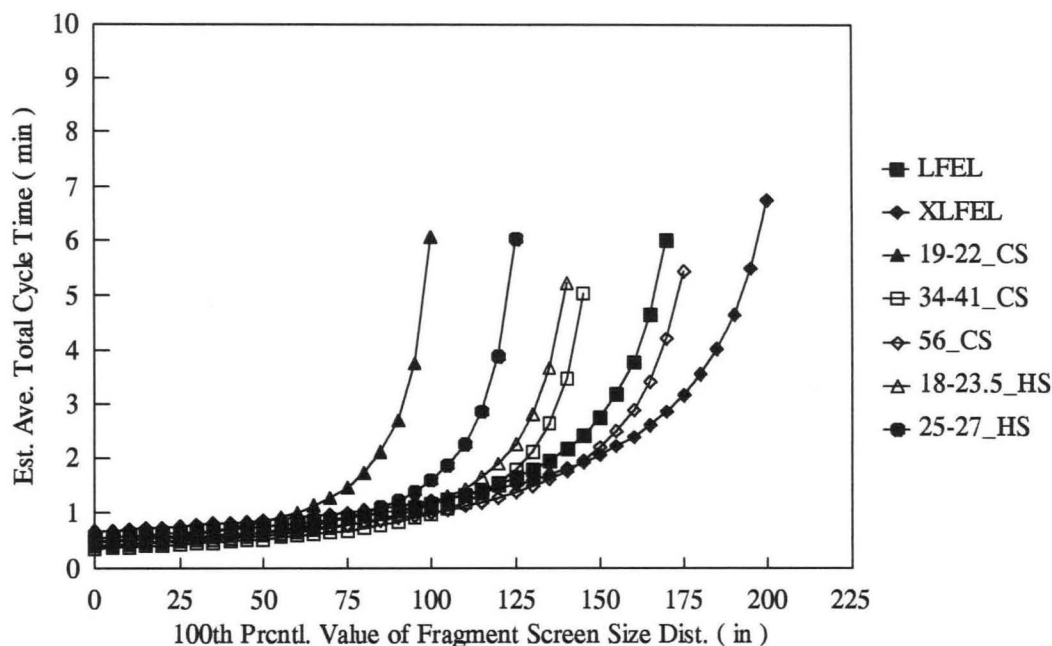


Figure 5.5 - Estimated Average Total Cycle Times for the Different Machine Ranks

The largest fragment size observed at the sites was about 85 inches. Then Figure 5.6 shows the total average estimated cycle times for the different machine ranks over a 100th percentile fragment screen size range of 90 inches. The cycle time scale is held to less than 1.5 minutes:

- The 34 to 41 yd³ class of cable shovels have the lowest estimated total cycle times regardless of the 100th percentile value of fragment screen size;
- the extra-large front end loaders have the highest total estimated cycle times below 100th percentile screen size values of about 50 inches;
- above 50 inches, the 19 to 22 yd³ class of cable shovels have the largest cycle times;
- for any 100th percentile value of fragment screen size, the total cycle time differentials between machine ranks represented by the large front end loaders, extra-large front end loaders, 56 yd³ cable shovels, and 34 to 41 yd³ cable shovels appears uniformly equal;

- the total cycle time differentials between machine ranks represented by the 19 to 22 yd³ cable shovels, 25 to 27 yd³ hydraulic shovels, and 18 to 23.5 yd³ hydraulic shovels is not equal at any 100th percentile value of fragment screen size.

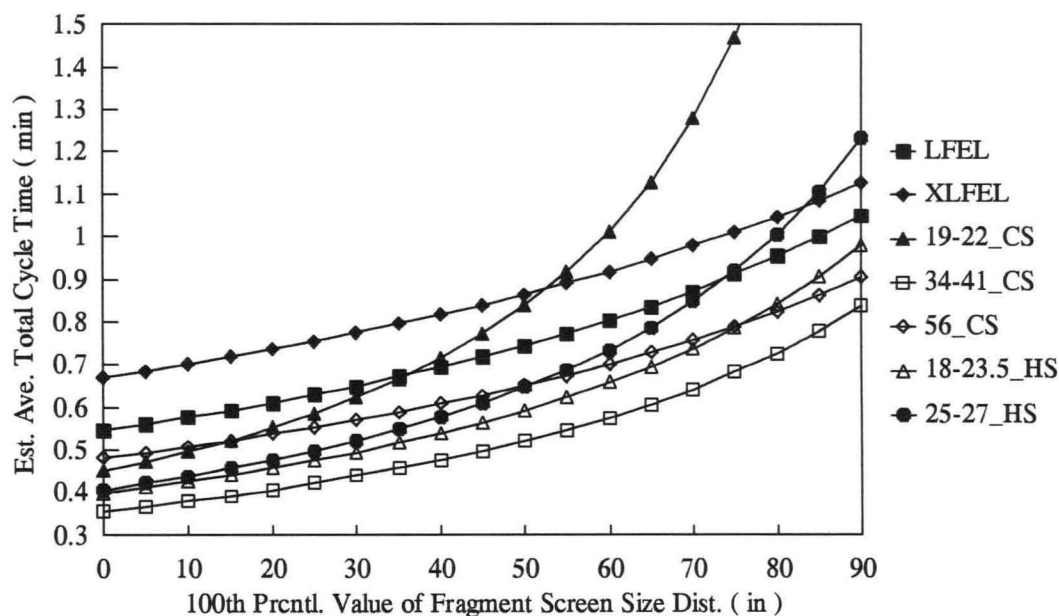


Figure 5.6 - Estimated Average Total Cycle Times for the Different Machine Ranks over 90 inches of 100th Percentile Screen Size Range

Figure 5.7 below shows the relationships between estimated total machine productions and 100th percentile fragment screen sizes. The 100th percentile size range exhibited is taken at 225 inches to correspond to the maximum observed value of bucket width (the extra large front end loaders). The lines intercept the horizontal axis (i.e. zero production) at fragment size values corresponding to the machine bucket widths. The vertical axis intercepts (i.e. zero 100th percentile size) correspond to the machine's perfect production. Figure 5.7 shows that when machine production is expressed as a function of 100th percentile fragment size, production is inversely proportional to the

machine's sensitivity to fragment size:

- The cable shovels exhibit the highest total estimated production but the greatest sensitivity (greatest slope) to 100th percentile screen size;
- the front end loaders exhibit the lowest total estimated production but the lowest sensitivity;
- the production and sensitivity of the hydraulic shovels is between that of front end loader and cable shovels.

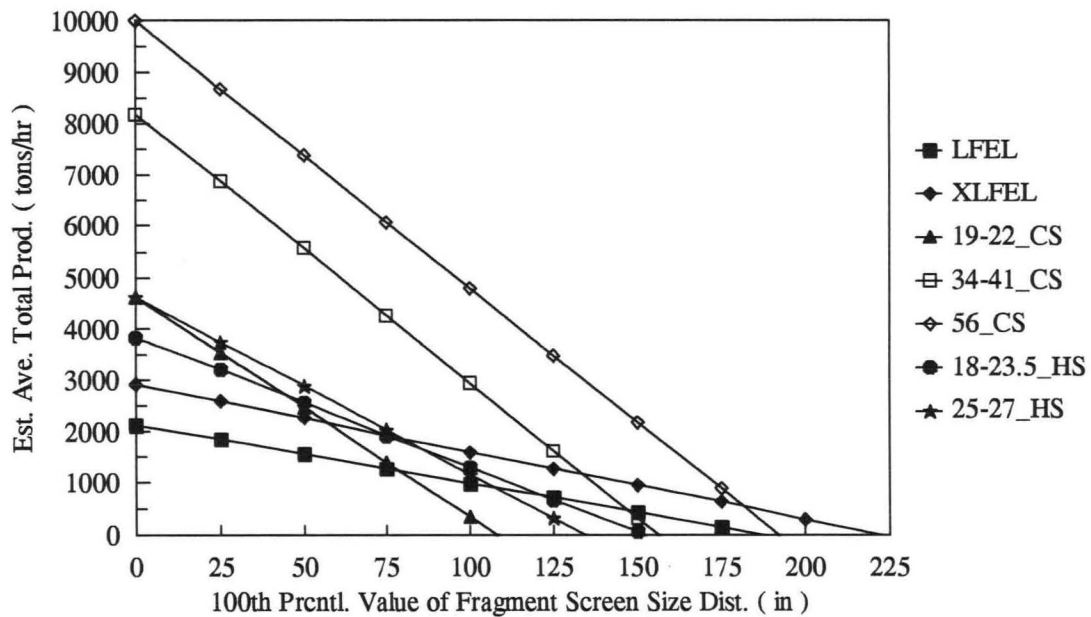


Figure 5.7 - Estimated Average Total Productions for the Different Machine Ranks over 225 inches of 100th Percentile Screen Size Range

5.5 The Machine Cost Estimator

In Section 2.2, average machine cost (Equation 2.18) was developed as:

$$C_m = \frac{\left(\frac{k_m}{W_b}\right)}{\left(1 - \frac{s_f}{W_b}\right)} \left(\frac{a_m + b_m}{\bar{\rho}_h V_b \bar{F}_b}\right) \tag{5.15}$$

where a_m and b_m represented the total costs (\$/hr) of owning (or leasing) and operating the excavating machine, respectively. The operating cost term was conveniently defined to include machine availability and utilization. The average machine cost estimator can be expressed as:

$$\hat{C}_m = \frac{\left(\frac{\hat{k}_m}{W_b} \right)}{\left(1 - \frac{x_f 100}{W_b} \right)} \left(\frac{a_m + b_m}{\hat{C}_\rho^F V_b} \right) \quad (5.16)$$

This estimator for machine cost is then utilized in the total excavation cost model developed in Chapter 7. The cost estimator for drilling machines is developed within the next Chapter.

6. DRILL PRODUCTIVITY AND THE STRENGTH OF ROCK MASS

“ It was in Spokane on October 25, 1901, that Walt Bradshaw and Joe Freethy, another Butte driller, drove fifty-five inches into hard rock in fifteen minutes, a world record that has never been surpassed. Some old-timers refuse to accept this achievement as a world record, claiming that Gunnison granite was not used. This type of rock, quarried at Gunnison Colorado, is known as the hardest of granites. Old-timers contend that no marks were considered as official unless Gunnison Granite was used. Ed Chamberlain, Cripple Creek, and Carl Maka, Leadville, drilled what is said to be the deepest hole ever put down in Gunnison Granite by two men. Their record is 46 and 5/8 inches, made at Bisbee, Arizona, in 1903.”

Marsh (1943) --- Copper Camp .

The goal of this Chapter is the development of estimators for the productivity and cost of drilling machines. This goal required a model relating rock mass strength to drill penetration rate. The blasting models presented in Chapter Four demonstrated that the fragmentation of a rock mass is related to the uniaxial compressive strength of the rock mass. The uniaxial rock strength values used in the fragmentation regression analysis were obtained by performing laboratory tests upon cores bored from rock mass grab samples after the rocks composing the sites were blasted. Because such tests are impractical for implementation into a computer based system of rock mass size reduction, rock mass strength will have to be determined through the drilling function. This Chapter is summarized as:

1. The observed data is presented (Section 6.1);
2. the observed data is modeled with an empirical penetration rate formula obtained from the literature (Section 6.2);
3. the penetration rate formula is utilized to obtain an estimate of rock mass strength (Section 6.3);

4. production and cost estimators for the drilling machine are developed (Section 6.4). These estimators are then utilized in the excavation cost model developed in Chapter 7.

6.1 The Observed Drill and Strength Data

Gathering and assessment of drilling data was not included as part of the original Caterpillar Contract (Section 3.1), but when the field note information portions of the original data set were catalogued into a series of site data bases, it was revealed that the penetration rates of rotary production drills had been inadvertently recorded at three sites within the same Copper mine. After the results of laboratory rock strength tests had been entered into the database, it was discovered that these same three sites could also be characterized with uniaxial compressive strength data. From a statistical standpoint, the amount of drilling data obtained is inadequate, and moreover the data is incomplete because variables such as bit thrust and r.p.m. and cumulative bit hours of the drill are unknown. But the known information will be presented and interpreted in this section to demonstrate the use of a previously published empirical drilling formula. Table 6.1 summarizes this information, and Figure 6.1 shows the form of the graphical relationship between penetration rate and the measured uniaxial compressive strength of the rock.

Table 6.1 - Rotary Penetration Rate, Bit Diameter, and Rock Strength Data for Three Sites at Mine Cu2

Site	Drill Penetration Rate r_d (ft/hr)	Bit Diameter ϕ (in)	Uniaxial Compressive Strength S (lbf/in ²)
Cu2SD	72	10.625	22,600
Cu2SG	66	10.625	25,700
Cu2SF	78	10.625	15,200

The equation of the linear trend line shown on Figure 6.1 shows that for the 3 sites at Mine Cu2, the penetration rate decreases by about one one-thousandths of a foot per hour per unit increase in rock strength:

$$r_d = (-1.080 \times 10^{-3}) S + 94.90 \quad [R^2 = 0.947, \text{Sig } F = 0.147] \quad (6.1)$$

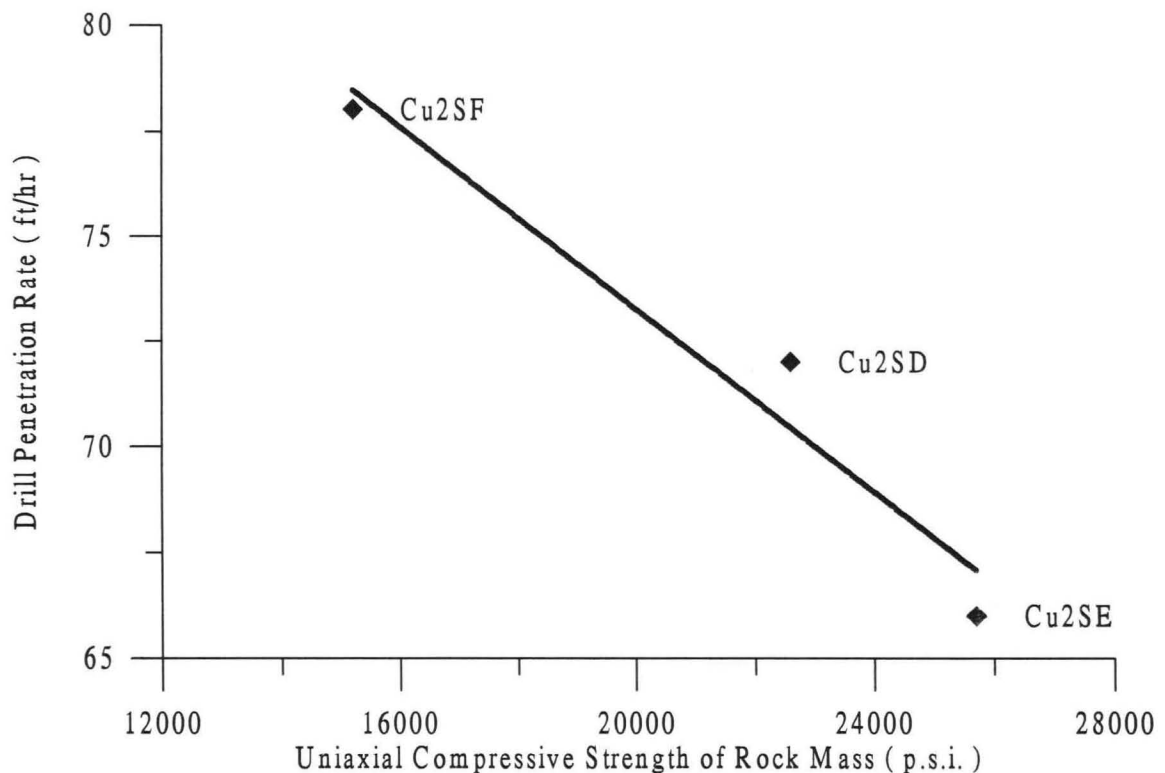


Figure 6.1 - Rotary Drill Penetration Rate Vs. Observed Rock Strength for Three Sites at Mine Cu2

6.2 The Bauer and Calder Rotary Drilling Penetration Rate Formula

In the late 1960's, two Canadian Engineers published an empirical equation for the penetration rate of a rotary rock drill. The form of the equation was derived by regression analysis performed upon an extensive set of field and laboratory observations [Bauer and Calder, 1967]:

$$r_d = \frac{(61 - 28 \log_{10}(S)) T \dot{\theta}}{250 \phi} \quad (6.2)$$

where:

- r_d = drill penetration rate (ft/hr);
- S = uniaxial compressive rock strength (lbf/in² x 10⁻³);
- T = axial thrust on drill bit (lbf x 10⁻³);
- $\dot{\theta}$ = bit rotation rate (rev/min);
- ϕ = hole diameter (in).

Equation 6.2 can be back-solved for rock strength:

$$S = 147.9 \cdot 10^{-0.035 \left[\frac{r_d \phi}{T \dot{\theta}} \right]} \quad (6.3)$$

Therefore if the four variables on the right hand side of the above equation can be monitored, then the strength of the rock mass within which the drill operates can be determined. This strength value can then be utilized within the fragmentation model (Chapter 4) to help determine the amount of explosive loaded into the drill hole to blast the rock mass into fragment sizes that minimize the machine loading cost.

It would be useful to compare the recorded rock strength values for the sites with the values predicted by Equation 6.3. However, from Table 6.1, only two of the four required variables are known (penetration rate and bit diameter); there is no thrust or rotation rate data for the bits used to drill the three sites. Therefore it is proposed to simplify Equation 6.2 into the following form:

$$\bar{r}_d = \frac{\hat{d}_{m1} - \hat{d}_{m2} \log_{10}(S)}{\phi} \quad (6.4)$$

where \hat{d}_{m1} and \hat{d}_{m2} are drill machine constants. Performing a regression of the above form on the data of Table 6.1 results in:

$$\hat{r}_d = \frac{2984.4 - 514.3 \log_{10}(S)}{\phi} \quad [R^2 = 0.920] \quad (6.5)$$

so from known observations on penetration rate, rock strength, and bit diameter, the drilling machine can be calibrated. Then the drill can be used for estimating the strength of the rock it perforates, as shown below.

6.3 An Estimator for Rock Mass Strength

Back-solving Equation 6.4 above for the base 10 logarithm of strength results in:

$$\log_{10}(S) = \frac{\hat{d}_{m1}}{\hat{d}_{m2}} - \frac{\bar{r}_d \phi}{\hat{d}_{m2}} \quad (6.6)$$

from which S can be solved as:

$$S = 10^{\left(\frac{\hat{d}_{m1}}{\hat{d}_{m2}} - \frac{\bar{r}_d \phi}{\hat{d}_{m2}} \right)} \quad (6.7)$$

Substituting the drill constants determined from the Mine Cu2 drill (Equation 6.5) results in a strength estimator of:

$$\hat{S} = 630,957 \cdot 10^{-1.94 \cdot 10^{-3} (\bar{r}_d \phi)} \quad (6.8)$$

Figure 6.2 shows the results of plotting the estimated rock mass strengths (Equation 6.8) against the observed penetration rates at the 3 sites. The equation of the linear trend line is:

$$\hat{S} = -995.6 \bar{r}_d + 92,947 \quad [R^2 = 0.99, \text{Sig } F = 0.051] \quad (6.9)$$

- The total height of the 95% prediction interval for a new estimated value of rock mass strength on any new individual observation of penetration rate is large, and is about 20,000 p.s.i.;
- one reason for the large 95% prediction interval value is the wide range and limited amount of observed penetration rate data, which results in a large value of sample standard deviation;
- larger penetration rate and rock strength sample populations may or may not improve the predictive accuracy of the rock strength model.

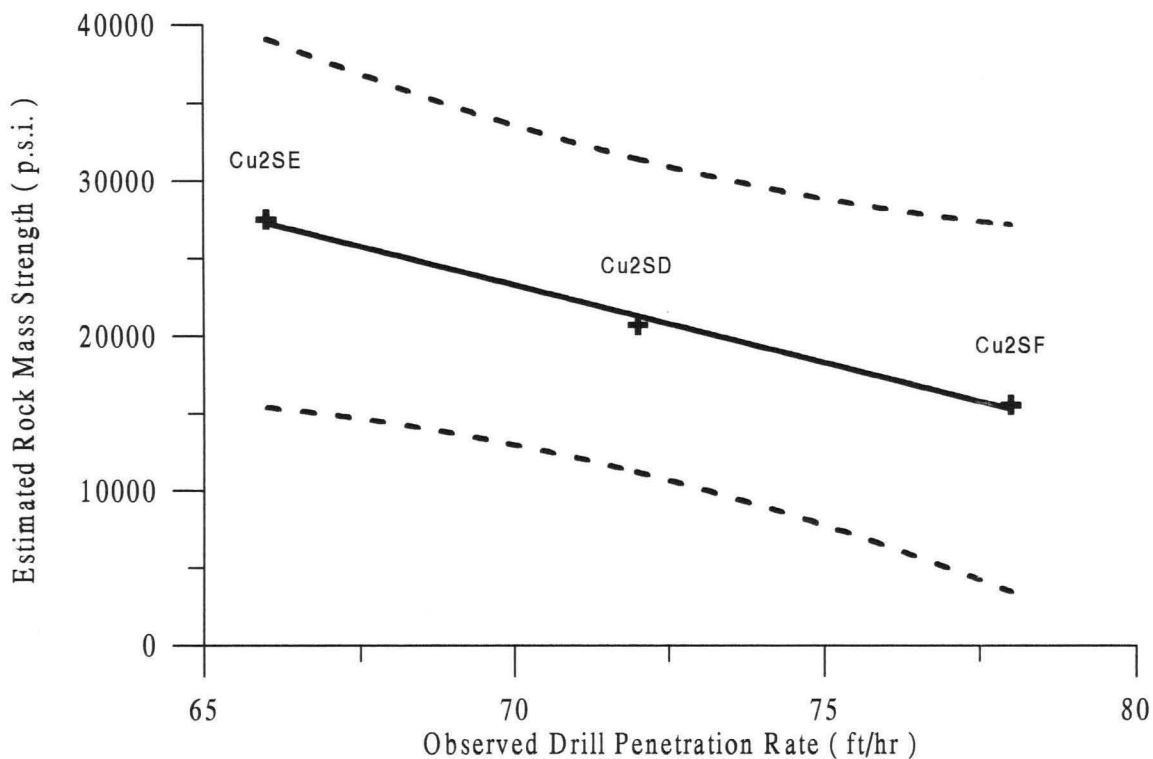


Figure 6.2 - Estimated Rock Mass Strength (Bauer & Calder Model) Vs. Observed Drill Penetration Rate for Three Sites at Mine Cu2

6.4 Drilling Machine Costs

Equations 2.1 through 2.3 from Chapter 2 are here respectively repeated:

$$t_d = \frac{k_d}{V_{rm}} \quad (6.10)$$

$$k_d = \frac{V_{rm} (H + sd)}{r_d} \quad (6.11)$$

$$P_d = \frac{\rho_b (V_{rm})^2}{k_d} = \frac{\rho_b V_{rm} \bar{r}_d}{H + sd} \quad (6.12)$$

where t_d was the drill time (hr), k_d was the drill machine constant ($yd^3 \cdot hr$), V_{rm} was the rock mass volume (yd^3), H was the bench height (ft), sd was the subdrill (ft), r_d was the drill penetration rate (ft/hr), and P_d was the drill productivity (ton/hr). Then if the penetration rate can be observed, then drill cost (\$/ton) can be defined as:

$$C_d = \frac{a_d + b_d}{P_d} = \frac{k_d (a_d + b_d)}{\rho_b (V_{rm})^2} = \frac{(a_d + b_d) (H + sd)}{\rho_b V_{rm} \bar{r}_d} \quad (6.13)$$

where the $a_d + b_d$ terms are drill owning and operating costs, respectively (\$/hr). The operating cost includes the utilization and availability of the machine. This drill cost term is utilized in the total excavation cost model developed in the subsequent Chapter.

In certain instances the penetration rate will be unknown, for example a mass of rock in queue for excavation and size reduction. Then the strength of the rock must be estimated from the strength of the surrounding rock mass. Provided regions of this surrounding mass have been perforated with a calibrated drill, then rock strength at known locations could be determined with an expression similar to Equation 6.8 above. (The constant terms in 6.8 apply to one 10 and 5/8 inch rotary drill at Mine Cu2.) Then from

the strength of discrete locations, the spatial distribution of strength would be estimated with “Kriging”. Then this strength is “Kriged” into the queue volume in much the same manner as commodity grade is Kriged. The cost of drilling could then estimated as:

$$\hat{C}_d = (a_d + b_d) \frac{1}{(\hat{d}_{m1} - \hat{d}_{m2} \log_{10}(\hat{S}_K))} \frac{(H + sd) \phi}{\rho_b V_{rm}} \quad (6.14)$$

where \hat{S}_K is the Kriged estimate for uniaxial compressive rock mass strength.

7. THE TOTAL EXCAVATION COST MODEL

“ To find models for these complex patterns turned out to be much more difficult than I thought. Of course, before making a simulation I was convinced that I had found the correct model. Using the simulation I learned frequently where mistakes in my thinking were and to what patterns my hypothesis really would lead. This led to new insights and new models. I am far from having a satisfactory model for every shell . ”

H. Meinhardt (1995) --- *The Algorithmic Beauty of Sea Shells*

This Chapter presents the final form of the model for total estimated excavation

cost:

1. Certain terms within the total excavation cost equation (originally developed in Chapter 2) are re-formulated because of the results of Chapters 4, 5, and 6 (Section 7.1);
2. the total excavation cost is formulated for minimization with respect to powder column length and rock mass volume, and the solution is observed to be unbounded (Section 7.2);
3. a powder column constraint is formulated for the model resulting in powder column solutions in good agreement with observation, but rock mass volume solutions much larger than those observed in practice (Section 7.3);
4. a rock mass volume constraint is added to the model, resulting in feasible solutions for both the powder column and the rock volume (Section 7.4);
5. the range of ground conditions used to characterize the rock mass used in the modeling are presented (Section 7.5);
6. data for three different types (front loader, cable shovel, hydraulic shovel) of 20 yd³ loading machines used in the modeling are presented (Section 7.6);
7. the hourly costs of the machines are equilibrated at mean ground conditions (Section 7.7).

7.1 The Total Excavation Cost Estimator

Equation 2.22 for the total excavation cost was:

$$C_{\text{tot}} = (C_d + C_e) + \bar{C}_m = C_b + \bar{C}_m = (a_d + b_d) \frac{(H + sd)}{\rho_b V_m \bar{r}_d} + (a_e + b_e) \left(\frac{k_{me} f \left(\frac{s_m}{s_f} \right)}{e_m} \right) + \frac{\left(\frac{k_m}{W_b} \right)}{\left(1 - \frac{s_f}{W_b} \right)} \left(\frac{a_m + b_m}{\bar{\rho}_h V_b \bar{F}_b} \right) \quad (7.1)$$

The work presented within the previous 3 Chapters resulted in Equations 6.13, 4.57, and 5.16 which determined the costs of the drill, powder rig, and loading machine as respectively:

$$C_d = \frac{(a_d + b_d)(H + sd)}{\rho_b V_m \bar{r}_d} \quad (7.2)$$

$$\hat{C}_e = (a_e + b_e) \frac{\hat{k}_{me}}{e_m} \left(\frac{\theta_m^{0.321}}{\theta_f^{2.118}} \right) \quad (7.3)$$

$$\hat{C}_m = (a_m + b_m) \hat{k}_m \frac{1}{(W_b - x_f^{100}) (\hat{C}_p^F V_b)} \quad (7.4)$$

Combining the 3 terms above results in a new formulation for total estimated excavation cost (\$ /ton):

$$\hat{C}_{\text{tot}} = (a_d + b_d) \frac{(H + sd)}{\rho_b V_m \bar{r}_d} + (a_e + b_e) \left[\frac{\hat{k}_{me}}{e_m} \left(\frac{\theta_m^{0.321}}{\theta_f^{2.118}} \right) \right] + (a_m + b_m) \hat{k}_m \frac{1}{(W_b - x_f^{100}) (\hat{C}_p^F V_b)} \quad (7.5)$$

The units of the bracketed term to the immediate right of the powder rig owning and operating cost term $(a_e + b_e)$ are lb/ton, and were originally formulated (Section 2.1) to represent pounds of explosive per ton of rock mass. The estimated explosive cost (\$/ton) can be re-formulated as simply:

$$\hat{C}_e = (a_e + b_e) \left(\frac{\pi \phi^2 \rho_e \hat{L}}{(144)4 \rho_b V_{rm}} \right) \quad (7.6)$$

where ϕ is the drill hole diameter (in), ρ_e is the explosive density (lb/ft³), ρ_b is the rock mass bank density (ton/yd³), V_{rm} is the rock mass volume (yd³), and \hat{L} is the estimated length of the powder column (ft). However this reformulation of the explosive cost term results in a more complex expression for loading machine cost. The estimated machine cost \hat{C}_m (\$/ton) of Equation 7.5 above is a function of the 100th percentile value of the fragment screen size distribution. Equation 5.8 showed how the 100th percentile size could be approximated as a function of the fragment screen size distribution parameters as:

$$x_f^{100} \cong \theta_f (6.90)^{1/n_f} \quad (7.7)$$

Then the machine cost estimator becomes:

$$\hat{C}_m = (a_m + b_m) \hat{k}_m \frac{1}{\left(W_b - (\hat{\theta}_f (6.90)^{1/\hat{n}_f}) \right) (\hat{C}_p^F V_b)} \quad (7.8)$$

and the total estimated excavation cost (Equation 7.5) can now be expressed as:

$$\hat{C}_{tot} = (a_d + b_d) \frac{(H + sd)}{\rho_b V_{rm} \bar{I}_d} + (a_e + b_e) \left(\frac{\pi \phi^2 \rho_e \hat{L}}{(144)4 \rho_b V_{rm}} \right) +$$

$$(a_m + b_m) \hat{k}_m \frac{1}{(W_b - (\hat{\theta}_f (6.90)^{1/\hat{n}_f})) (\hat{C}_p^F V_b)} \quad (7.9)$$

7.2 Minimization of the Total Cost of Excavation

The total estimated excavation cost can be minimized with respect to different variables. For defined equipment fleets at operating mines, minimization with respect to drill diameter ϕ (in), powder column length L (ft), and rock mass volume V_m (yd^3) would appear to give the most useful results. However, as noted in Chapter 6, the drilling cost term was developed with a limited amount of data that did not include variation of the diameter term. Then for the following development ϕ will be held constant, and the total cost estimator will be minimized with respect to the powder column length and the rock mass volume only. Symbolically differentiating 7.9 with respect to L and V_m results in:

$$\frac{\partial \hat{C}_{tot}}{\partial \hat{L}} = \frac{\partial C_d}{\partial \hat{L}} + \frac{\partial \hat{C}_e}{\partial \hat{L}} + \frac{\partial \hat{C}_m}{\partial \hat{L}} \quad (7.10)$$

$$\frac{\partial \hat{C}_{tot}}{\partial V_{rm}} = \frac{\partial C_d}{\partial V_{rm}} + \frac{\partial \hat{C}_e}{\partial V_{rm}} + \frac{\partial \hat{C}_m}{\partial V_{rm}} \quad (7.11)$$

but because:

$$\hat{C}_m = u(\hat{\theta}_f, \hat{n}_f), \text{ and } \hat{\theta}_f = v(V_{rm}, \hat{L}), \text{ and } \hat{n}_f = z(V_{rm}, \hat{L})$$

where u , v , and z are different functions, the chain rule is applied to 7.10 and 7.11

resulting in:

$$\frac{\partial \hat{C}_m}{\partial \hat{L}} = \frac{\partial \hat{C}_m}{\partial \hat{\theta}_f} \cdot \frac{\partial \hat{\theta}_f}{\partial \hat{L}} + \frac{\partial \hat{C}_m}{\partial \hat{n}_f} \cdot \frac{\partial \hat{n}_f}{\partial \hat{L}} \quad (7.12)$$

and:

$$\frac{\partial \hat{C}_m}{\partial V_{rm}} = \frac{\partial \hat{C}_m}{\partial \hat{\theta}_f} \bullet \frac{\partial \hat{\theta}_f}{\partial V_{rm}} + \frac{\partial \hat{C}_m}{\partial \hat{n}_f} \bullet \frac{\partial \hat{n}_f}{\partial V_{rm}} \quad (7.13)$$

then Equations 7.10 and 7.11 become:

$$\frac{\partial \hat{C}_{tot}}{\partial \hat{L}} = \frac{\partial C_d}{\partial \hat{L}} + \frac{\partial \hat{C}_e}{\partial \hat{L}} + \frac{\partial \hat{C}_m}{\partial \hat{\theta}_f} \bullet \frac{\partial \hat{\theta}_f}{\partial \hat{L}} + \frac{\partial \hat{C}_m}{\partial \hat{n}_f} \bullet \frac{\partial \hat{n}_f}{\partial \hat{L}} \quad (7.14)$$

$$\frac{\partial \hat{C}_{tot}}{\partial V_{rm}} = \frac{\partial C_d}{\partial V_{rm}} + \frac{\partial \hat{C}_e}{\partial V_{rm}} + \frac{\partial \hat{C}_m}{\partial \hat{\theta}_f} \bullet \frac{\partial \hat{\theta}_f}{\partial V_{rm}} + \frac{\partial \hat{C}_m}{\partial \hat{n}_f} \bullet \frac{\partial \hat{n}_f}{\partial V_{rm}} \quad (7.15)$$

Performing the indicated partial derivatives results in:

$$\frac{\partial C_d}{\partial \hat{L}} = 0 \quad (7.16)$$

$$\frac{\partial C_d}{\partial V_{rm}} = \frac{-(a_d + b_d)(H + sd)}{\rho_b V_{rm}^2 \bar{r}_d} \quad (7.17)$$

$$\frac{\partial \hat{C}_e}{\partial \hat{L}} = (a_e + b_e) \left(\frac{\pi \phi^2 \rho_e}{(144) 4 \rho_b V_{rm}} \right) \quad (7.18)$$

$$\frac{\partial \hat{C}_e}{\partial V_{rm}} = -(a_e + b_e) \left(\frac{\pi \phi^2 \rho_e \hat{L}}{(144) 4 \rho_b V_{rm}^2} \right) \quad (7.19)$$

$$\frac{\partial \hat{C}_m}{\partial \hat{L}} = \frac{(a_m + b_m) \hat{k}_m}{\hat{C}_p^F V_b} \frac{1}{[W_b - \hat{\theta}_f (690)^{1/\hat{n}_r}]^2} \left[\frac{\partial \hat{\theta}_f}{\partial \hat{L}} (690)^{1/\hat{n}_r} + \hat{\theta}_f (690)^{1/\hat{n}_r} \ln(690) \left(\frac{-1}{\hat{n}_r^2} \right) \frac{\partial \hat{n}_f}{\partial \hat{L}} \right] \quad (7.20)$$

$$\frac{\partial \hat{C}_m}{\partial V_{rm}} = \frac{(a_m + b_m) \hat{k}_m}{\hat{C}_p^F V_b} \frac{1}{[W_b - \hat{\theta}_f (690)^{1/\hat{n}_r}]^2} \left[\frac{\partial \hat{\theta}_f}{\partial V_{rm}} (690)^{1/\hat{n}_r} + \hat{\theta}_f (690)^{1/\hat{n}_r} \ln(690) \left(\frac{-1}{\hat{n}_r^2} \right) \frac{\partial \hat{n}_f}{\partial V_{rm}} \right] \quad (7.21)$$

where $\hat{\theta}_f$ and \hat{n}_f were previously presented in Equations 4.55 and 4.33 respectively as:

$$\hat{\theta}_f = 2.05 \hat{S}^{0.077} \hat{\theta}_{rm}^{0.152} \frac{V_{rm}^{0.385}}{\hat{E}_{ag}^{0.472}} = \hat{A}_\theta \frac{V_{rm}^{0.385}}{\hat{E}_{ag}^{0.472}} \quad (7.22)$$

and:

$$\hat{n}_f = 2.830 \times 10^{-9} (\hat{E}_{ag})^{2.58} + 1.17 \left(\frac{H}{\hat{L}} \right)^{0.20} \quad (7.23)$$

and where the estimated strength in 7.22 can be determined with Equation 6.7:

$$S = 10^{\left(\frac{\hat{d}_{m1}}{\hat{d}_{m2}} - \frac{\bar{r}_d \phi}{\hat{d}_{m2}} \right)} \quad (7.24)$$

The above grade energy (\hat{E}_{ag}) term for 7.22 and 7.23 above can be expressed as:

$$\hat{E}_{ag} = \frac{\pi \phi^2 (\hat{L} - \hat{s}d) \rho_e e_m}{(144)4} \quad (7.25)$$

where e_m is the mass specific energy of the explosive (MJ/lb). With these definitions in

hand, the remaining partial derivatives are determined as:

$$\frac{\partial \hat{\theta}_f}{\partial \hat{L}} = \frac{-0.472 \hat{A}_\theta V_{rm}^{0.385}}{\left(\frac{\pi \phi^2 \rho_e e_m}{(144)4} \right)^{0.472} (\hat{L} - \hat{s}d)^{1.472}} \quad (7.26)$$

$$\frac{\partial \hat{\theta}_f}{\partial V_{rm}} = \frac{0.385 \hat{A}_\theta V_{rm}^{-0.615}}{(\hat{E}_{ag})^{0.472}} \quad (7.27)$$

$$\frac{\partial \hat{n}_f}{\partial \hat{L}} = 2.83 \times 10^{-9} \left(\frac{\pi \rho_e e_m}{(144)4} \right)^{2.58} \phi^{5.16} 2.58 (\hat{L} - \hat{s}d)^{1.58} - 0.2 \frac{1.17 H^{0.20}}{\hat{L}^{1.2}} \quad (7.28)$$

$$\frac{\partial \hat{n}_f}{\partial V_{\text{rm}}} = 0 \quad (7.29)$$

To solve for the powder column length and rock mass volume for which the total excavation cost is minimized:

1. Equation 7.24 is substituted into 7.22;
2. Equation 7.25 is substituted into both 7.22 and 7.23;
3. Equations 7.16 through 7.21 and 7.26 through 7.29 above are substituted into Equations 7.14 and 7.15;
4. Equations 7.14 and 7.15 are equated to zero and solved simultaneously.

The full substitutions will not be presented. The symbolic representation is merely:

$$\frac{\partial \hat{C}_{\text{tot}}}{\partial \hat{L}} = \frac{\partial C_d}{\partial \hat{L}} + \frac{\partial \hat{C}_e}{\partial \hat{L}} + \frac{\partial \hat{C}_m}{\partial \hat{\theta}_f} \cdot \frac{\partial \hat{\theta}_f}{\partial \hat{L}} + \frac{\partial \hat{C}_m}{\partial \hat{n}_f} \cdot \frac{\partial \hat{n}_f}{\partial \hat{L}} = 0 \quad (7.30)$$

$$\frac{\partial \hat{C}_{\text{tot}}}{\partial V_{\text{rm}}} = \frac{\partial C_d}{\partial V_{\text{rm}}} + \frac{\partial \hat{C}_e}{\partial V_{\text{rm}}} + \frac{\partial \hat{C}_m}{\partial \hat{\theta}_f} \cdot \frac{\partial \hat{\theta}_f}{\partial V_{\text{rm}}} + \frac{\partial \hat{C}_m}{\partial \hat{n}_f} \cdot \frac{\partial \hat{n}_f}{\partial V_{\text{rm}}} = 0 \quad (7.31)$$

A personal computer was programmed to solve the above system of equations by iteration. Machine and physical constants were selected to correspond to one of the database mining sites. One step before the solution crashed due to an exponent overflow, the L value corresponded to a length of 9.76×10^{44} light years, and the rock volume corresponded to about 18.2×10^9 cubic light years. The conclusion is that in order for the computer to output useful solutions, constraints must be formulated. First the powder column will be constrained, then the model will be re-run. The result will show if a constraint for the rock mass volume is required; perhaps it can be avoided. Constrained

solution formulations for this model are mathematically intensive, as shown in the subsequent section.

7.3 Minimization of the Total Cost of Excavation Subject to a Powder Column Constraint

The powder column constraint will be formulated via slack variable substitution.

The powder column length (ft) can be defined as:

$$L = sd + (H - stm) \quad (7.32)$$

where sd is the subdrill distance (ft), H is the bench (ft), and stm is the stemming (ft).

the constraint on the estimated powder column length is formulated as:

$$\hat{L} \leq \hat{sd} + (\hat{H} - \hat{stm}) \quad (7.33)$$

Linear regression was utilized upon the blast data (Table A1 of Appendix) to estimate the subdrill, bench, and stemming. These terms were each regressed against multiple variates that consisted of the rock mass chunk size distribution scale and shape parameters (θ_{rm} and n_{rm} respectively), the rock mass strength (S), the drill hole diameter (ϕ), and the above grade energy (E_{ag}). The results show that the subdrill, bench and stemming can always be accurately predicted by hole diameter and above grade energy. Neither the rock mass “chunk” size distribution scale and shape parameters, nor the rock mass strength were observed to enter the regressions as predictive variables at the 95% confidence level:

$$\hat{sd} = 1.347 (\phi) - 0.00281 (E_{ag}) - 4.976 \quad [R^2 = 0.889, \text{Sig. F} = 0.000] \quad (7.34)$$

[0.0000] [0.0002] [0.0002]

$$\hat{H} = 3.900 (\phi) + 0.00741(E_{ag}) - 7.552 \quad [R^2 = 0.934, \text{Sig. F} = 0.000] \quad (7.35)$$

$$\begin{array}{ccc} [0.0000] & [0.0016] & [0.0451] \end{array}$$

$$\hat{stm} = 4.983 (\phi) - 0.00761(E_{ag}) - 20.760 \quad [R^2 = 0.953, \text{Sig. F} = 0.000] \quad (7.36)$$

$$\begin{array}{ccc} [0.0000] & [0.0001] & [0.0000] \end{array}$$

The bracketed terms below the variables and constants are the individual t statistic values, i.e. the probability that the individual term immediately above is not linearly related to the dependent variable on the left hand side. 7.33 above can be transformed back into an equality by subtracting a slack variable:

$$\hat{L} = \hat{sd} + (\hat{H} - \hat{stm}) - \chi_1^2 \quad (7.37)$$

where the slack variable is squared so that it always assumes a value greater than zero.

After 7.34 through 7.36 are substituted into 7.37, it becomes:

$$\hat{L} = 0.264\phi + 0.0122 E_{ag} + 8.232 - \chi_1^2 \quad (7.38)$$

and following the necessary substitutions, estimated above grade energy (Equation 7.25 above) also becomes a function of χ_1 :

$$\hat{E}_{ag} = \frac{\frac{\pi\phi^2 \rho_e e_m}{(144)4} (-1.083\phi + 13.208 - \chi_1^2)}{1 - 0.01520 \frac{\pi\phi^2 \rho_e e_m}{(144)4}} \quad (7.39)$$

and it follows that the subdrill, bench, and stemming (Equations 7.34 through 7.36 above) have become functions of χ_1 . Then for minimization, the total cost must be differentiated with respect to V_{mm} and χ_1 and equated to zero according to:

$$\frac{\partial \hat{C}_{tot}}{\partial V_{mm}} = \frac{\partial \hat{C}_d}{\partial V_{mm}} + \frac{\partial \hat{C}_e}{\partial V_{mm}} + \frac{\partial \hat{C}_m}{\partial V_{mm}} = 0 \quad (7.40)$$

and:

$$\frac{\partial \hat{C}_{\text{tot}}}{\partial \chi_1} = \frac{d\hat{C}_d}{d\chi_1} + \frac{\partial \hat{C}_e}{\partial \chi_1} + \frac{\partial \hat{C}_m}{\partial \chi_1} = 0 \quad (7.41)$$

For Equation 7.40, the form of the derivative terms are identical to certain previous formulations presented in Section 7.2 above, except Equations 7.34 through 7.36 would be substituted wherever sd , H , and stm appear, respectively, and 7.38 and 7.39 would be substituted wherever \hat{L} or \hat{E}_{ag} appear, respectively. Performing the derivatives indicated

for 7.41 above results in:

$$\frac{d\hat{C}_d}{d\chi_1} = \frac{(a_d + b_d)}{\rho_b V_{\text{rm}} \bar{r}_d} \left(\frac{d\hat{H}}{d\chi_1} + \frac{d\hat{s}d}{d\chi_1} \right) \quad (7.42)$$

$$\frac{\partial \hat{C}_e}{\partial \chi_1} = \frac{\partial \hat{C}_e}{\partial \hat{L}} \bullet \frac{\partial \hat{L}}{\partial \chi_1} \quad (7.43)$$

$$\frac{\partial \hat{C}_m}{\partial \chi_1} = \frac{\partial \hat{C}_m}{\partial \hat{\theta}_f} \bullet \frac{\partial \hat{\theta}_f}{\partial \chi_1} + \frac{\partial \hat{C}_m}{\partial \hat{n}_f} \bullet \frac{\partial \hat{n}_f}{\partial \chi_1} \quad (7.44)$$

where:

$$\frac{d\hat{H}}{d\chi_1} = 0.00741 \frac{d\hat{E}_{\text{ag}}}{d\chi_1} \quad (7.45)$$

$$\frac{d\hat{s}d}{d\chi_1} = -0.00281 \frac{d\hat{E}_{\text{ag}}}{d\chi_1} \quad (7.46)$$

$$\frac{d\hat{E}_{\text{ag}}}{d\chi_1} = \frac{-2\pi\phi^2 \rho_e e_m \chi_1}{(144)4 - 0.01520\pi\phi^2 \rho_e e_m} \quad (7.47)$$

$$\frac{\partial \hat{C}_e}{\partial \hat{L}} = (a_e + b_e) \left(\frac{\pi \phi^2 \rho_e}{(144) 4 \rho_b V_{mm}} \right) \quad (7.48)$$

$$\frac{\partial \hat{L}}{\partial \chi_1} = 0.0122 \left(\frac{d \hat{E}_{ag}}{d \chi_1} \right) - 2 \chi_1 \quad (7.49)$$

$$\frac{\partial \hat{C}_m}{\partial \hat{\theta}_f} = \frac{(a_m + b_m) \hat{k}_m}{\hat{C}_\rho^F V_b} \frac{1}{\left(W_b - (\hat{\theta}_f (6.90)^{1/\hat{n}_f}) \right)^2} (6.90)^{1/\hat{n}_f} \quad (7.50)$$

$$\frac{\partial \hat{\theta}_f}{\partial \chi_1} = \frac{-0.472 \hat{A}_\theta V_{mm}^{0.385}}{\hat{E}_{ag}^{1.472}} \left(\frac{d \hat{E}_{ag}}{d \chi_1} \right) \quad (7.51)$$

$$\frac{\partial \hat{C}_m}{\partial \hat{n}_f} = - \frac{(a_m + b_m) \hat{k}_m}{\hat{C}_\rho^F V_b} \frac{\hat{\theta}_f (6.90)^{1/\hat{n}_f} \ln(6.90)}{\left(W_b - (\hat{\theta}_f (6.90)^{1/\hat{n}_f}) \right)^2 \hat{n}_f^2} \quad (7.52)$$

$$\begin{aligned} \frac{\partial \hat{n}_f}{\partial \chi_1} = & 2.830 \times 10^{-9} 2.58 (\hat{E}_{ag})^{1.58} \left(\frac{d \hat{E}_{ag}}{d \chi_1} \right) + \\ & 1.17(0.20) \left(\frac{1}{\hat{L}^{0.20} \hat{H}^{0.80}} \left(\frac{d \hat{H}}{d \chi_1} \right) - \frac{\hat{H}^{0.2}}{\hat{L}^{1.2}} \left(\frac{d \hat{L}}{d \chi_1} \right) \right) \end{aligned} \quad (7.53)$$

Following the necessary substitutions, 7.40 and 7.41 are solved simultaneously for the V_{mm} and χ_1 values that result in minimum total cost. Then the powder column length is obtained by back-solving it out of 7.37. Re-running the column constrained model with the same inputs used before (end of Section 7.2 above) resulted in a stemming, subdrill, bench, and powder column of 28.9, 8.13, 37.07, and 16.3 feet respectively, and a rock mass volume of 6,725 yd^3 . Exact burden and spacing values are unknown, because they were not formulated. But since the bench (H) and rock mass volume (V_{mm}) are known,

a square pattern (ft) can be estimated as:

$$p \approx \sqrt{\frac{27 V_{\text{rm}}}{H}} \approx \sqrt{\frac{27(6,725)}{37.07}} \approx 70 \quad (7.54)$$

which is over twice the pattern (32' x 32') observed at the site (Cu2SG). The model predicts a mean fragment size of 11.8 inches, which offers an important insight as to how the current form of the model minimizes cost: The powder column is maximized subject to the constraint, then the rock volume is steadily increased lowering drill and explosive cost per ton, until the large fragment sizes that result begin to ramp up the loading cost. Because the rock volume output value is well beyond the maximum recorded observation within the blast data (2,444 yd³ at sites Cu5SA and Cu5SE , Appendix), the conclusion is that the model will require a volume constraint.

7.4 Minimization of the Total Cost of Excavation Subject to Powder Column and Rock Mass Volume Constraints

When burden (B), spacing (S), and bench (H) are defined in foot units, the rock mass volume (V_{rm}) in yd³ units can be obtained as:

$$V_{\text{rm}} = \frac{BSH}{27} \quad (7.55)$$

The constraint on the estimated rock mass volume will be:

$$\hat{V}_{\text{rm}} \leq \frac{\hat{B}\hat{S}\hat{H}}{27} \quad (7.56)$$

An estimator for the bench (\hat{H}) has already been presented (Equation 7.35 above).

Estimators for burden and spacing were determined similarly and are presented as:

$$\hat{B} = 1.755 (\phi) + 0.008036 (E_{ag}) + 1.963 \quad [R^2 = 0.798, \text{Sig. F} = 0.000] \quad (7.57)$$

[0.0009] [0.0024] [0.6287]

$$\hat{S} = 1.356 (\phi) + 0.005709 (E_{ag}) + 5.469 \quad [R^2 = 0.851, \text{Sig. F} = 0.000] \quad (7.58)$$

[0.0001] [0.008] [0.0406]

Now 7.56 above is transformed into an equality by subtracting another slack variable:

$$\hat{V}_{\text{rm}} = \frac{\hat{B}\hat{S}\hat{H}}{27} - \chi_2^2 \quad (7.59)$$

where the “ 2 ” subscript denotes that the slack variable differs from that used for the powder column constraint (Equation 7.37). Because \hat{B} , \hat{S} , and \hat{H} are functions of above grade energy, and because above grade energy is a function of χ_1 , it follows that now $\hat{V}_{\text{rm}} = f(\chi_1, \chi_2)$. Then for minimization, the total estimated cost must be

differentiated with respect to both χ_1 and χ_2 and equated to zero according to:

$$\frac{\partial \hat{C}_{\text{tot}}}{\partial \chi_1} = \frac{\partial \hat{C}_d}{\partial \chi_1} + \frac{\partial \hat{C}_e}{\partial \chi_1} + \frac{\partial \hat{C}_m}{\partial \chi_1} = 0 \quad (7.60)$$

and:

$$\frac{\partial \hat{C}_{\text{tot}}}{\partial \chi_2} = \frac{\partial \hat{C}_d}{\partial \chi_2} + \frac{\partial \hat{C}_e}{\partial \chi_2} + \frac{\partial \hat{C}_m}{\partial \chi_2} = 0 \quad (7.61)$$

where the derivatives within the two terms above are equivalent to:

$$\frac{\partial \hat{C}_d}{\partial \chi_1} = \left(\frac{a_d + b_d}{\rho_b \bar{r}_d} \right) \left[\frac{1}{\hat{V}_{\text{rm}}} \left(\frac{d\hat{H}}{d\chi_1} \right) + \frac{1}{\hat{V}_{\text{rm}}} \left(\frac{d\hat{s}d}{d\chi_1} \right) - \frac{(\hat{H} + \hat{s}d)}{\hat{V}_{\text{rm}}^2} \left(\frac{\partial \hat{V}_{\text{rm}}}{\partial \chi_1} \right) \right] \quad (7.62)$$

$$\frac{\partial \hat{C}_e}{\partial \chi_1} = \frac{(a_e + b_e)\pi\phi^2\rho_e}{(144)4\rho_b} \left(\frac{1}{\hat{V}_{\text{rm}}} \left(\frac{d\hat{L}}{d\chi_1} \right) - \frac{\hat{L}}{\hat{V}_{\text{rm}}^2} \left(\frac{\partial \hat{V}_{\text{rm}}}{\partial \chi_1} \right) \right) \quad (7.63)$$

$$\frac{\partial \hat{C}_m}{\partial \chi_1} = \frac{\partial \hat{C}_m}{\partial \hat{\theta}_f} \bullet \frac{\partial \hat{\theta}_f}{\partial \chi_1} + \frac{\partial \hat{C}_m}{\partial \hat{n}_f} \bullet \frac{\partial \hat{n}_f}{\partial \chi_1} \quad (7.64)$$

$$\frac{\partial \hat{C}_d}{\partial \chi_2} = \frac{2(a_d + b_d)(\hat{H} + \hat{s}d)\chi_2}{\rho_b \bar{r}_d \hat{V}_{rm}^2} \quad (7.65)$$

$$\frac{\partial \hat{C}_e}{\partial \chi_2} = \frac{(a_e + b_e)\pi\phi^2\rho_e}{(144)4\rho_b} \hat{L} \left(2 \frac{\chi_2}{\hat{V}_{rm}^2} \right) \quad (7.66)$$

$$\frac{\partial \hat{C}_m}{\partial \chi_2} = \frac{\partial \hat{C}_m}{\partial \hat{\theta}_f} \bullet \frac{\partial \hat{\theta}_f}{\partial \chi_2} + \frac{\partial \hat{C}_m}{\partial \hat{n}_f} \bullet \frac{\partial \hat{n}_f}{\partial \chi_2} \quad (7.67)$$

where $\frac{d\hat{H}}{d\chi_1}$, $\frac{d\hat{s}d}{d\chi_1}$, $\frac{d\hat{L}}{d\chi_1}$, $\frac{\partial \hat{C}_m}{\partial \hat{\theta}_f}$, $\frac{\partial \hat{C}_m}{\partial \hat{n}_f}$, and $\frac{\partial \hat{n}_f}{\partial \chi_1}$ have been previously defined. The

remaining undefined terms include:

$$\frac{\partial \hat{V}_{rm}}{\partial \chi_1} = \frac{1}{27} \left(\hat{H} \hat{S} \left(\frac{d\hat{B}}{d\chi_1} \right) + \hat{B} \hat{S} \left(\frac{d\hat{H}}{d\chi_1} \right) + \hat{B} \hat{H} \left(\frac{d\hat{S}}{d\chi_1} \right) \right) \quad (7.68)$$

$$\frac{\partial \hat{\theta}_f}{\partial \chi_1} = \hat{A}_\theta \left[\left(\frac{\partial \hat{\theta}_f}{\partial \hat{V}_{rm}} \right) \left(\frac{\partial \hat{V}_{rm}}{\partial \chi_1} \right) + \left(\frac{\partial \hat{\theta}_f}{\partial \hat{E}_{ag}} \right) \left(\frac{d\hat{E}_{ag}}{d\chi_1} \right) \right] \quad (7.69)$$

where $\frac{d\hat{E}_{ag}}{d\chi_1}$ has been previously defined, leaving:

$$\frac{d\hat{B}}{d\chi_1} = 0.008036 \left(\frac{d\hat{E}_{ag}}{d\chi_1} \right) \quad (7.70)$$

$$\frac{d\hat{S}}{d\chi_1} = 0.00709 \left(\frac{d\hat{E}_{ag}}{d\chi_1} \right) \quad (7.71)$$

$$\frac{\partial \hat{\theta}_f}{\partial \hat{V}_{rm}} = \frac{0.385 \hat{A}_\theta}{\hat{E}_{ag}^{0.472}} V_{rm}^{-0.615} \quad (7.72)$$

$$\frac{\partial \hat{\theta}_f}{\partial \hat{E}_{ag}} = (-0.472) \frac{\hat{A}_\theta \hat{V}_{rm}^{0.385}}{\hat{E}_{ag}^{1.472}} \quad (7.73)$$

$$\frac{\partial \hat{\theta}_f}{\partial \chi_2} = \frac{-2 \hat{A}_\theta}{\hat{E}_{ag}^{0.472}} (0.385) V_{rm}^{-0.615} (\chi_2) \quad (7.74)$$

$$\frac{\partial \hat{n}_f}{\partial \chi_2} = 0 \quad (7.75)$$

Now solving for the powder column length and rock mass volume for which the total excavation cost is minimized consists of solving 7.60 and 7.61 simultaneously for values of χ_1 and χ_2 , and then back-solving the powder column length and rock volume out of 7.37 and 7.59 respectively. Testing the model with the same machine and physical values used before (end of Section 7.3 above) resulted in the same stemming, subdrill, bench, and powder column as the previous run (28.9, 8.15, 37.07, and 16.22 feet respectively) but the rock mass volume shrunk from 6,711 yd³ (previous run) to 737 yd³. The burden and spacing values output were 24.06 and 22.33 feet, respectively. Running the model with the 50 foot bench observed at the site (Cu2SG) resulted in a burden and spacing of 33.2 and 28.8 feet, which now correspond very well with the observed 32' x 32' pattern. The mean fragment size output was 5.03 inches, which corresponds almost exactly to the 5.08 inch mean size observed at the site with the SPLIT software. These results indicate that that the model can duplicate observed drill patterns, powder loads, and fragment sizes. But the purpose of constructing the model was not to duplicate observation, but

rather to determine the minimum cost per ton patterns and loads that should be used for the mining equipment (the drill, powder rig, and loading machine) subject to changing ground conditions.

7.5 The Range of Ground Conditions used for the Excavation Cost Modeling

The results of Chapter 4 showed that from the standpoint of the cost of explosive induced size reduction, a set of three different descriptors describe the ground conditions: 1) The size distribution of the solid chunks composing the rock mass; 2) the strength of the rock mass, and 3) the density of the rock mass. Chapter 3 described how image analysis can be utilized to determine the chunk size distribution, Chapter 6 showed how rock strength can be estimated from the drill, and Chapter 4 provided the fragmentation model that related all three of the ground descriptors to the cost of the explosive used to fragment the mass. Table 7.1 presents the ground conditions used to characterize the hypothetical rock mass within the cost model. θ_m and ρ_b are taken from the blast data (Appendix).

Table 7.1 - The Ground Condition Variables used in the Cost Model

Variable	Variable Description (units)	Min	Max	Range	Mean [Std Dev]
θ_m	Weibull scale parameter of rock mass chunk screen size distribution (in)	15.0	37.8	22.8	24.8 [6.4]
S	rock mass strength (psi)	15,200	25,700	10,500	21,166 [5,394]
ρ_b	rock mass bank density (ton/yd ³)	1.7	2.3	0.6	1.96 [0.18]

The range of strength data shown in the table is the same range used to derive the drill constants (Table 6.1), and is considerably less than the total observed range (3,649 to 25,700 p.s.i.) from the blast data listed in the Appendix. The drill penetration rate function (Equation 6.5) will not be extrapolated outside of the range of strength data utilized to determine the drill constants.

7.6 Loading Machines used for the Excavation Cost Modeling

Chapter 5 showed how the ton per hour production of the different types and classes of loading machines could be characterized as a function of fragment screen size. The bucket volumes within the machine database were observed to range from 11.7 to 56 yd³ (Table 5.1). The cost modeling will investigate the relationships between the 20 yd³ class machines only. Table 7.2 lists the pertinent machine data for the 3 different types of machines used in the modeling.

Table 7.2 - Summary of Loading Machine Data Used in the Cost Modeling

Machine Class and Type	\hat{C}_ρ^F Bucket Density (tons/yd ³)	\hat{k}_m Machine Constant (in - hrs)	\bar{V}_b Struck Bucket Volume (yd ³)	\bar{W}_b Bucket Width (in)
extra-large front end loaders (21.3 yd ³)	1.530 [0.054] ¹	2.477 [0.163]	21.3 [0]	222 [0]
medium cable shovels (19 to 22 yd ³)	1.673 [0.053]	0.809 [0.044]	20.6 [1.58]	108 [0]
medium hydraulic shovels (18 to 23.5 yd ³)	1.206 [0.065]	1.002 [0.058]	21 [2.03]	151.5 [16.20]

Note 1: Numbers in square brackets are standard deviations.

7.7 Machine Cost Equilibration for the Excavation Cost Modeling

The objective of the cost modeling is to investigate how total excavation cost changes subject to different loading machines and changing ground conditions. Then cost comparisons become a relative issue, and absolutely accurate cost information is not necessary. Machine cost information was not a deliverable of the original Caterpillar contract (Section 3.1). The hourly owning and operating cost for the extra - large front end loader (Table 7.2) was estimated from the manufacturers handbook at 250 \$/hr. The dollar per pound explosive cost of owning and operating the powder rig was estimated at ten cents per pound. Then the model was set up for the extra-large front loader and run with the mean ground condition values listed in Table 7.1. The target price total cost per ton was rather arbitrarily set to 0.20 \$/ton. This corresponded to a drill rig cost of 160 \$/hr. Then the ground conditions, drill cost, and powder rig costs were held constant, and the model was set up to back-solve for the hourly costs of the shovels that resulted in the same 0.20 \$/ton total cost value, resulting in hourly costs of 350.9 and 312.0 \$/hr for the cable and hydraulic shovel (Table 7.2), respectively.

The next Chapter presents results and pertinent conclusions for the excavation cost modeling.

8. RESULTS AND CONCLUSIONS

“ Shoveling, being one of the ancient occupations, is not usually considered worthy of serious thought. Some attention is given to the kind of tool used, but very little to the process itself. Some years ago, a scientific study was made of the shoveling operation and it was demonstrated that a first class shoveler could do the most work with the least effort by using a shovel that would have a load of 21 pounds. It is evident, of course, that no shoveler can always take a load of exactly 21 pounds on his shovel, but, although the load may vary 3 or 4 pounds one way or the other, he will do his biggest day's work and be less tired when his average for the day is about 21 pounds per shovel load. ”

Wilson, Cunningham, and Butler (1934) --- *Arizona Lode Gold Mines and Gold Mining*

This Chapter shows how total estimated excavation cost changes according to different ground conditions and different loading machines. The ground condition variables include the strength, size, and density of the pre-blasted rock mass. The loading machines include front loaders, cable shovels, and hydraulic shovels, all having bucket capacities of approximately 20 yd³. Loading machine cost per ton was formulated as a function of fragment screen size. The model was used to equilibrate machine costs per ton at average ground condition values. Then the excavation cost model was run for each machine over the observed range of each ground condition variable, where the remaining two ground condition variables were held constant at their mean values. The principal objective of this exercise is to determine whether excavation cost savings can be attained with a cost model that includes the assessment of ground conditions. The added cost of excavation that would be imposed by the utilization of the model was neglected. For an excavation system consisting of blasting sandwiched between drilling and loading machines, the modeling results show that:

- Although variations in both the size and the strength of the rock mass will affect the muckpile fragment size, on average the fragment size changes are so small they have a negligible affect on the resulting machine cost and hence the total cost (Sections 8.1 and 8.2);
- total excavation cost is mainly affected by changes in drilling cost and explosive cost. The drilling cost changes are brought about by changing rock mass strength and density (Sections 8.2 and 8.3, respectively). The explosive cost change is caused by changes in rock mass density (Section 8.3).

Conclusion: There appears to be no economic merit for gathering and assessing the rock mass strength and fracture data required for an excavation cost model that minimizes the costs of drilling, blasting, and loading, because the estimated fragment size differentials that result from blasting rock mass characterized over the range of modeled ground conditions are small.

However, certain subsequent work suggests that loading machine production (Chapter 5) was perhaps formulated to be too insensitive to fragment size. The response of the model subject to a reformulated production-fragment size relationship for large front end loaders is presented within Section 9.1 of the next Chapter. Also, excavation is merely the preliminary stage of many mining operations which include subsequent stages of comminution. For example a crusher included model would no longer be concerned with the cost of excavating rock mass; such a model would become a rock mass *size reduction* cost model. It is inferred that a model formulated to include a crusher will result in much smaller estimated fragment sizes to save crushing cost, at the expense of drilling and explosive cost. Such small fragment sizes will perhaps render the productive performance of loading machines as a function of the fragmentation descriptor a low priority issue; it is inferred that the strategic issues will become ground control and slope stability problems incurred by the explosives assault. In any event, such a size reduction cost model will also have to include penalty functions to account for the for the cost of

forgone production opportunity. Consider for example that the baseline throughput of the crushing plant at some mine is 100,000 tons per day. The production of the drills and explosives at this mine could be increased by expanding the patterns. But the larger fragment sizes resulting from such a setup could “choke” the crushing plant into a throughput less than the baseline production. Then the lost opportunity of this choked throughput would be accounted for via a penalty cost attached to the blasting cost. A considerable amount of research effort will have to be performed to attain a crusher included model; the nature of this work is outlined in Section 9.2 of the next Chapter.

The reader is also reminded that because of the limited amount of drilling data, the range of rock mass strengths utilized for the drilling function within the model were but the upper 50% of the total observed range representing the different mining sites. The lower half of the total observed strength range was not utilized in the model, because of the fact that drill penetration rates could not reliably be extrapolated into this region (Section 7.5). It is inferred that if the drill had been calibrated to allow the inclusion of such a low strength rock mass within the model, higher total cost differentials would have resulted. The importance of the drilling function is further discussed in Section 9.3.

8.1 Total Estimated Excavation Costs for the Different Machines over the Range of Observed Rock Mass Chunk Screen Size Distribution Scale Parameters

Figure 8.1 shows the results of holding the density and strength of the model rock mass constant at the mean observed values (Table 7.1), and then solving the model for incremental steps over the range of observed rock mass chunk size scale parameters. The loading machine input was the extra-large front end loader. The cost inputs utilized are

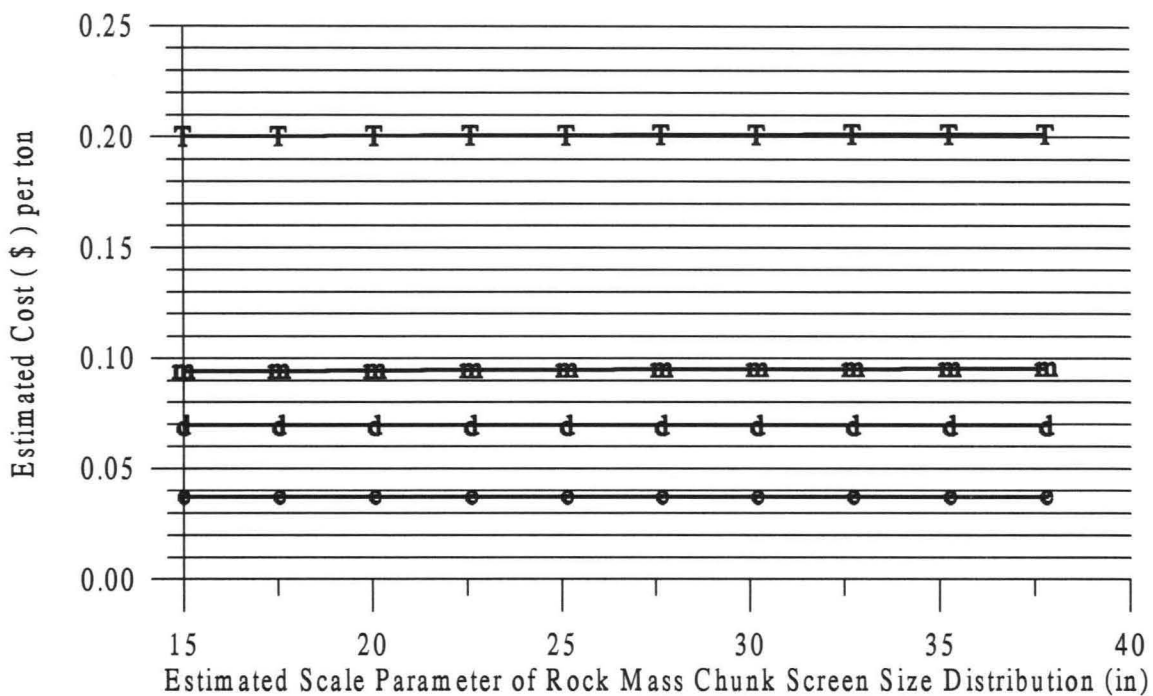


Figure 8.1 - Estimated Excavation Costs over the Rock Mass Chunk Screen Size Scale Parameter Range

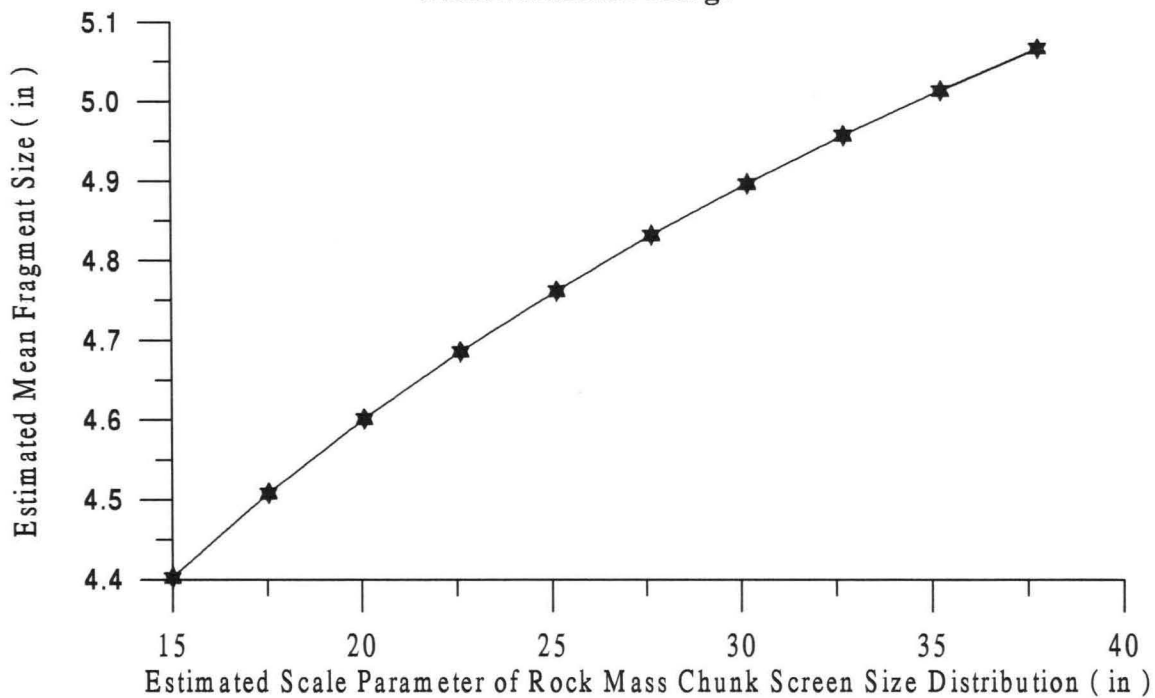


Figure 8.2 - Mean Fragment Sizes Estimated by the Model over the Rock Mass Chunk Screen Size Scale Parameter Range

listed in Section 7.7. For Figure 8.1 and subsequent Figures, “ T ” represents the total cost per ton, and “ e ”, “ d ”, and “ m ” represent the cost per ton for the explosive loading rig, drill, and loading machine respectively. Referring to Figure 8.1:

- the \$/ton costs do not appear to change over the rock mass chunk size scale parameter range.

The form of the cost Vs. scale parameter plots for the medium cable shovel and medium hydraulic shovel appear the same as Figure 8.1 and will not be presented. Figure 8.2 shows how the mean fragment sizes output by the model change proportionally to the rock mass chunk size scale parameters input to the model:

- the mean fragment sizes increase by about ½ inch in approximately linear fashion over the 23 inch wide range of observations representing the chunk size scale parameters.

Machine costs were formulated as a function of fragment size, and fragment size is affected by the chunk size within the pre-blasted rock mass. Figure 8.3 shows the results of plotting the chunk scale parameters against a cost scale expanded in the vicinity of the machine cost curves representing the different machine types. The \$/ton machine costs appear equal at a scale parameter value of about 25 inches, because the costs were equilibrated at the mean observed scale value of 24.8 inches (Section 7.7). On either side of the mean scale value, the machine costs change, but the changes are small:

- the \$/ton costs for the different machines change by only fractions of a cent per ton over the rock mass chunk size scale parameter range.

Conclusions: Variation of the rock mass scale parameters over a range representative of those observed in open pit mines results in a negligible variation of the total excavation cost estimated by the model. The very small increases in total cost are caused by increases in estimated loading machine costs, which are caused by increases in fragment size. But the total range of this fragment size increase is so slight it hardly affects the loading machine operating

cost, regardless of the machine type used.

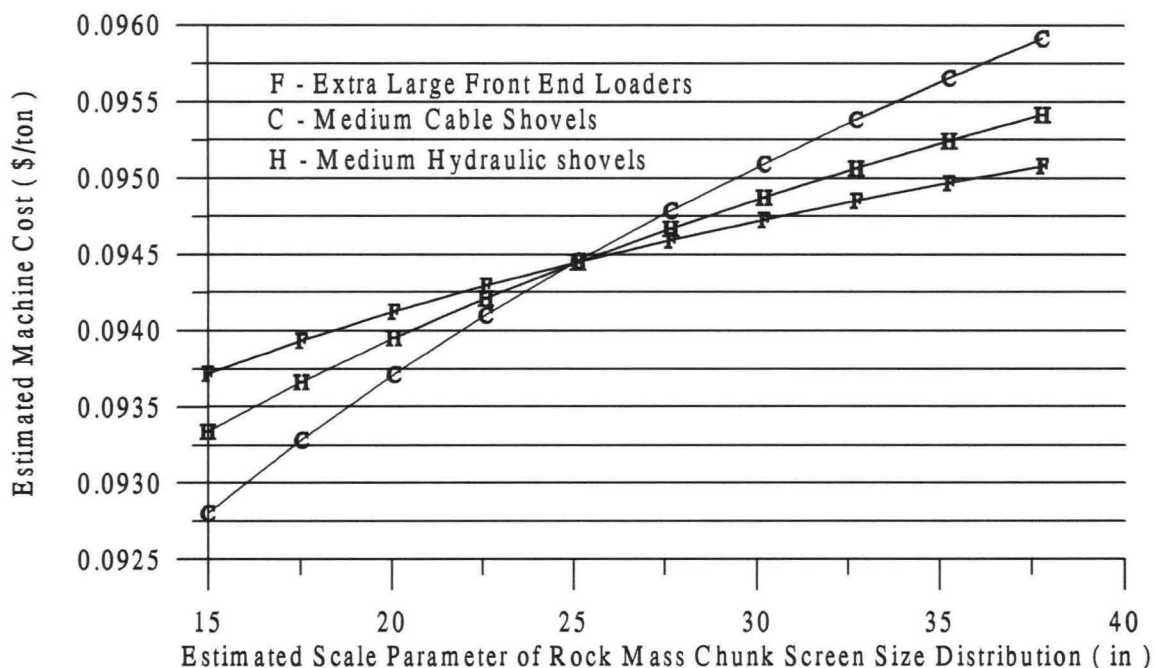


Figure 8.3 - Machine Costs Vs. Rock Mass Chunk Screen Size Scale Parameter

8.2 Total Estimated Excavation Costs for the Different Machines over the Range of Rock Mass Strengths

Figure 8.4 shows the results of holding the density and chunk size scale parameter constant at their mean observed values, and then solving the model for incremental steps over the range of rock mass strengths that characterized the drilling function. The loading machine input was the extra-large (20 yd³) front end loader:

- the total \$/ton cost increases by about \$0.01/ton over the rock mass strength range;
- the total cost increase appears to be wholly caused by the increase in drill cost.

The forms of the Cost Vs. Strength plots for the medium cable and hydraulic shovels appear the same as Figure 8.4 and will not be presented. Figure 8.5 shows how the

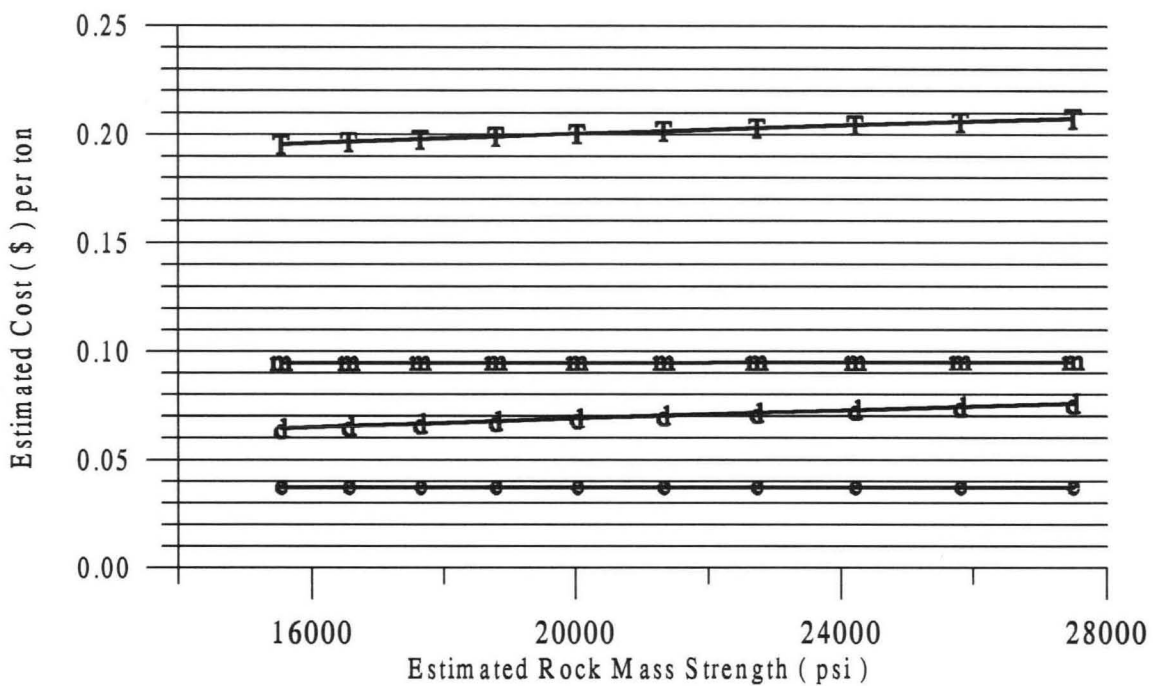


Figure 8.4 - Estimated Excavation Costs over the Range of Rock Mass Strength

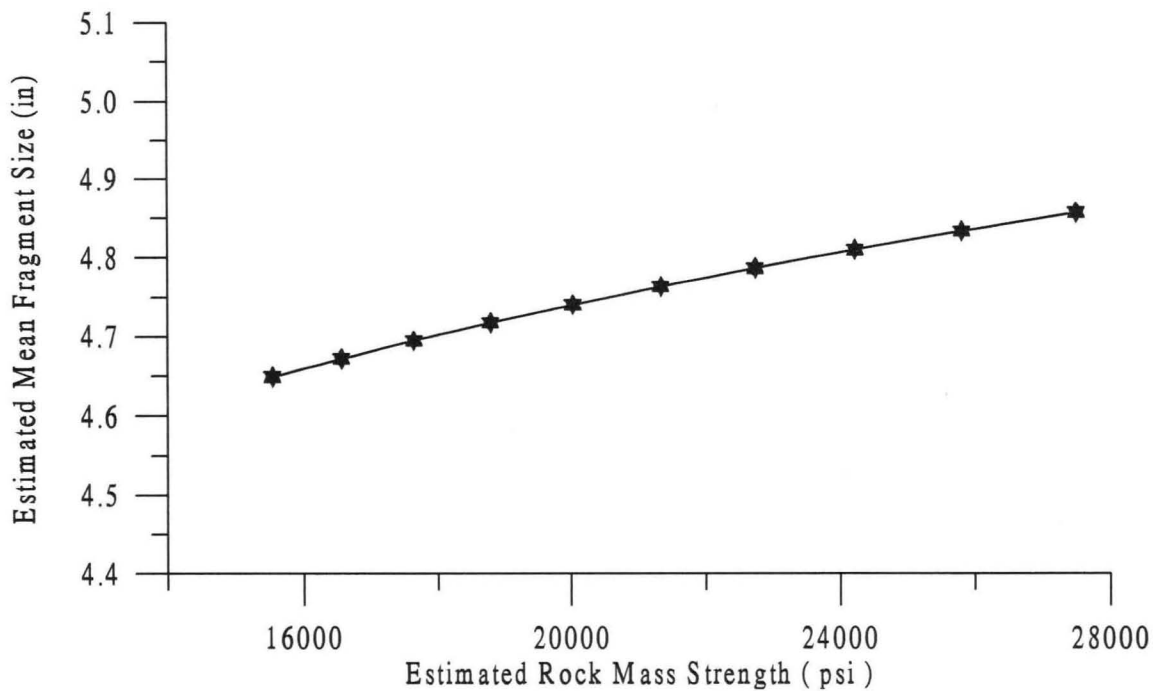


Figure 8.5 - Mean Fragment Sizes Estimated by the Model over the Range of Rock Mass Strength

mean fragment sizes output by the model change proportionally to the rock mass strengths input to the model:

- the mean fragment sizes increase by about 0.20 inch in approximately linear fashion over the 10,500 p.s.i. wide range of observations representing rock mass strength.

Machine costs were formulated as a function of fragment size, and fragment size is affected by the strength of the pre-blasted rock mass. Figure 8.6 shows the results of plotting rock strength against machine costs. The \$/ton machine costs appear equal at a strength of about 21,000 p.s.i., because the costs were equilibrated at the mean observed strength value of 21,166 (Section 7.7). According to Figure 8.6, the model predicts that:

- The \$/ton costs for the different machines will change by only about a tenth of a cent per ton over the rock mass strength range.

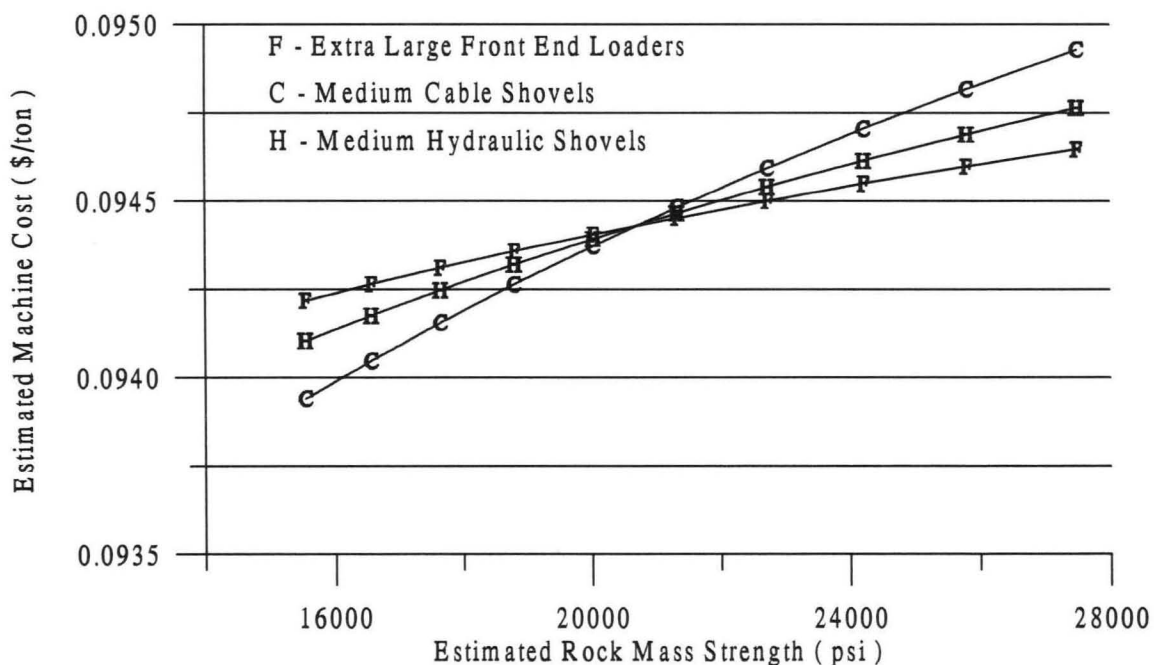


Figure 8.6 - Machine Costs Vs. Rock Mass Strength

Conclusions: Variation of rock mass strength over a range representative of that used to calibrate the drill results in a very small variation in the total estimated excavation cost. The very small increases in total cost that are observed are caused primarily by increases in drill cost, simply because as rock strength increases, penetration rate decreases, and the ton per hour block out rate of the drill goes down. Increasing rock strength also results in increased fragment size, but the total range of this fragment size increase has a negligible effect upon machine operating cost, regardless of the machine type used.

8.3 Total Estimated Excavation Costs for the Different Machines over the Range of Rock Mass Densities

Figure 8.7 shows the results of holding the strength and chunk size scale parameter of the model rock mass constant at their mean observed values, and then solving the model for incremental steps over the range of observed rock mass densities.

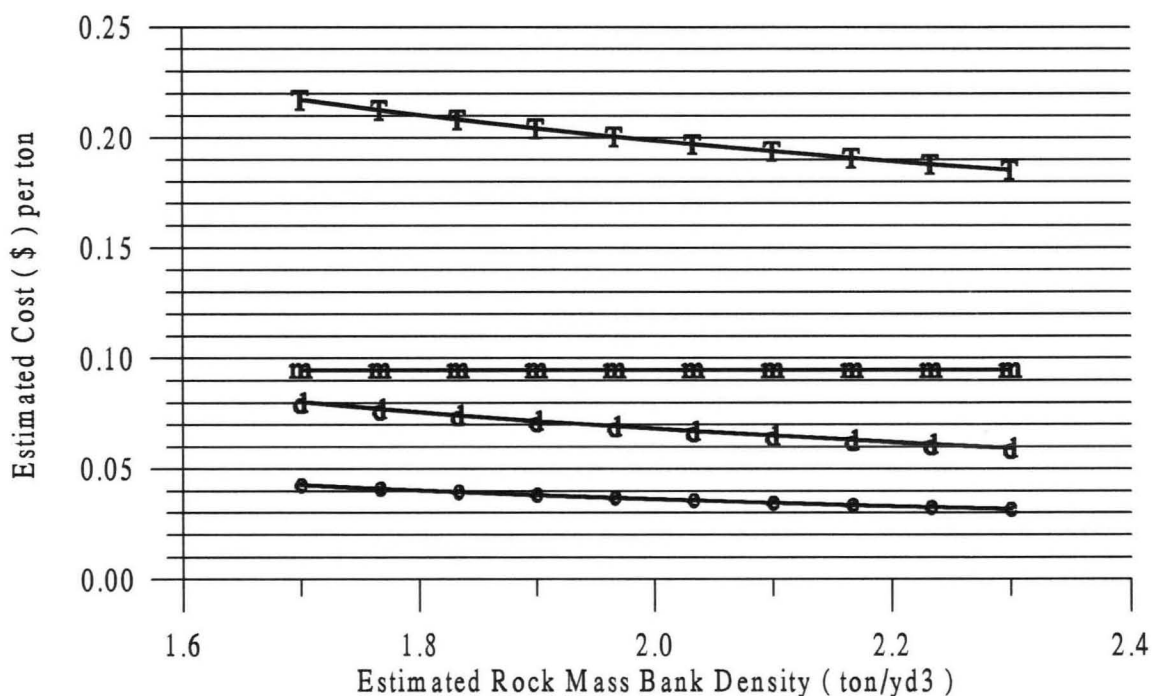


Figure 8.7 - Estimated Excavation Costs over the Rock Mass Density Range

The loading machine input was the extra-large front end loader:

- the total \$/ton cost decreases by about \$0.03/ton over the model rock mass density range;
- the total cost decrease appears to be caused by decreases in both drill cost (about \$ 0.02/ton) and explosive cost (about \$ 0.01/ton);
- drill and explosive costs decrease simply because tonnage per unit volume increases according to density.

The forms of the cost Vs. density plots for the medium cable shovel and medium hydraulic shovel appear the same as Figure 8.7 and will not be presented. Figure 8.8 shows the relationship between the mean fragment sizes output by the model and the rock mass densities input to the model:

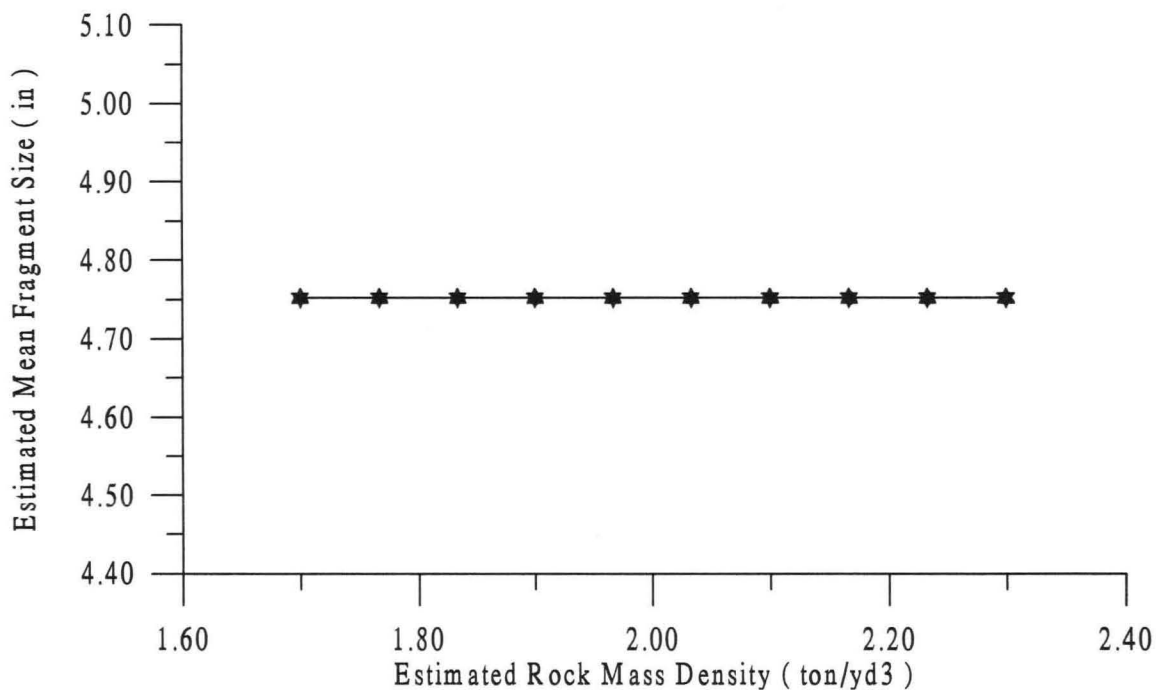


Figure 8.8 - Mean Fragment Sizes Estimated by the Model over the Range of Rock Mass Density

- the mean fragment sizes is constant at 4.75 inches over the 0.60 ton/yd³ wide range of observations representing the rock mass density.

Thus the estimated loading machine costs will not change, and the plot of machine costs with respect to estimated rock mass density will not be exhibited. This anti-intuitive result simply reflects the fact that machine production was never formulated as a function of bank density, but rather as a function of the regressed product of fill factor and heaped density (Equation 5.4). In addition, the fragmentation estimators utilized for the model (Equations 7.22 and 7.23) do not include a density parameter. The modeled decreases in drill and blast cost (Figure 8.7) is caused by the bank density parameter in the denominators of the terms defining these costs (Equation 7.9).

Conclusions: Variation of the rock mass densities over a range representative of those observed at open pit mines results in the highest variation in total excavation cost estimated by the model, when compared to the total costs obtained by ranging over rock mass size and strength. The decreases in total cost that are observed are caused primarily by decreases in drill cost, followed by decreases in explosive cost. Loading machine cost does not contribute to the total cost decrease.

8.4 An Inconsistency of the Current Form of the Excavation Cost Model

The current form of the excavation cost model exhibits an inconsistency in that it never appears to alter control values representing the estimated rock mass volume (Equation 7.59) and the length of the explosive column (Equation 7.37). The model always maximizes the constraints imposed on these variables. One reason for this constraint maximization is that the loading machine production functions (Chapter 5) were perhaps defined to be too insensitive to fragment screen size. The next Chapter shows that when machine production becomes more sensitive to fragment size, the model

reacts to minimize total cost by increasing the powder column length in order for the explosive to produce smaller fragments and thereby reduce the machine cost. This result hints that when the model is finally formulated to include an even higher gain relationship between the variables of money and produced fragment size (i.e. comminution), the model will react by attempting to create ever smaller fragment sizes via the drill and explosive functions. But the cost reaction of the loading machine will be lower, regardless of how its productivity is defined, because of the reduced range of the produced fragment sizes. For such a scenario it is perhaps ironic that formulations for loading machine productivity as a function of fragment size will become less significant. However, size is but one of a total of discrete 20 descriptors used to characterize the fragments (Section 3.4). Some of the regressions performed for this work showed that the productive performance of the same class and type of loading machine is variable at constant average fragment size. Then for example, although a blast at two different sites will produce the same average fragment size, the two blasts also produce two different particle interaction configurations, one of which results in a faster machine load cycle time. In Section 2.2, it was inferred that some sort of particle shape descriptor was partially responsible for the variations in heaped density and bucket fill factors observed at the sites; but in order to simplify the mathematics, (particularly the fragmentation modeling) it was assumed that the shape descriptor was independent of the fragment size. A more complete understanding of the relationship between machine production and the fragmentation descriptor set can be uncovered by further research effort, as discussed within Section 9.1 of the next Chapter.

9. FUTURE WORK

“ Mining for the precious metals has assumed such vast proportions, and the bullion product has reached such a seemingly fabulous amount, that the attention of nations and individuals in all parts of the world has been arrested, and the people living in the mineral belts are themselves amazed. Shall New York City become the great reservoir into which shall flow the vast products of these mineral fields? Shall New York manufacturers build the machinery that shall disembowel the mountains and crush or smelt the ores of the rich mineral fields of the South and West? Shall the enterprising people of New York own the controlling interest in the grand list of mines now being developed all over the Pacific Coast States and Territories - shall their general offices be located here - shall their supplies be purchased in this market - shall the idle capital of the East and Europe flow to this city for investment in mines and mining stocks? These are the paramount questions of the hour. *The telegraph annihilates distance.* Shall the great commercial and financial center of the United States make the prices of the stocks in which its people deal, or shall they continue at the mercy of San Francisco manipulations? The opportunity is presented. Shall it be embraced? ”

Anonymous (1879) --- *The United States Annual Mining Review
and Stock Ledger for 1879*

The results of the previous Chapter demonstrated that a mathematical model can indeed utilize ground condition inputs, and then go on and minimize the total estimated cost of excavating rock mass. But the fact, and it may as well be faced, is that the current form of the model poses little or no economic merit. The future work presented within this Chapter shows how the model could be forged into formidable economic tool.

To form a digital system for minimizing the cost of rock mass size reduction, the principal challenges are not concerned with advances in image analysis, but rather with whether the costs of the comminutive processes (crushing and grinding) can be accurately expressed as functions of remotely sensed ground condition parameters,

particularly the strength of the rock mass.

The material within Section 9.1 below shows how the model reacts to shrink fragment size when the cost of machine operation with respect to fragment size becomes more sensitive. These results indicate that an assumption utilized to define machine productivity, i.e. that machine cycle time is infinite for 100th percentile fragment sizes greater than the buckets width (Section 5.2) was probably too conservative. Section 9.1 shows how machine productivity can be easily redefined.

To be of practical use, the cost model will have to include a comminutive process. Locally, certain mines are already beginning to outfit crusher mass streams with digital fragment delineation systems. Section 9.2 shows that in order for the model to incorporate a crusher, for which the relationship between cost and fragment size is extremely sensitive, crusher production will have to be formulated as a multivariate function of remotely sensed variables, one of which must describe the strength of the rock mass from which the fragments were blasted. The work presented in Chapter 6 already showed how the strength of the rock mass can be estimated with the drill.

Finally Section 9.3 discusses the future work required for more completely characterizing the relationship between rock strength and the penetration rate of drilling machines.

9.1 Redefining Loading Machine Productivity

In Chapter 5, loading machine cost was defined as a function that included the 100th percentile fragment screen size and the machine's bucket width (Equation 5.16).

Excavation cost model results from the previous Chapter showed that machine cost changes were marginal over the estimated fragment sizes output by the model. In retrospect, it would have been more sensible to have defined productivity as a function that utilized the bucket's height, as opposed to its width. Figure 9.1 shows the resulting average total cycle times for the large front end loaders (12 yd³) modeled for the full bucket width (W_b), and at half bucket width. (This Figure is an adaptation of Figure 5.2. For data point locations, please refer to Figure 5.1). Figure 9.1 shows that when the bucket width term is halved, an entirely new cycle time curve results. Total cycle time now ramps up rapidly beyond about 25 inches of 100th percentile size, and will now go on to infinite time (i.e. zero production) near a 100th percentile size of 93.5 inches.

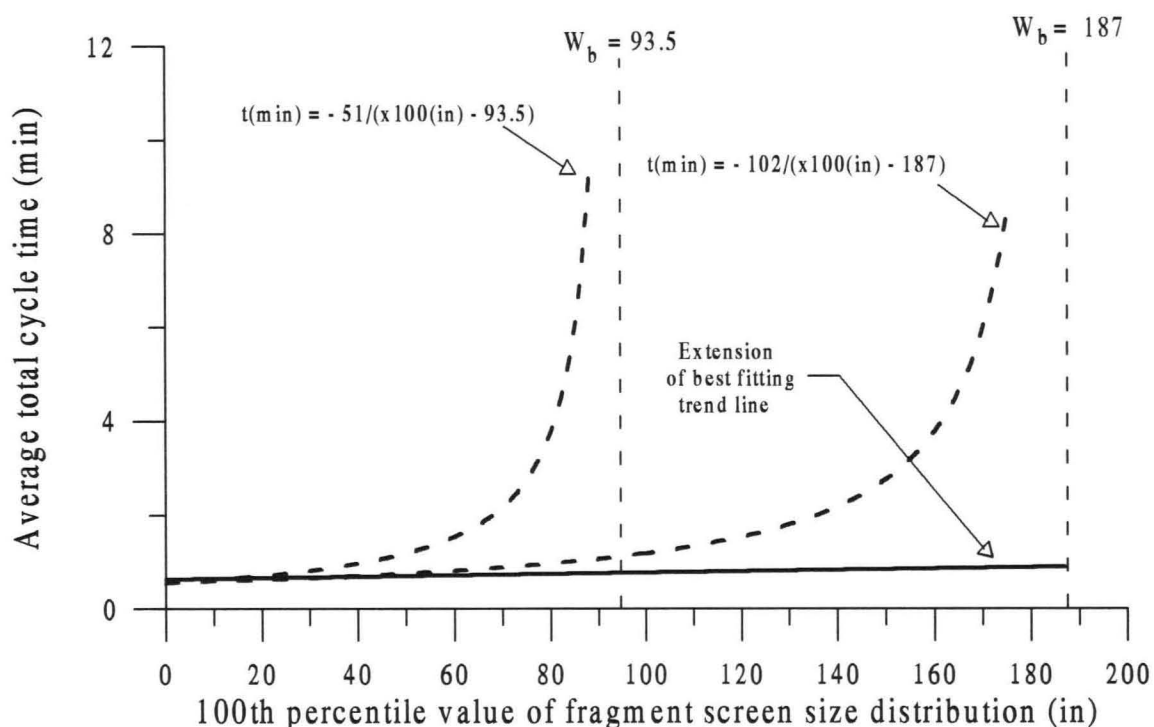


Figure 9.1 - Modeled Average Total Cycle Times for Large Front End Loaders Corresponding to 2 Different Bucket Widths

These redefined large front loading machines can easily be put into the cost model.

Machine cost (\$156/hr) was determined according to the procedure of Section 7.7. The results will be presented in the same sequence used to present the results of the previous Chapter. Figure 9.2 shows the estimated costs for the excavation system that now utilizes the large front loader having the redefined production function, over the range of rock mass scale parameter size:

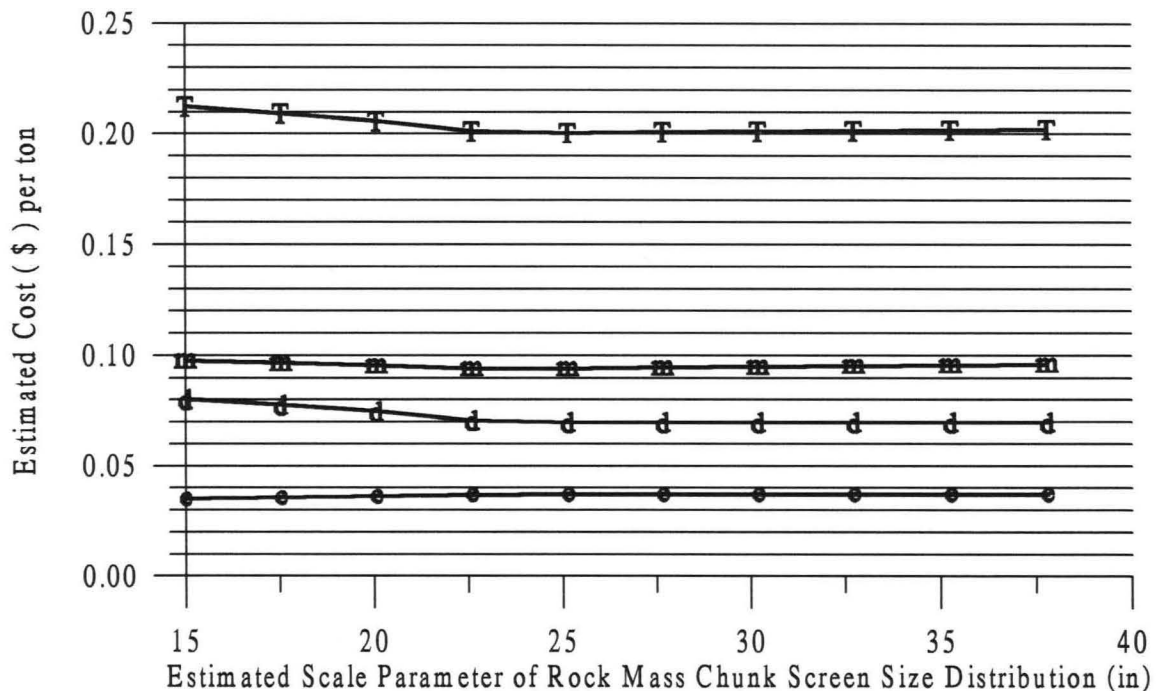


Figure 9.2 - Estimated Excavation Costs over the Rock Mass Chunk Screen Size Scale Parameter Range: Large Front End Loader with Redefined Production Function

- The total estimated cost (symbol “T”) exhibits a linear ramp from \$0.21/ton (at 15 inches) to \$0.20/ton (at about 22.5 inches);
- the ramp in total costs is caused by a drilling cost ramp (“ d ”) of similar magnitude and location.

The relationships between mean fragment size and chunk size, and machine cost and chunk size are presented on Figures 9.3 and 9.4 respectively.

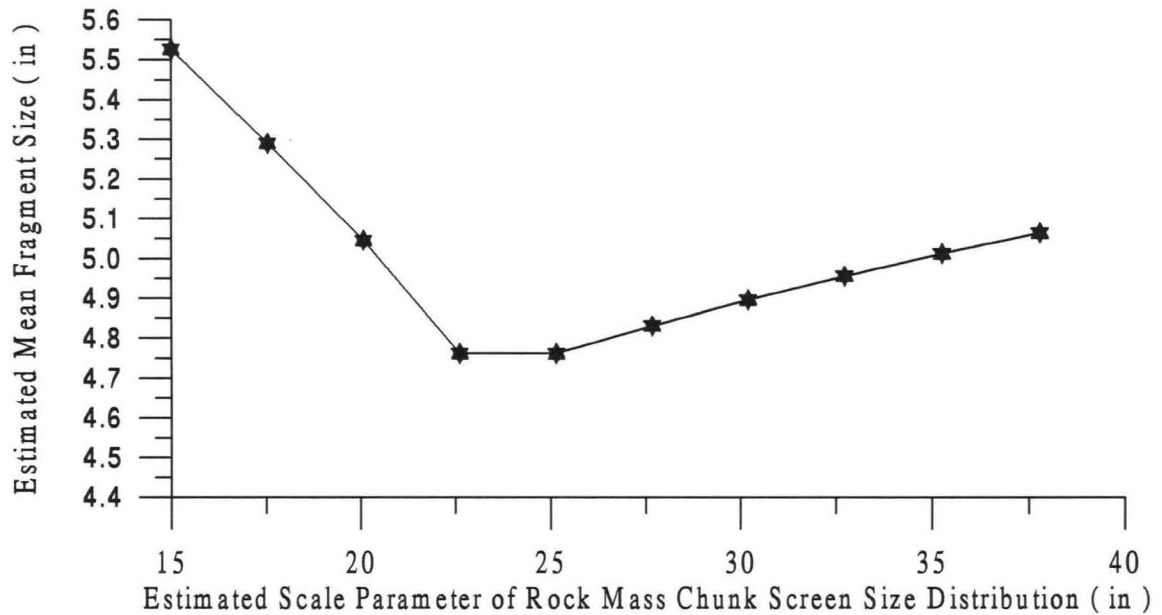


Figure 9.3 - Mean Fragment Sizes Estimated by the Model over the Rock Mass Chunk Screen Size Scale Parameter Range: Large Front End Loader with Redefined Production Function

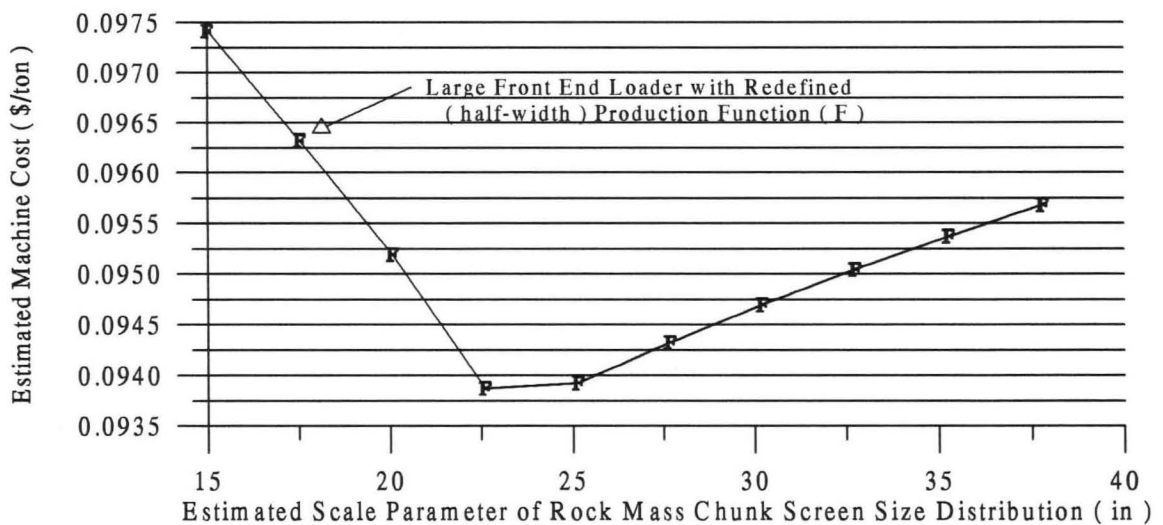


Figure 9.4 - Machine Costs Estimated by the Model over the Rock Mass Chunk Screen Size Scale Parameter Range: Large Front End Loader with Redefined Production Function

The form of these plots are concave, and are unlike any previously presented:

- Mean fragment size and machine cost maximums occur at a chunk size scale parameter value of 15 inches;
- local mean fragment size and machine cost minimums occur at a chunk size scale parameter value of about 22.5 inches.

The form is best explained by showing how the redefined machine function now forces the model to alter the powder length and the rock volume over the chunk size range to compute the minimum excavation cost, as in Figure 9.5 below:

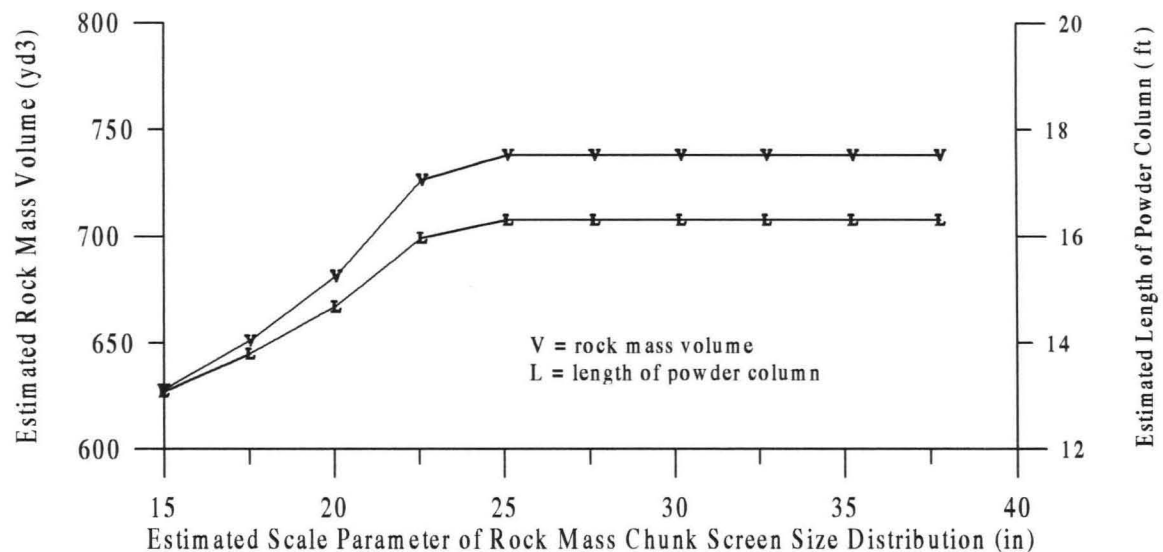


Figure 9.5 - Rock Volumes and Powder Columns Estimated by the Model over the Rock Mass Chunk Screen Size Scale Parameter Range: Large Front End Loader with Redefined Production Function

- At the 15 inch chunk size scale parameter value associated with maximum loader cost (see Figure 9.4), the model has determined that a powder column of about 13 feet and a rock volume of about 625 yd³ will result in the lowest total excavation cost;
- between chunk size scale parameter values of 15 and 25 inches, the model minimizes total cost by increasing both powder and rock volume (at different rates) to produce smaller fragments, which decreases the loader cost;
- beyond chunk size scale parameter values of 25 inches, the model has constrained both the rock volume and the powder column at constant values.

Therefore above chunk size scale parameters of 25 inches, the model can no longer decrease fragment size with explosive to lower machine cost. The machine cost begins to ramp up away from its local minima (Figure 9.4) simply because the size of the raw rock mass material blasted to produce the fragments is increasing, while powder and rock volume are constrained to constant values. Thus when machine cost becomes more sensitive to fragment size change, the model behaves as intended by altering both the rock volume and the explosive column.

The productivity models for all of the different machines presented in Chapter 5 (Table 5.1) could readily be redefined in the manner of the above example. However, the results for redefined cable shovels and hydraulic shovels will not nearly be as marked as that for the front loaders, simply because the aspect ratios (width/height) of the shovel buckets appear to be near unity.

Aside from the above considerations, there is still a considerable amount of work that can be performed to more completely characterize machine production as a function of the fragmentation descriptor. However, from the standpoint of an excavation cost model, this work will be particularly challenging. For example, consider that after a considerable amount of regression analysis, machine productivity could be very accurately estimated as a multivariate function (size, shape, orientation, etc.) of variables within a fragmentation descriptor set. Then the challenge becomes attaining an immensely complicated goal of how to design and control these different variables with the explosive. The fragmentation modeling presented in Chapter 4 was concerned with only two fragmentation descriptor variables: The uniformity and shape parameters that describe the

distribution of fragment screen size.

The necessary work to adapt the model to include a crushing machine, the cost for which is extremely sensitive to fragment size, is presented within the next Section.

9.2 Crushing Implications

The behavior of the excavation cost model will be radically transformed by the inclusion of a crushing cost function, because crushing is extremely cost intensive. The results of the previous Chapter showed how the model allocates the expense of the drill, explosive, and machine into a minimum total excavation cost arrangement. But the cost intensive nature of a crusher will act like a cost throttle upon the model, and force it into blast intensive behavior. Thus a crusher included model is no longer purely concerned with minimizing the cost of excavation, but rather principally concerned with minimizing the cost of the explosive and crushing modes of size reduction.

Crushing and grinding can account for up to 85% of the total power consumption at open pit mines utilizing concentrators [Hartman, 1992]. The actual portion of the total power budget consumed in the crushing stage of a size reduction sequence that includes a subsequent grinding stage is highly variable. Bond's comminution work formula, originally presented as Equation 1.2, is here repeated as:

$$W = 10 W_i \left(\frac{1}{\sqrt{P}} - \frac{1}{\sqrt{F}} \right) \quad (9.1)$$

where W is the mass specific work consumption (kW-hr/ton) of the comminutive machine, W_i is the Bond work index (kW-hr/ton) for the mass moving through the

machine, and F and P are the screen size values (microns) for which 80% of the feed and product particles pass. Then for an excavation mass flow consisting of loading, conveyance (trucks or belts), and crushing, and neglecting any size reducing processes occurring during loading and conveyance, F can be taken as the 80th percentile size of the blasted rock mass fragments. If maintenance and spare parts costs are neglected, then the cost (\$/ton) of the crushing machine can be determined as:

$$C_c = \frac{a_c}{P_c} + b_c W = \frac{a_c}{P_c} + b_c \left[10 W_i \left(\frac{1}{\sqrt{P}} - \frac{1}{\sqrt{F}} \right) \right] \quad (9.2)$$

where a_c is the cost of owning or leasing the machine (\$/hr), P_c is the crusher production (tons/hr), and b_c is the operating cost, here taken as electricity cost (\$/ kW-hr).

Consider that a crusher has been outfitted with cameras at it's entrance and exit; then P and F can be estimated a digital image analysis software such as SPLIT. Furthermore, assume the work index (W_i) of the material is known. Neglecting any recirculating fragment mass flow, then the dollar per ton crushing cost (C_c) can be estimated if the mass flow (P_c (ton/hr)) into or out of the crusher can be measured with a belt scale, and if the owning and electrical costs are known. But from the standpoint of a model for estimating size reduction cost, this dollar per ton cost value is worthless, because it presupposes that the mass flow and work index of the rock moving through the crusher are always known.

Chapter 3 showed how the size distributions of rock mass and fragments are estimated with digital image analysis. The fragmentation model presented in Chapter 4 detailed how fragment size distributions are produced from rock mass of known size and

strength. Chapter 5 showed how machine production can be expressed as a function of the fragment size distribution, and Chapter 6 presented a way of estimating rock mass strength through drill production. Thus the physical nature of the rock mass, mass which must eventually be fed through the crusher, has been remotely sensed by the camera and the drill. Another formidable challenge that is now posed for subsequent research is to formulate an expression for crusher production (ton/hr) in terms of these remotely sensed variables.

By purely intuitive reasoning, the crusher's production must be proportional to the size of it's product (x_P), and inversely proportional to both the strength (S) and size (x_F) of it's feed, or:

$$P_c \propto \frac{x_P}{S x_F} \quad (9.3)$$

so following this intuition it is proposed that experimentation be performed upon crushing machinery to gather observational data to permit the following regression:

$$\hat{P}_c = \frac{\hat{k}_c (\hat{x}_P^?)^{C_3}}{(\hat{S})^{C_1} (\hat{x}_F^?)^{C_2}} \quad (9.4)$$

where \hat{k}_c is a constant characterizing the crushing machine size and type, \hat{S} is the rock strength as estimated by the drill (p.s.i.), $\hat{x}_P^?$ is some percentile value of the fragment size distribution fed to the crusher (in), $\hat{x}_F^?$ is some percentile value of the crusher's product size distribution (in), and C_1 through C_3 are constants. It is not clear whether the regression represented above will have to include a separate " throttle " estimator term,

for instance that corresponds to the mantle (gyratory crusher) or the gape (jaw crusher) setting of the machine.

The next logical step would be to avoid the time and expense imposed by Bond Work Index determinations, and perform experimentation to permit a regression for estimating mass specific work consumption (kW-hr/ton) as:

$$\hat{W} = C_4 \hat{S}^{C_5} \left[(\hat{x}_P^?)^{C_6} - (\hat{x}_F^?)^{C_7} \right] \quad (9.5)$$

where $\hat{x}_P^?$ and $\hat{x}_F^?$ are some percentile values (not necessarily the same as the percentile values of 9.4 above) of the crusher product and feed, respectively, in inches, and C_4 through C_7 are constants. Crusher cost per ton can then be estimated as a function of remotely sensed variables:

$$\hat{C}_c = a_c \left[\frac{(\hat{S})^{C_1} (\hat{x}_F^?)^{C_2}}{\hat{k}_c (\hat{x}_P^?)^{C_3}} \right] + b_c \left\{ C_4 \hat{S}^{C_5} \left[(\hat{x}_P^?)^{C_6} - (\hat{x}_F^?)^{C_7} \right] \right\} \quad (9.6)$$

but the determination of the constants within this equation will require a considerable amount of research effort.

Once the model incorporates the crushing cost per ton expression, then it will react by attempting to shrink rock mass volume to a very low value that will be determined by the drill cost per ton. It is inferred that a lower bound constraint will have to be formulated for the rock volume estimator, because of considerations involving flyrock and slope stability. But it must be emphasized that the relationships between these phenomena and rock volume, as well as the powder column's length and diameter, are not

well characterized. A commonly held view within the industry is that slope stability considerations already limit the extent to which explosives are used for size reduction within most open pit mines. This view is supported by certain of the field note data utilized for this thesis. For instance where volume was being blasted right up against the ultimate pit limit, some of the mines would either increase the volume (via the burden) and use a standard load, or else keep volume constant (with a standard pattern) and use reduced loads in the holes. These simple procedures limit back break and increase the stand time of the bench faces. But exactly how a slope stability constraint would be formulated for the model is unclear; certainly this issue qualifies for future geotechnical research.

The easiest way to answer some of these uncertainties is not necessarily by performing blast experiments, but perhaps by simply observing the behavior and results of a crusher included model subject to different constraint conditions, and comparing this information with observational data.

A “bigger is better” mode of thought appears to influence both the design and the procurement of machinery within the modern mining industry. It is not entirely clear whether this way of thinking is the real view of the machine suppliers; more likely they are simply responding to market demand. Loading machine bucket volumes increase, and require larger trucks. Drilling machines drill ever larger holes, requiring larger powder loads, and permitting larger volumes of rock to be affected by the subsequent blast. Then average fragment sizes increase, requiring larger crushing resources. Given a set of variables describing the range of rock mass conditions within which these machines must

operate, then exactly what allocation of machine types and sizes, what rock mass block size, and what hole diameter and powder load will result in the lowest total cost? This thesis has attempted to demonstrate that this seemingly straightforward problem is so complicated it will never be solved without the aid of a mathematical model formulated to minimize the total cost incurred in reducing the size of the rock mass. The boundary conditions, or constraints, are a crucially important aspect of such a model. Chapter 7 showed that control variable constraint formulations always appear as functions of drill diameter. The future work required to more completely characterize the drilling function is presented within the following section.

9.3 Drilling Work

The drilling machine data utilized for this thesis was inadequate. As shown in Chapter 6, only three observations from Mine Cu2 were used to characterize the relationship between drill penetration rate and rock strength. Section 7.5 showed how the range of rock strengths used in the model had to be limited to the range of strengths generated by the Mine Cu2 drill. Then as noted in Section 7.2, which was concerned with minimizing excavation cost, drill diameter could not be included along with rock volume and powder length as a control variable simply because the observational data for the drill did not include any variation of diameter; the rotary drill observed at Mine Cu2 utilized a 10 & 5/8 inch diameter bit of unknown life (bit hours) and make.

The drilling function is crucially important to any rock mass excavation or size reduction cost model, because the drill is the remote strength sensing device from which

the cost and efficiency of subsequent size reduction can be estimated. Chapter 4 demonstrated that rock mass strength is a fundamental parameter required for accurately estimating fragmentation. The formulations presented in Section 9.2 above predict that rock mass strength can be utilized to estimate both mass specific work consumption and crusher production.

30 years ago Bauer and Calder showed how rock strength could be estimated with the drill (Chapter 6). But correlating a drill's penetration rate to the uniaxial compressive strength of the rock it penetrates will require that the drill be outfitted with sensors to record the thrust, linear translation, and r.p.m. of the drill stem. This data would then have to be sampled (at some determined frequency) and then composited into bench strength intervals, much the same way as drill hole assay values are composited from their assay per interval foot averages into bench assay values. The bench rock strengths thus estimated would also have to include some sort of function to account for bit wear. It is anticipated that the effect of bit wear upon estimated rock strength will be worked out as a simple power function acting upon a time variable describing total bit hours.

APPENDIX
DATA TABLES

Site Codes		Hole Data						Explosive Length/ Hole (ft.)					Total Equivalent ANFO Weights per Hole			
Mine Site Code	Mine Site Code (Plots)	Brdn (ft)	Speng (ft)	Hole Dia. (in)	Bench (ft)	Sub-Drill (ft)	Stm (ft)	ANFO (ft)	Slurry (Wet Holes) (ft)	Other (ft.)	Total (ft)	above grade (ft)	Total (lbs)	Total (kg)	Total above grade (lbs)	Total above grade (kg)
Au7SA	a	15	15	7.88	20	3.0	16.0	7.00			7.00	4.00	125.5	56.9	71.7	32.5
Au9SB	b	24	24	7.88	20	5.0	8.9	16.10			16.10	11.10	288.7	131.0	199.0	90.3
Au9SA	c	18	18	7.88	20	5.0	17.0	8.00			8.00	3.00	143.5	65.1	53.8	24.4
Au7SF	d	15	15	6.75	20	3.0	16.0	7.00			7.00	4.00	92.2	41.8	52.7	23.9
Au7SB	e	15	15	6.75	20	3.0	16.0	7.00			7.00	4.00	92.2	41.8	52.7	23.9
Au12SA	f	17	17	7.88	20	5.0	13.4		11.64		11.64	6.64	295.1	133.9	119.1	54.0
Au11SE	g	15	15	7.30	25	5.0	13.0	17.50			17.50	12.50	269.6	122.3	192.6	87.4
Au6SB	h	15	15	6.50	25	5.0	12.0	12.21		0.73	12.94	7.94	161.7	73.4	97.0	44.0
Au11SB	i	15	15	7.30	25	5.0	13.0	17.50			17.50	12.50	269.6	122.3	192.6	87.4
Cu2SG	j	32	32	10.63	50	6.0	26.0	18.19	13.94		32.13	26.13	1237.0	561.1	852.8	387.0
Cu5SD	k	40	30	12.75	50	9.9	31.3	8.51	20.12		28.63	18.73	1737.0	787.9	880.2	399.4
Cu5SF	l	40	27	12.75	50	7.6	33.5	7.18	11.95		19.13	11.53	1132.0	513.5	542.2	246.0
Cu2SE	m	22	22	10.63	50	7.0	26.0	5.97	23.87		29.84	22.84	1296.7	588.2	745.6	338.3
Cu5SE	n	40	33	12.75	50	8.1	35.6	22.45			22.45	14.35	1055.3	478.7	674.5	306.0
Cu5SA	o	40	33	12.75	50	7.4	28.9	28.48			28.48	21.08	1338.6	607.2	990.8	449.6
Cu5SB	p	30	30	12.75	50	6.1	28.0	28.13			28.13	22.03	1322.2	599.8	1035.5	469.8
Cu4SE	q	27	27	13.75	50	13.0	46.0	17.00			17.00	4.00	929.3	421.5	218.7	99.2
Cu4SB	r	27	27	13.75	50	13.0	46.0	17.00			17.00	4.00	929.3	421.5	218.7	99.2
Cu4SA	s	27	27	13.75	50	13.0	46.0	17.00			17.00	4.00	929.3	421.5	218.7	99.2
Cu4SC	t	27	23	13.75	50	13.0	44.7	18.30			18.30	5.30	1000.4	453.8	289.7	131.5

Notes:

- 1) The density value used for ANFO was 53.04 lbs/ft³.
- 2) The Relative Bulk Strength used for ANFO was 100; the ANFO Specific Energy = 740 cal/cc.
- 3) A wide variety of different slurry explosives were used; their density value was taken as 75 lbs/ft³.
- 4) The Relative Bulk Strength of the Slurry Explosives was taken as equivalent to ANFO

Table A1 - Site Blast and Fragmentation Data

Site Codes		Rock Volume per Hole		Powder Factor		Kuz-Ram Fragmentation Model Data		
Mine Site Code	Mine Site Code (Plots)	(yd3)	(m3)	Total Hole (lbs/yd3)	above grade (lbs/yd3)	Kuz Fnctn	Cnnnghm Rock Factor	Kuz Mean Size (cm)
Au7SA	a	166.7	127.4	0.753	0.43	5.9	8.6	50.6
Au9SB	b	426.7	326.2	0.68	0.47	6.6	3.9	25.7
Au9SA	c	240.0	183.5	0.60	0.22	9.4	6.3	59.1
Au7SF	d	166.7	127.4	0.553	0.32	7.1	7.0	50.3
Au7SB	e	166.7	127.4	0.553	0.32	7.1	7.9	56.4
Au12SA	f	214.1	163.7	1.379	0.56	5.2	4.2	21.9
Au11SE	g	208.3	159.3	1.294	0.92	3.8	5.8	22.1
Au6SB	h	208.3	159.3	0.776	0.47	5.8	7.5	43.4
Au11SB	i	208.3	159.3	1.294	0.92	3.8	6.7	25.1
Cu2SG	j	1896.3	1449.9	0.652	0.45	8.7	8.6	74.7
Cu5SD	k	2222.2	1699.1	0.78	0.40	9.6	7.4	70.8
Cu5SF	l	2000.0	1529.2	0.566	0.27	12.0	7.3	88.2
Cu2SE	m	896.3	685.3	1.447	0.83	5.2	8.0	41.6
Cu5SE	n	2444.4	1869.0	0.43	0.28	12.3	7.2	88.6
Cu5SA	o	2444.4	1869.0	0.55	0.41	9.6	7.3	70.3
Cu5SB	p	1666.7	1274.3	0.79	0.62	6.9	6.9	47.8
Cu4SE	q	1350.0	1032.2	0.69	0.16	15.5	7.7	120.2
Cu4SB	r	1350.0	1032.2	0.69	0.16	15.5	6.9	107.6
Cu4SA	s	1350.0	1032.2	0.69	0.16	15.5	6.9	107.7
Cu4SC	t	1150.0	879.3	0.87	0.25	11.4	7.3	83.6

Notes:

- 1) The "Kuz Fnctn" entry is defined as $((V_o/Q_{ag})^{0.80}) * (Q_{ag})^{0.17} * (100/115)^{-0.63}$
- 2) The "Cunningham Rock Factor" was determined by visual interpretation of scaled Rock Mass Cell images.
- 3) The density used for the C. Rock Factor was constant 2.33 mt/m³.

Table A1 (Continued) - Site Blast and Fragmentation Data

Site Codes		Kuz-Ram Fragmentation Model Data				Uniaxial Compressive Rock Strength	
Mine Site Code	Mine Site Code (Plots)	Kuz Mean Size (in)	n Kuz	Kuz Scale (cm)	Kuz Scale (in)	(psi)	(N/m ²)
Au7SA	a	19.9	0.55	98.16	38.65	13156	90644840
Au9SB	b	10.1	1.24	34.51	13.59	10440	71931600
Au9SA	c	23.3	0.64	104.97	41.33	18883	1.3E+08
Au7SF	d	19.8	0.54	99.52	39.18	8003	55140670
Au7SB	e	22.2	0.54	111.54	43.91	16950	1.2E+08
Au12SA	f	8.6	0.90	32.95	12.97	5906	40692340
Au11SE	g	8.7	1.18	30.11	11.86	8022	55271580
Au6SB	h	17.1	0.81	68.09	26.81	13972	96267080
Au11SB	i	9.9	1.18	34.27	13.49	17896	1.2E+08
Cu2SG	j	29.4	1.04	106.19	41.81	25700	1.8E+08
Cu5SD	k	27.9	0.81	111.12	43.75	12402	85449780
Cu5SF	l	34.7	0.52	179.50	70.67	3649	25141610
Cu2SE	m	16.4	1.03	59.32	23.35	13841	95364490
Cu5SE	n	34.9	0.65	156.26	61.52	10352	71325280
Cu5SA	o	27.7	0.86	107.95	42.50	11534	79469260
Cu5SB	p	18.8	0.96	69.99	27.56	6213	42807570
Cu4SE	q	47.3	0.60	221.98	87.40	9246	63704940
Cu4SB	r	42.4	0.60	198.80	78.27	6233	42945370
Cu4SA	s	42.4	0.60	198.94	78.32	6304	43434560
Cu4SC	t	32.9	0.61	153.00	60.24	11767	81074630

Notes:

- 1) The Kuz-Ram mean fragment size was determined with Equation 4.9 (Section 4.4.1).
- 2) The Kuz-Ram uniformity parameter "n" was determined with Equation 4.13 (Section 4.4.3).

Table A1 (Continued) - Site Blast and Fragmentation Data

Site Codes		SPLIT Fragment Size Distribution Data					
Mine Site Code	Mine Site Code (Plots)	Shape Prmtr "n"	Scale Prmtr "theta" (in)	Mean (in)	Median (in)	Mode (in)	Stndrd Dvtn (in)
Au7SA	a	1.57	6.62	5.97	5.20	3.23	4.03
Au9SB	b	1.20	4.24	4.09	3.04	0.48	3.72
Au9SA	c	1.43	6.69	6.10	5.15	2.73	4.41
Au7SF	d	1.28	6.51	6.17	4.76	1.25	5.29
Au7SB	e	1.41	6.30	5.83	4.73	1.92	4.59
Au12SA	f	1.25	4.31	4.02	3.22	1.19	3.23
Au11SE	g	1.31	3.63	3.34	2.74	1.21	2.57
Au6SB	h	1.33	2.20	2.02	1.67	0.77	1.53
Au11SB	i	1.34	5.53	5.12	4.15	1.69	4.03
Cu2SG	j	1.71	5.70	5.08	4.60	3.41	3.06
Cu5SD	k	1.89	2.98	2.64	2.45	2.00	1.45
Cu5SF	l	1.52	4.84	4.37	3.81	2.39	2.93
Cu2SE	m	1.52	4.23	3.81	3.32	2.09	2.56
Cu5SE	n	1.54	4.76	4.28	3.75	2.41	2.84
Cu5SA	o	1.85	3.10	2.75	2.54	2.04	1.54
Cu5SB	p	2.00	3.07	2.72	2.56	2.17	1.42
Cu4SE	q	1.41	8.04	7.32	6.20	3.35	5.27
Cu4SB	r	1.55	7.08	6.37	5.59	3.63	4.20
Cu4SA	s	1.48	6.49	5.87	5.07	3.03	4.04
Cu4SC	t	1.65	5.39	4.82	4.31	3.06	3.00

Table A1 (Continued) - Site Blast and Fragmentation Data

Site Codes		Average Fragment Shape Data							
Mine Site Code	Mine Site Code (Plots)	Area (in2)	Prmtr (in)	Major Axis (in)	Minor Axis (in)	Angle Rel. to Hor.	Angle Rel. to Vert.	Elngtn	Rghnss
Au7SA	a	14.24	14.70	4.59	2.67	94.95	4.95	0.416	0.890
Au9SB	b	2.91	5.98	1.83	1.06	92.68	2.68	0.414	0.688
Au9SA	c	1.80	4.42	1.30	0.75	90.40	0.40	0.435	0.510
Au7SF	d	11.16	12.67	3.75	2.16	93.07	3.07	0.418	0.868
Au7SB	e	6.44	9.45	2.81	1.66	91.19	1.19	0.413	0.811
Au12SA	f	2.10	5.58	1.64	0.91	81.52	8.48	0.439	0.677
Au11SE	g	1.94	5.34	1.58	0.93	81.39	8.61	0.416	0.674
Au6SB	h	1.70	5.21	1.60	0.93	84.40	5.60	0.407	0.701
Au11SB	i	3.67	6.83	2.05	1.17	82.24	7.76	0.434	0.702
Cu2SG	j	3.32	6.34	1.91	1.07	94.15	4.15	0.437	0.673
Cu5SD	k	3.97	8.05	2.46	1.43	88.54	1.46	0.407	0.815
Cu5SF	l	2.72	6.01	1.76	1.01	81.56	8.44	0.428	0.672
Cu2SE	m	6.35	9.64	2.96	1.72	82.07	7.93	0.420	0.817
Cu5SE	n	6.12	9.65	2.95	1.72	86.55	3.45	0.416	0.826
Cu5SA	o	5.18	9.05	2.82	1.60	88.11	1.89	0.422	0.830
Cu5SB	p	5.09	9.33	2.93	1.70	83.36	6.64	0.412	0.854
Cu4SE	q	10.97	12.04	3.69	2.16	90.10	0.10	0.413	0.856
Cu4SB	r	6.71	9.41	2.77	1.62	86.71	3.29	0.423	0.794
Cu4SA	s	11.91	13.07	3.98	2.24	86.08	3.92	0.434	0.843
Cu4SC	t	12.11	13.64	4.20	2.46	88.47	1.53	0.411	0.883

Table A1 (Continued) - Site Blast and Fragmentation Data

Site Codes		SPLIT Fragment Shape Distribution Data			
Mine Site Code	Mine Site Code (Plots)	Major Axis Shape Prmtr	Major Axis Scale Prmtr (in)	Minor Axis Shape Prmtr	Major Axis Shape Prmtr (in)
Au7SA	a	1.44	5.06	1.30	2.89
Au9SB	b	1.10	1.90	0.92	1.02
Au9SA	c	0.90	1.24	0.79	0.65
Au7SF	d	1.17	3.96	1.03	2.19
Au7SB	e	1.17	2.96	1.04	1.68
Au12SA	f	1.12	1.71	1.03	0.92
Au11SE	g	1.22	1.69	1.11	0.96
Au6SB	h	1.49	1.77	1.37	1.02
Au11SB	i	1.03	2.08	0.94	1.13
Cu2SG	j	0.97	1.88	0.89	1.01
Cu5SD	k	1.50	2.73	1.38	1.57
Cu5SF	l	1.01	1.77	0.95	0.98
Cu2SE	m	1.35	3.23	1.17	1.82
Cu5SE	n	1.39	3.24	1.23	1.84
Cu5SA	o	1.48	3.12	1.33	1.74
Cu5SB	p	1.81	3.29	1.63	1.90
Cu4SE	q	1.14	3.87	1.08	2.22
Cu4SB	r	1.06	2.84	0.96	1.59
Cu4SA	s	1.19	4.23	1.08	2.31
Cu4SC	t	1.46	4.64	1.30	2.67

Table A1 (Continued) - Site Blast and Fragmentation Data

Site Codes		SPLIT Rock Mass Size Distribution Data					
Mine Site Code	Mine Site Code (Plots)	Shape Prmtr "n"	Scale Prmtr "theta" (in)	Mean (in)	Median (in)	Mode (in)	Stndrd Dvtn (in)
Au7SA	a	1.49	24.63	22.25	19.26	11.67	15.20
Au9SB	b	1.32	31.45	28.96	23.83	10.75	22.15
Au9SA	c	1.48	21.62	19.55	16.88	10.10	13.44
Au7SF	d	1.44	20.59	18.69	15.97	9.04	13.18
Au7SB	e	1.31	35.47	32.71	26.81	11.80	25.19
Au12SA	f	1.41	20.54	18.70	15.84	8.55	13.44
Au11SE	g	1.27	37.80	35.08	28.32	11.17	27.82
Au6SB	h	1.56	26.03	23.40	20.58	13.50	15.32
Au11SB	i	1.40	22.01	20.06	16.94	9.00	14.52
Cu2SG	j	1.20	31.52	29.65	23.22	7.08	24.81
Cu5SD	k	1.15	14.97	14.24	10.88	2.55	12.42
Cu5SF	l	1.22	23.06	21.60	17.07	5.66	17.79
Cu2SE	m	1.58	24.09	21.62	19.10	12.77	14.00
Cu5SE	n	1.51	16.40	14.80	12.87	7.99	9.99
Cu5SA	o	1.85	20.85	18.52	17.10	13.69	10.38
Cu5SB	p	1.41	19.28	17.55	14.87	8.03	12.62
Cu4SE	q	1.53	22.43	20.20	17.65	11.22	13.47
Cu4SB	r	1.94	35.84	31.78	29.67	24.67	17.08
Cu4SA	s	1.48	22.92	20.73	17.90	10.71	14.25
Cu4SC	t	1.39	24.50	22.35	18.82	9.82	16.29

Table A1 (Continued) - Site Blast and Fragmentation Data

Gold Mining Site Rock Strengths			Copper Mining Site Rock Strengths		
Site	UCS (psi)	UCS (Pa)	Site	UCS (psi)	UCS (Pa)
Au10SB	7096	48891440	Cu2SD	22785	156988650
Au11SA	18337	126341930	Cu2SE	13841	95364490
Au11SB	17896	123303440	Cu2SG	25855.15	178141984
Au11SE	8022	55271580	Cu3SA	14000	96460000
Au11SF	8556	58950840	Cu3SB	10560	72758400
Au12SA	5906	40692340	Cu3SC	2600	17914000
Au12SB	7500	51675000	Cu4SA	6304	43434560
Au12SC	39250	270432500	Cu4SB	6233	42945370
Au12SD	39250	270432500	Cu4SC	11767	81074630
Au6SB	13972	96267080	Cu4SD	10789	74336210
Au6SC	11762	81040180	Cu4SE	9246	63704940
Au6SE	11805	81336450	Cu5SA	11534	79469260
Au6SF	12822	88343580	Cu5SB	6213	42807570
Au7SA	13156	90644840	Cu5SC	6318	43531020
Au7SB	16950	116785500	Cu5SD	12402	85449780
Au7SF	8003	55140670	Cu5SE	10352	71325280
Au7SG	10850	74756500	Cu5SF	3649	25141610
Au8SC	20703	142643670			
Au8SD	20202	139191780			
Au9SA	18883	130103870			
Au9SB	10440	71931600			
Au9SD	2069.15	14256444			

Table A2 - Site Rock Mass Uniaxial Compressive Strength Data

REFERENCES

- Anonymous, 1879. *The United States Annual Mining Review and Stock Ledger for 1879*, pp. 22-24, The Mining Review Publishing Company, No. 16 Dey Street, New York.
- Atlas Powder Company, 1987. *Explosives and Rock Blasting*, p. 176, Atlas Powder Company, Field Technical Operations, Dallas, Texas.
- Bauer, A., Calder, P.N., 1967. "Open Pit Drilling - Factors Influencing Drilling Rates", *Proceedings of the 4th Rock Mechanics Symposium*, pp. 1 - 34, Department of Energy, Mines and Resources, Ottawa, 1967.
- Cunningham, C.V.G., 1983. "The Kuz-Ram Model for Prediction of Fragmentation from Blasting", *First International Symposium on Rock Fragmentation by Blasting*, Lulea, Sweden.
- Cunningham, C.V.G., 1987. "Fragmentation Estimations and the Kuz-Ram Model - Four Years On", *Proc. 2nd Int. Symp. Rock Fragmentation*, pp. 475-487, Keystone, Colorado.
- Evans, M., Hastings, N., Peacock, B., 1993. *Statistical Distributions*, John Wiley and Sons, Inc., New York.
- Girdner, K., Kemeny, J., Srikant, A., McGill, R., 1996. "The Split System for Analyzing the Size Distribution of Fragmented Rock", *Measurement of Blast Fragmentation*, pp. 101-108, Franklin & Katsabanis (Eds.), Balkema, Rotterdam.
- Hartman, H. L., *SME Mining Engineering Handbook*, 2nd Edition, 1992, p. 407, Society for Mining, Metallurgy, and Exploration Inc., Littleton, Colorado.
- Hessen, B., 1939. *The Social and Economic Roots of Newton's Principia*, p. 26, Howard Fertig Inc., 1971, New York.
- Holman, J.P., 1978. *Experimental Methods for Engineers*, p. 45, McGraw-Hill, New York.
- Kemeny, J., Devgan, A., Hagaman, R., and Wu, X., 1993. "Analysis of Rock Fragmentation Using Digital Image Processing", pp. 1144-1160, *J. Geotechnical Eng.*, Vol. 119, No. 7.

- Koch, G., Link, R., 1971, *Statistical Analysis of Geological Data*, p. 35, Dover Inc., New York.
- Konya, C., Walter, E., 1990. *Surface Blast Design*, p. 135, Prentice Hall, Englewood Cliff, N.J.
- Kreyszig, E., 1988. *Advanced Engineering Mathematics*, 6th Edition, p. 1287, John Wiley and Sons, New York.
- Kuznetsov, V.M., 1973. "The Mean Diameter of the Fragments Formed by Blasting Rock", pp. 144-148, *Soviet Mining Science*, Vol. 9, No. 2.
- Lilly, P., 1986. "An Empirical Method of Assessing Rock Mass Blastability", *The Aus. IMM/IE Aust Newman Combine Group, Large Open Pit Mining Conference, Oct. 1986*.
- Marsh, G.D., 1943. *Copper Camp - Stories of the World's Greatest Mining Town Butte Montana*, p. 223, Hastings House, New York.
- Meinhardt, H., 1995. *The Algorithmic Beauty of Sea Shells*, p. Viii, Springer-Verlag, Berlin.
- Morrison, D.F.M., 1983. *Applied Linear Statistical Methods*, p.68, Prentice Hall Inc., Englewood Cliffs, New Jersey.
- Pfeiffer, E.W. and Westing, A.W., 1971. "Land War", *Environment*, November 1971.
- Philostratus the Athenian, 2nd/3rd Century. *Life of Appolonius of Tyana*, Charles Blount Translation, Nathaniel Thompson, London, 1680.
- Rammler, E., and Rosin, R., 1933. "Laws Governing the Fineness of Powdered Coal", *J. Institute of Fuels*, Vol. 7.
- Shigley, J. E. , 1977. *Mechanical Engineering Design*, p. 146, McGraw-Hill, New York.
- Steinbeck, J. 1939. *The Grapes of Wrath*, p. 45, Viking Penguin Inc., New York.
- Suetonius, Gaius Tranquillus, 1st/2nd Century. *The Twelve Caesars*, p. 145, Robert Graves Translation, Penguin Books Ltd, Harmondsworth, England 1957.
- United States Army, 1965. *Field Manual FM 31-20, Special Forces Operational Techniques*, p. 331, Headquarters, Department of the Army, Washington, D.C.

- Weibull, W., 1939. "A Statistical Theory of the Strength of Materials", *Proc. Roy. Swedish Acad. Eng. Sci.*, 151.
- Whitman, W., 1881. *Leaves of Grass*, p. 169, Everyman, J.M. Dent, Orion Publishing Group, Orion House, 5 Upper St. Martin's Lane, London 1993.
- Wills, B.A., 1992. *Mineral Processing Technology*, p. 193, Pergamon Press Inc., Tarrytown, N.Y.
- Wilson, E.D., Cunningham, J.B., and Butler, G.M., 1934. *Arizona Lode Gold Mines and Gold Mining*, pp. 206-207, The Arizona Bureau of Mines Bulletin 137, Revised 1967, University of Arizona, Tucson.